UNIVERSITY OF CALIFORNIA, SAN DIEGO

INTERPRETATION OF MAMMALIAN BRAIN RHYTHMS OF SENSORIMOTOR PROCESSING

A Dissertation submitted in partial satisfaction of the requirements for the

degree Doctor of Philosophy

in

Biology with specialization in Computational Neurobiology

by

Diane J. Whitmer

Committee in charge:

Terrence J. Sejnowski, Chair
Gert Cauwenberghs
Eric Halgren
David Kleinfeld
Scott Makeig
Pamela Reinagel
Gregory Worrell

2008

The Dissertation of Diane J. Whitmer is approved, and it is acceptable in quality and form for publication on microfilm and electronically:

Chair

University of California, San Diego

2008

DEDICATION

This work is dedicated to the loving memory of my grandfather, Martin Littman, who passed away April 16, 2006. He was proud of my accomplishments, supportive of my career goals, and would have very much enjoyed celebrating the completion of my doctorate.

TABLE OF CONTENTS

LIST OF FIGURES

LIST OF TABLES

ACKNOWLEDGEMENTS

I am grateful for the support and guidance of my thesis advisor, Dr. Scott Makeig, without whom this dissertation would not have been possible. Through this research, Scott has encouraged me to think more clearly and to tackle problems as quantitatively as possible. As a pioneer in the application of ICA to EEG recordings, Scott has also taught me both the power and limitations of using ICA. I would also like to thank Dr. Greg Worrell, who provided the exceptional opportunity to acquire data from epilepsy patients at the Mayo Clinic, and has served as a role model to me both scientifically and interpersonally. I would like to thank my advisor Professor David Kleinfeld, who was an invaluable role model for deriving solutions from first principles, developing and building technology to answer scientific questions, and for careful interpretation of signal processing. I would additionally like to thank Professor Terrence Sejnowski for his support and leadership as the chair of my committee and as the director of my graduate program. I am grateful for the extensive guidance, mentoring, and scientific feedback from committee member Professor Eric Halgren, and only wish I had met him earlier during my graduate career. I thank Professor Pamela Reinagel for her mentoring, advice, and feedback through this process and for serving on my thesis committee, along with Professor Gert Cauwenberghs who also served on my thesis committee.

There are many additional people whose support has been instrumental in my completing my dissertation. On the administrative side, I thank Tom Tomp and Cathy Pugh of the Division of Biological Sciences for helping me navigate through the administrative aspects of the process, and system administrator Bob Buffington who

keeps everything running smoothly at the Swartz Center. I am grateful to all of my friends for their companionship and support through this process. A special thanks goes to Alicia Bicknell, Kim Ditomasso, Jody Harrell, Andra Ghent, Daniel Keller, Jessica Kleiss, Zoe Langsten, Ifije Ohiorhenuan, Jeff Slattery, Ben Sullivan, Corinne Teeter, Jean Verrette, Shane Walker, and Amaya Becvar Weddle.

Finally, I am thankful for the ongoing love and support from my family, especially my parents Ellen and Roger Whitmer, my grandmother Priscilla, and my sister Dr. Rachel Whitmer who was the first in our family to complete a doctorate and has set an example as a successful scientist.

Chapter II is a reprint, in full, of the material as it appears in *PLoS Biology*, 2007 Feb;5(2):e15. The dissertation author is the second author on this paper from work completed in the Kleinfeld lab. I would like to thank the first author, Samar Mehta, for his mentoring and collaboration on this project, co-author Rodolfo Figueroa for his teamwork in the acquisition of behavioral data, co-author Professor Ben Williams, and senior author Professor David Kleinfeld.

Chapter III is a reprint, in full, of the material as it appears as in the *Journal of Neuroscience*, 2006 Jun 14; 26(24):6518-22. The dissertation author is the second author on this paper from work performed in collaboration with first author Rune Berg while we were in the laboratory of senior author David Kleinfeld.

Chapter IV is a preprint of a manuscript to be submitted to *Human Brain Mapping*. The dissertation author is the primary author of this work. I would like to thank Scott Makeig and Greg Worrell for co-authoring this work. Co-author Matthew Stead was instrumental in setting up the data acquisition system for the recordings, and co-

author Il Keun Lee was responsible for designing the behavioral paradigm. I'd also like to thank Karla Crockett for her assistance in acquiring behavioral data from patients, and Andrey Vankov for his development of software that helped import the data into Matlab.

CURRICULUM VITA

Education:

Ph.D., Biology with specialization in Computational Neurobiology, UC San Diego, 2008
BA, Cognitive Science, Dartmouth College, 1997

Research Experience:

Graduate dissertation student, Swartz Center for Neural Computation, UC San Diego
Advisor: Dr. Scott Makeig, currently. Multi-scale Dynamics of Visually-Cued Finger Movements in Human Epilepsy Patients

Graduate student researcher, Laboratory of Dr. David Kleinfeld, UCSD, 2003-2005
Sensorimotor processing in the rat whisker system

Graduate rotation student, Computational Neurobiology Lab of Dr. Terry Sejnowski, Salk Institute, 2001. Spike timing reliability

Undergraduate researcher, Laboratory of Dr. Jeff Taube, Dartmouth College, 1995-1996
Spatial Cognition in Rats: Encoding 3rd Dimension of Space with Head Direction Cells

Undergraduate research assistant, Laboratory of Dr. Janet Metcalfe,
Dartmouth College, 1995-1997. Human cognition in face recognition

Peer Reviewed Publications:

S. B. Mehta, D. Whitmer, R. Figueroa, B. A. Williams and D. Kleinfeld. Haptic Perception in a Scanning Sensorimotor System. *Public Library of Science:Biology*, 5(2):e15, 2007.

R.W. Berg, D. Whitmer, D. Kleinfeld. Exploratory Whisking in Rat is Not Phase-Locked to the Hippocampal Rhythm. *Journal of Neuroscience*, 26: 6518-6522, 2006.

Manuscripts in Preparation:

D. Whitmer, G. Worrell, M. Stead, I.K. Lee, F. Meyer, and S. Makeig. Dynamics of Visually-Cued Finger Movements and Epilepsy Signals based on Independent Component Analysis (ICA) of Electrocorticogram (ECoG) and EEG. *In preparation,* 2008.

Conference Proceeding Publications:

S. Schreiber, J.M. Fellous, D. Whitmer, P.H.E. Tiesinga, and T.J. Sejnowski, A New Correlation-based Measure of Spike Timing Reliability. *Neurocomputing*, 52-54: 925-931, 2003.

Abstracts:

Whitmer, D., Worrell, G., Stead, M., Lee, I.K., Meyer, F., Makeig, S. Cortical Dynamics of Visually-Cued Finger Movements in ECoG with ICA. *NIPS 2007: Large-Scale Brain Dynamics Workshop poster*, Whistler, BC, Canada. Neural Information Processing Systems, 2007.

Whitmer, D., Worrell, G., Stead, M., Lee, I.K., Meyer, F., Makeig, S. Cortical Mapping Based on Independent Component Analysis and Spectral Changes in the Electrocorticogram. Program No. 389-TH-AM. *Human Brain Mapping Abstract*, Chicago, IL, USA. Organization for Human Brain Mapping, 2007.

Mehta, S. B., Whitmer, D., Figueroa, R., Williams B. A., Kleinfeld, D. Behavioral Evidence for Sensorimotor Integration in the Rat Vibrissa System. Program No. 144.1, *Society for Neuroscience Abstract*. Washington, DC: Society for Neuroscience, 2006.

Whitmer, D. Relationships Between Intracranial EEG and Scalp EEG in Human Epilepsy Patients. *Annual Spring Retreat in Cognitive Neuroscience*, UC San Diego, 2006.

D. Whitmer, I.K. Lee, G. Worrell, S. Makeig. Separating Proximal from Distal Activities in Concurrent Scalp and Intracranial EEG Data. Program No. 185-T-AM. *Human Brain Mapping Abstract*, Florence, Italy: Organization for Human Brain Mapping, 2006.

S.B. Mehta, D.J. Whitmer, D. Kleinfeld, Spatial Localization in the Rat Vibrissa System: Behavioral Discrimination. Program No. 978.6. *Society for Neuroscience Abstract.* Washington, DC: Society for Neuroscience, 2004.

D.J. Whitmer, R.W. Berg, D. Kleinfeld. The Coupling Between Hippocampal Theta Rhythm and Whisking is Weak and Independent of Sensory Feedback. Program No. 59.4. *Society for Neuroscience Abstract.* Washington, DC: Society for Neuroscience, 2003.

Teaching Experience:

Teaching Assistant, Cellular Neuriology, Professors: Dr. Massimo Scanziani and Dr. Anirvan Ghosh, UCSD Division of Biological Sciences, Winter 2008.

Teaching Assistant, Cellular Neurobiology, Professors: Dr. Nick Spitzer and Dr. Darwin Berg, UCSD Division of Biological Sciences, Fall 2007.

Clinical Cases Discussion Section Leader, Basic Neurology, Professor: Dr. Mark Kritchevsky, UCSD School of Medicine, Spring 2007.

Teaching Assistant, Introduction to Signals and Systems, Professor: Dr. Alexander Vardy, UCSD Dept. of Electrical and Computer Engineering, Fall 2004.

Guest Lecturer (single lecture), Undergraduate Computational Neurobiology, Professor: Dr. Terrence Sejnowski, UCSD Division of Biological Sciences, Spring 2004.

Teaching Assistant, Undergraduate Computational Neurobiology, Professor: Dr. Terrence Sejnowski, UCSD Division of Biological Sciences, Spring 2003.

Additional Training:
Neuroinformatics Course, Woods Hole Marine Biological Labs, Summer 2007
HHMI Medical Specialty Training (Neurology), Winter, 2007

Awards and Fellowships:
Travel Award for Human Brain Mapping Conference, Chicago, IL, June 2007
NSF IGERT Fellowship for Graduate Training at UCSD, 2001-2005
Howard Hughes Undergraduate Research Fellowship, Dartmouth College, 1995
Presidential Scholars Program, Dartmouth College, 1995-1996

ABSTRACT OF THE DISSERTATION

INTERPRETATION OF MAMMALIAN BRAIN RHYTHMS

OF SENSORIMOTOR PROCESSING

by

Diane J. Whitmer

Doctor of Philosophy

in

Biology with specialization in Computational Neurobiology

University of California, San Diego, 2008

Professor Terrence Sejnowski, Chair

A fundamental goal of neuroscience is to relate neural signals with external sensory stimuli and with complex behaviors such as movement. In many sytems and brain regions, brain oscillations correlate with movement. The body of work presented here examines the role of oscillations in both sensory representation and motor output, spanning multiple scales of measurement from local field potential recordings to the large-scale electrical activity of the whole human brain. The vibrissa system of rats is an active sensory motor system where the whiskers are actively moved to explore the environment. The work described in Chapter II uses a behavioral paradigm to test coding

strategies within the rat vibrissa system. We ask whether rats can discriminate the position of objects in the plane within which the whiskers move and whether discrimination can be accomplished with a single vibrissa. We report that rats can locate the position of objects in space relative to its body position with a single whisker, suggesting a neural code based on timing of the whisking cycle. Chapter III examines a salient, widespread oscillation associated with movements in rats (the theta rhythm), to determine whether this signal might drive whisking behavior. We find that hippocampal theta and the whisking rhythm are not coherent although they are oscillatory signals within the same spectral band. In humans, invasive brain measurements are possible in the cases of focal refractory epilepsy patients who are undergoing neurosurgical evaluation. Chapter IV uses intracranial measurements from epilepsy patients who performed a visually-cued finger movement task, to understand the electrical signals that enable a complex sensory motor action. We analyze signals spectrally, examining oscillations with a linear systems approach, specifically using independent component analysis (ICA) to interpret the signals. We find that ICA can separate pathological brain signals from motor signals and decompose intracranial signals into its underlying sources. Together, these results demonstrate that oscillations of peripheral sensors can encode the representation of spatial information, that neural rhythms in overlapping frequency bands are not necessarily entrained, and that ICA is a useful tool for ummixing motor and other signals in the human brain.

Chapter I. Electrophysiological Measurements, Oscillations, and Sensorimotor Processing

The goal of neuroscience is to relate brain function with behavior, cognition, and perception. How are complex stimuli from the external environment represented in neuronal function, such that an animal can make real-time decisions to take action? The issue is further complicated when the animal's sensors are moving and when a variety of information sources compete for attention. Furthermore, what level of the nervous system, from single neurons to whole brain structures, is the relevant scale from which to measure brain signals to answer these questions?

The brain operates in many paradigms, including at the chemical level of signaling molecules in neurotransmitters and second messenger cascades, at the energetic level of metabolic processes, and at the biophysical level of electromagnetic fields. Since the discovery that the stereotyped discrete electrical signals of action potentials enable inter-neuronal communication, circuit and systems level inquiry in neuroscience has focused on the electrical properties of the brain and how information is conveyed through electrical signals. Even within the electromagnetic framework, measurements can range from the single neuron level to the whole brain, providing completely different viewpoints of the same external event or experimental paradigm. The body of work presented here spans multiple scales of measurement from local field potential recordings to the large-scale electrical activity of the whole human brain.

Although we are ideally interested in better understanding the human brain, neuroscience is often conducted in animal models to overcome the limitations of using

human subjects, and because animal models sometimes provide simpler yet homologous systems to their human counterparts. The rat whisker (vibrissa) system is one animal model ideally suited for asking questions about sensorimotor processing. The vibrissa system is a well-characterized system with discrete, topographical representation of individual whiskers through multiple levels of the nervous system, providing an experimental preparation in which it is relatively easy to record from functionally identifiable neurons. Moreover, the vibrissa system of rats is an active sensory motor system where the whiskers are actively moved to explore the environment, called "whisking behavior." This lends itself to questions about how sensory information and movement information can be integrated and/or segregated, allowing the rat to gain an accurate model of its environment and make quick decisions to navigate, identify food sources, and avoid predators.

Human measurements are typically restricted to non-invasive whole-brain imaging techniques that bear the challenges of limited spatial and/or temporal resolution. Invasive electrical measurements of the human brain, with improved spatial resolution, are possible in the cases of focal refractory epilepsy patients who are undergoing neurosurgical evaluation. We use intracranial measurements from epilepsy patients who performed a visually-cued finger movement task to understand the nature of electrical signals that allow a complex sensory motor action like this to occur. We analyze signals spectrally, examining oscillations in a linear systems approach and specifically using independent component analysis (ICA) to aid the interpretation of these signals.

The work described in Chapter II uses a behavioral paradigm to test coding strategies within the rat vibrissa system. We report results that answer the question of

whether and how the rat can locate the position of objects in space relative to body position. Chapter III uses a salient, widespread oscillation associated with movements in rats (the theta rhythm), to determine whether this signal might drive whisking behavior. Chapter IV measures the electrical signals directly from the human brain of epilepsy patients who performed a sensorimotor task, and determine the brain signals associated with the movement. Specifically, we use independent component analysis to separate pathological brain signals from motor signals and to decompose intracranial signals into its underlying sources.

The themes linking this work are electrophysiological measurements of sensorimotor processing and oscillations as a neural code. The overarching questions this work addresses at a lower level are: 1) what is the neural code of sensorimotor processing, and 2) how do brain oscillations encode sensory information and motor movements? In this first chapter, a body of neuroscience literature is presented to provide the necessary context of the dissertation research. I will first discuss techniques for measuring the electrical activity of the brain and the trade-offs between the different methods. Next, I will present the taxonomy of brain oscillations measured at the level of field potentials and discuss the functional meaning of each type of oscillation as revealed by the work of other researchers. Finally, I will discuss the issues of sensorimotor processing and compare the rat vibrissa system to the primate somatomotor system.

1.1 Scales of Measurement for Electrophysiology

Spikes

The action potential is the smallest functional unit of information processing by neurons for inter-neuronal communication. Action potentials are stereotyped changes in the potential difference across the membrane of axons, generated by the flow of ions through voltage-gated channels (Cole 1939). Action potentials can be recorded either intracellularly, by inserting typically glass pipette electrodes into the cytoplasm of neurons (Becker 1959), or extracellularly, with the use of metal microelectrodes (Davies 1956; Hubel 1959). Action potentials are an "all-or-nothing" physiological event resulting in large voltage changes when a threshold is exceeded, and can be conceptualized as a digital signal called a "spike." Therefore, the only information carried by the spike of a single neuron is the time of occurrence.

Spikes ("action currents") were first observed in recordings of the sciatic nerve in a frog leg, using a string galvanometer (Forbes 1920). Building upon this work, Liddell and Sherrington (Liddell 1924) demonstrated that the firing rate of "action currents" was modified according to the amount of stretch on the muscle. It thereafter became standard practice to sum the number of spikes that occur over a time window and average over repeated trials to create a histogram, or probability density, representing the firing rate of a neuron. This representation of stimulus features by the firing rate of the neuron became known as a "rate code." A common feature of a rate code is cosine tuning, wherein stimuli that vary continuously along some parameter are represented by variable firing rates.

In subsequent studies over the next few decades, it was discovered that the firing rate of action potentials is selective for specific stimulus features. A classic example is the center-surround receptive field of retinal ganglia in frogs (Barlow 1953) and cats (Kuffler 1953), of the lateral geniculate nucleus of cats (Hubel 1960), and of the cat visual cortex (Hubel and Wiesel 1959). Neurons with center-surround receptive fields fire maximally in response to a light circle surrounded by a dark ring, or a dark circle surrounded by a light ring. Subsequent studies demonstrated that complex features could be represented by a combination of lower features. For example, a bar of light can be modeled by an array of center-surround stimuli. Neurons in "later" stages of the nervous system, along the afferent pathway, were found to respond to increasingly complex stimuli.

The concept of receptive fields was then extended to the spatial dimension in cortical mapping studies. In the earliest example, the cat visual cortex was found to be organized topographically and functionally, based on receptive fields (Mountcastle 1955; Mountcastle 1957). It is now known that spatially organized cortical maps based on receptive fields are ubiquitous in the nervous system (Kaas 1997), existing in every sensory system, as well as in the cortical representation of basic motor movements. For example, the specialized rat vibrissa somatosensory system is represented in topographic cortical maps called whisker "barrels" (Woolsey and Van der Loos 1970). In the motor system, topographically arranged single units are responsive to two-dimensional arm movements (Georgopoulos, Kalaska et al. 1982).

A paradigm shift in the interpretation of single unit activity took place when researchers demonstrated in a variety of brain areas that the precise timing of spikes

carries more information than the firing rate, and could in fact be an encoding strategy used by the nervous system. For example, single units in the frontal cortex of a monkey fire in repeatable complex patterns when responding to behavioral task conditions (Abeles, Bergman et al. 1993). In the hippocampus of a rat, the precise timing of place cells carry information about the rat's location in space (O'Keefe and Recce 1993). Additionally, rat neocortical cells fire with sub-millisecond precision in response to noisy stimuli (Mainen and Sejnowski 1995).

With the move toward quantifying spike timing came a shift in the direction of measuring multiple single units to look for a neural code based on the joint activity of multiple neurons. Vaadia and colleagues (Vaadia, Haalman et al. 1995) extended the work of Abeles to demonstrate that the pattern of correlations among the precise firing patterns of single units in the frontal cortex of monkeys carried information about the behavioral task. In area MT of the monkey visual system, two single units located in spatially discontiguous areas of cortex, but with overlapping receptive fields, engaged in synchronous activity when responding to a single moving bar stimulus (Singer, Kreiter et al. 1996). Directional tuning of the motor units described above was found to be better decoded based on the firing rates of a population of neurons than the firing rates of single units (Georgopoulos, Schwartz et al. 1986).

Technological advances in the 1980s enabled researchers to record simultaneously from populations of single neurons using multi-electrode arrays (Kruger 1983; Nicolelis and Ribeiro 2002). These advances pointed the quest for the neural code toward population codes. Numerous research studies demonstrated that a population of neurons can decode information about the environment or behavior of an animal. For

example, the activity of an ensemble of place cells accurately predicts the spatial location of the rat (Wilson and McNaughton 1993). Furthermore, information about visual stimuli can be decoded by the synchrony among populations of neuron in all levels of the visual system, from the retina to the extra-striate cortex (Usrey and Reid 1999).

Recording spikes was instrumental for generating the fundamental concepts of rate coding, feature selectivity, and cortical mapping (Rieke 1997). As with any data acquisition methodology, however, there are technical challenges associated with single unit recordings. Separating the signal from background noise to obtain "clean" recordings, spike sorting (Schmidt 1984; Lewicki 1998), and the problem of spike classification (Fee, Mitra et al. 1996; Lewicki 1998) are a few examples. The single neuron approach nonetheless is advantageous for characterizing the precise relationship between a stimulus with parameterized properties and the output of a neuron in a pattern of spikes. One disadvantage of the approach is the limited spatial sampling of neural tissue in an organ with approximately 10^{12} neurons. To extrapolate how brain systems represent information and communicate based on recordings from such a small number of neurons is nearly impossible. Further, the approach of recording from one neuron fails to shed light on how neurons are connected into circuits, and how information might be encoded at the circuit level.

Local field potentials

Local field potentials (LFP) are the measurement of the electric fields generated by the currents of tens of thousands of neurons. The neural activity giving rise to these electric field measurements are believed to be the summation of dendro-somatic inputs,

as well as intrinsic currents from the transmembrane movement of ions through voltage-gated channels. The voltage differences between the intracracellular and extracellular space are distributed non-uniformly through different regions of a neuron, giving rise to current sources and sinks and producing the equivalent of small current dipoles. The size of the dipole generated is largely dependent upon the geometry of the neurons. For any particular neuron, a strong current dipole will result when the soma and dendrites are oriented in opposing directions. When the arbors of dendrites extend radially, the potential differences between the soma and dendrites tend to cancel each other out, producing a small net potential. The superposition of the current dipoles from an entire population of neurons creates the overall electric field, measured in LFP recordings as the voltage difference between two points in extracellular space. LFP recordings are biased toward detecting the ensemble activity of neurons arranged in a dipolar configuration with dendritic processes of populations of neurons aligned in parallel.

LFP recordings are made with electrodes implanted into the extracellular matrix between neurons. Essentially, LFP recordings measure slow oscillations relative to the sharp voltage changes of action potentials. Analysis of LFP recordings is typically performed by spectral decomposition of the signals and examination of relative power changes that occur in alignment with behavioral events. Changes in LFP amplitude can result from the recruitment of a different size population of neurons, or from changes in the degree of synchrony of post-synaptic potentials among a fixed number of neurons. Due to the flow of current through the volume conductor of the brain, LFP recordings can include the contribution of neural activity at some distance from the recording electrode. Current source density measurements based on a minimum of three electrodes and their

second spatial derivative is one technique for isolating focal neural activity proximal to the electrode array, and for more directly measuring the neurobiological generator (transmembrane currents) for which LFP is only an indirect measure (Pitts 1952; Nicholson and Freeman 1975; Mitzdorf 1985).

The advantages of local field potential recordings over spikes are that they: represent the activity over a larger population of neurons; are less technically challenging to record; and lack the issues associated with spike sorting. The disadvantage is that the average activity over a population of neurons is difficult to interpret. LFP activity is not necessarily local to the recording electrode, and some amount of information is missing from the recording due to cancellation of signals. The use of broadband filter settings to record simultaneous spikes and action potentials, and then separate the two types of signals offline, is one approach that circumvents making tradeoffs between spikes and LFPs.

Intracranial EEG

Intracranial EEG (iEEG) records electric fields produced by the same biophysical mechanisms as LFPs, but are based upon a larger population of neurons. Intracranial signals are recorded from surgically implanted subdural arrays or intraparyenchmal depth probes, typically 1-cm spaced electrodes with ~1-10 mm^2 surface area.

Intracranial recordings face the same inherent limitations of local field potentials. The electric field produced by the superposition of current dipoles biases the recording toward the contribution from neurons with their somae in teh same layers and with parallel dendrites in cortex, typically the apical dendrites of pyramidal neurons. In

addition, dipoles in opposing directions, either from oppositely oriented neurons or from folding of cortical tissue, cancel each other out, rending a significant fraction of neuronal activity absent from these measurements. Furthermore, the location of current sources that contribute to an intracranially recorded field can be at a distance from the recording electrode, but if local activity is not canceled out, the local activity likely dominates. Locality of current sources can be estimated as proximal to the electrodes in cases where the voltage gradients demonstrate a double polarity reversal, or when voltage gradients drop off steeply in neighboring electrodes (Halgren 2004). Because fields closest to the electrodes and with parallel oriented dendrites dominate the recordings, intracranial recordings are biased toward the activity of layers I and II of cortex.

Estimating the recording volume of intracranial electrodes is difficult, but a generally agreed upon order-of-magnitude approximation is a 10 mm^3 volume, encompassing approximately one million neurons. Correlation and coherence analyses of pair-wise electrodes have been used to estimate the spatial resolution of intracranial recordings. Bullock and McClune et al. (Bullock, McClune et al. 1995) report that at frequencies up to 60 Hz, coherence falls off significantly with 10 mm distances between electrodes, based on intracranial recordings two minutes in length. Menon et al. (Menon, Freeman et al. 1996) found that correlations of activity between electrode pairs during recordings of about five seconds dropped off significantly at approximately 1 cm distances. Spatial patterns based on phase relationships were found to drop off from 2 to 50 mm distances (Freeman, Holmes et al. 2006).

Despite the challenges described above, intracranial recordings are nonetheless considered to be the "gold standard" of human electrophysiology. This is because of the

sub-millisecond temporal resolution of recordings (limited only by the sampling rate of the data acquisition system), and better spatial resolution than non-invasive methods such as electroencelphalogram (EEG) and functional magnetic resonance imaging (fMRI). The use of intracranial recordings in humans was pioneered by Herbert Jasper and Wilder Penfield for the localization of seizure foci in epilepsy patients (Jasper & Penfield, 1949), and continues to serve as the standard practice for verifying the location of the epileptogenic zone (Engel and Crandall 1987; Luders, Awad et al. 1992), and for the localization of current sources estimated from magnetoencephalogram (MEG) and electrode encelphalogram (EEG) recordings (Lachaux, Rudrauf et al. 2003; Halgren 2004). Intracranial recordings are used to stimulate the brain in functional mapping studies, designed to identify brain regions involved in critical language, motor, and sensory function, to avoid these areas during surgical excision of the epileptogenic region (Engel 1996). This brain mapping technique is used today for the same purpose. The use of intracranial recordings has now been extended to cognitive neuroscience studies (Lachaux, Rudrauf et al. 2003; Engel, Moll et al. 2005) of language (Ojemann, Fried et al. 1989; Ojemann 1999), memory (Cameron, Yashar et al. 2001; Howard, Rizzuto et al. 2003), motor activity (Arroyo, Lesser et al. 1993; Crone, Miglioretti et al. 1998; Crone, Miglioretti et al. 1998), visually guided behaviors (Klopp, Marinkovic et al. 2001), face recognition (Halgren, Baudena et al. 1994; Halgren, Baudena et al. 1994; Klopp, Halgren et al. 1999), spatial cognition (Kahana, Caplan et al. 1999), attention (Ray, Niebur et al. 2008), and visual imagery (Kreiman, Koch et al. 2000; Kreiman 2002).

Electroencelphalogram

Electroencephalography (EEG), pioneered by Hans Berger in 1929, is the recording of the brain's electric fields with electrodes on the scalp (Berger 1929). EEG recordings have been used extensively for clinical applications including identifying stages of sleep, monitoring depth of anesthesia, monitoring seizures, diagnosing neurological disorders, and measuring propagation through sensory pathways using sensory-evoked potentials (Niedermeyer 1999). EEG has also been utilized for studying a wide range of cognitive and perceptual processes including motor activity, spatial tasks, verbal tasks, mathematical computations, short-term memory, memory encoding, and selective attention (Nunez 2006).

Like local field potential measurements and intracranial EEG, scalp EEG measures the electrical field produced by neurons at the population scale. Current dipoles produced by synchronous activity in neurons with parallel oriented fibers sum linearly to produce macroscopic fields. A gross approximation of the minimum volume of tissue that must be synchronous to produce a field detectable on the scalp is 6 cm^2 of cortical gyrus tissue, containing approximately 60 million neurons (Cooper, Winter et al. 1965; Ebersole 1997; Nunez 2006). Neuronal activity from non-parallel fibers, asynchronous activity, and oppositely oriented dipoles that cancel each other out, all fail to contribute to the signals recorded by EEG. EEG signals are of lower amplitude than intracranial signals due to attenuation by passage through the cerebral spinal fluid, skull, and scalp (Cooper, Winter et al. 1965). The skull also distorts the electric field (Hamalainen 1993).

The problem of localizing sources is challenging with subdurally recorded iEEG (also known as electrocorticography, or ECoG) because there are an infinite number of

configurations of current sources that can produce a particular pattern of electrical activity at the level of sensors. Solutions to the "inverse problem," of localizing current sources based on an observed pattern of electrical activity, require accurate head models for estimating the forward propagation of electric fields. Early forward models were based on a head volume conductor modeled as three concentric spheres representing the brain, scalp, and skull (Ary, Klein et al. 1981; de Munck 1988; Mosher, Leahy et al. 1999). Over the past few decades, spherical models have been replaced by realistic head models that take into account the irregular, non-spherical shape of the skull and its inhomogeneities due to variable thickness and from holes such as the eye sockets. A common solution for the forward problem is the boundary element method (BEM) where the volume conductor is decomposed into a mesh, and volume conduction is treated as isotropic and homogeneous in a piece-wise manner (Baillet 2001). Finite element models (FEM) have been developed to take into account anisotropies due to white matter tracts and irregularities in head morphology due to features such as the sinus cavities (Wolters, Kuhn et al. 2002). The inverse problem, because it does not have a unique solution, requires assumptions about the nature and numbers of sources. Typically, the comparison between a forward solution for a set of model sources and the recorded field is made and then iterated upon. A common assumption for current sources is the equivalent dipole model, in which the best fit is found for a dipole's position, orientation, and time function, to describe a particular field pattern.

The historically classic method of interpreting EEG signals is based on event-related potentials (ERPs), which are the average potential changes triggered by repeated presentations of the same stimulus. Interpretation of brain activity based on event-related

potentials is limited due to the fact that multiple underlying sources can generate what appears to be a single phenomenon when measured on the scalp. For example, the classic "P300" signal on the scalp in response to oddball stimuli is comprised of a combination of modality-specific sensory processing in association cortex, an attention-orienting signal in fronto-parietal-cingular cortices, and a ventro-tempero-frontal and hippocampal signal for gating contextual information (Halgren 2008).

The underlying model for the generation of ERPs is that the evoked activity has a fixed phase relationship with respect to the stimulus, and that averaging the evoked voltage over repeated trials improves the signal to noise ratio. "Noise" is defined as background voltage changes that vary from trial to trial. Because some stimuli produce changes in the amplitude of signals without necessarily changing the phase (for example, a decrease in the alpha rhythm in response to eyes opening), the ERP model is incomplete. Furthermore, there is a debate about whether ERP signals represent neuronal activity of spatially stationary dipoles at fixed latency to the triggering event among background electroencephalographic oscillations (evoked model), or whether they represent the partial phase synchronization of the ongoing EEG (oscillatory model). Note that these two models are not mutually exclusive and ERPs could arise from the combination of these two processes. Many researchers have looked to the spectral domain to better elucidate underlying mechanisms.

Computations that have been used extensively and which to some degree have replaced ERP measurements, are event-related desynchronizations (ERD) (Pfurtscheller and Aranibar 1977) and event-related synchronizations (ERS) (Pfurtscheller 1992). ERD

and ERS measurements are spectral power changes in specific frequency bands, over a time period triggered by the event of interest, relative to the power in that frequency band during some baseline period that typically precedes the trial. The terms "desynchronization" and "synchronization" are somewhat misleading because power decreases and increases can result from changes in the amount of phase locking within a population of neurons, or alternatively can result from changes in amplitude from changes in the numbers of neuronal sources participating. ERD/ERS measures therefore fail to disambiguate the evoked model from the oscillatory model because coherence measurements confound these two possibilities. Measures of phase-locking (Lachaux, Rodriguez et al. 1999; Le Van Quyen 2001)**,** when used in conjunction with coherence, can in some cases disambiguate these underlying mechanisms to explain observed event-related power increases and decreases. When there is an increase in phase-locking but not in spectral power in response to an event, then the underlying mechanism is likely to be phase resetting of oscillations. When there is an increase in both phase-locking and spectral power, then the interpretation is ambiguous because an event-triggered (time-locked) increase in neural activity can create a phase-locked response that is not necessarily a result of phase resetting of ongoing oscillations. A salient example of where the underlying causes of a classical event-related potential (ERP) signal were disambiguated was highlighted in the work of Makeig and colleagues (Makeig 2002). Through spectral and inter-trial coherence analysis of event-locked single trials, the "N100" average ERP signal, a sudden negative peak at 100 to 150 msec after presentation of visual stimuli, was shown to be attributed to partial phase resetting of alpha oscillations (Makeig 2002). In similar analyses, the decrement of the N100 signal

in response to attended auditory stimuli was accounted for by partial phase-resetting of oscillations, while the N100 response to unattended auditory stimuli was explained by both time-locked amplitude changes and partial phase-resetting (Fuentemilla, Marco-Pallares et al. 2006). Event-related potentials and phase coherence computations are nonetheless insufficient for clarifying the underlying source distribution of signals measured on the scalp. For example, the generators of the N10 0 and alpha rhythm appear similar on the scalp although the underlying phenomena are two completely different mechanisms that overlap temporally and spectrally.

Independent component analysis (ICA) is one data analysis technique that has been applied to EEG signals and has helped elucidate the nature of underlying sources (Bell and Sejnowski 1995; Makeig, AnlloVento et al. 1996). Makeig and colleagues (Makeig 2002) used ICA to decompose EEG data into independent components and found that many independent components had scalp patterns consistent with single equivalent dipole patterns and temporal dynamics corresponding to different aspects of a selective visual attention task. Since this seminal work, ICA has been used to separate brain sources in a variety of behavioral and cognitive experiments including studies of working memory (Onton, Delorme et al. 2005), processing of novel "oddball" sensory stimuli (Debener, Makeig et al. 2005), and separate of epileptic seizure data from non-seizure data (Nam, Yim et al. 2002), among others. The ICA algorithm will be described in further detail in Chapter IV.

The Problem of Multiple Scales

Most neurophysiology studies are based on the application of a single technique and are therefore biased toward the spatial and temporal resolution of that particular method. Each methodology offers its own advantages and disadvantages, and from each level of inquiry we can find relationships between brain activity and behavioral events, cognitive events, or external stimuli. The debate about the most appropriate scale or method with which to take measurements is perhaps not as critical as the question of how we can understand the relationships between neuroscience results obtained at vastly different scales of measurement.

Spike density measures and local field potentials are expected to be related because LFPs primarily capture a summation of input activity to neurons while spikes are a measure of neuronal outputs. Nonetheless, since the earliest neuronal recordings, the relationship between spikes and field potentials has not been obvious by inspection. Li and Jasper (Li and Jasper 1953) comment on the cat hippocampal recordings of Renshaw et al. (Renshaw 1940) that, "There seemed to be no clear relationship between the slow wave oscillations and the unitary spike potentials obtained from the pyramidal cells."

Simultaneous recordings of spikes and LFP are ideally suited to elucidate the relationships between these two types of signals. A consistent result from many research studies is that the gamma frequency band is the spectral band in which relationships between spikes and LFPs occur. A classic example is the recordings of Gray and Singer (Gray and Singer 1989) from the cat visual cortex. LFP oscillations and spiking activity was expressed at 40 Hz within a single orientation column of visual cortex during the presentation of a moving bar of light with ideal orientation, velocity, and direction of movement for the receptive field of the neurons. Spikes occurred during the negative

phase of the LFP oscillation. However, during spontaneous conditions without a stimulus, LFPs were large amplitude fluctuations in the 1-10 Hz frequency band and de-coupled to spikes. In another example, simultaneously recorded single units and LFPs from the macaque parietal cortex during a saccade-based working memory task were coherent in the gamma frequency band but not at lower frequencies (Pesaran, Pezaris et al. 2002). Recordings from the medial temporal lobe of humans show that both single units and the gamma power of LFP signals can be selective to semantic categories, but in these particular recordings there was little overlap between the spike-selective and LFP-selective electrodes (Kraskov, Quiroga et al. 2007). Similarly, recordings from human auditory cortex demonstrated high trial-to-trial variability between spiking and gamma LFP (Nir, Fisch et al. 2007). These two human studies just described, involved the presentation of complex stimuli and recordings from neurons with undetermined receptive fields, as compared to the cat and monkey studies described above.

Concurrent LFP recordings from microwires and field recordings from traditional intracranial macro-electrodes have been acquired from the human brain in a recent investigation of human seizure activity. This study by Worrell et al. (Worrell, Gardner et al. 2008) demonstrates that macro-electrodes filter out super high frequencies above the ripple band (> 250 Hz), while microwire recordings are inclusive of both the ripple band and fast-ripple band (Worrell, Gardner et al. 2008). These results lend supporting evidence to the hypothesis that oscillations in the very high frequency bands are generated by highly localized, sub-millimeter scale neuronal assemblies.

There are a small number of studies that attempt to describe the relationship between intracranial EEG and scalp EEG through simultaneous recordings. Abraham and

Marsan (Abraham and Marsan 1958) examined concurrent scalp and intracranial recordings of epileptic paroxysmal discharges and noted that only some fraction of intracranial signals can be detected on scalp EEG channels, that the size of cortical tissue within which epileptic events is related to whether they will appear on the scalp, and that the ratio of intracranial to scalp EEG amplitudes varies widely. In an early study by Cooper and Winter et al. (Cooper, Winter et al. 1965), simultaneous EEG and subdural intracranial recordings similarly demonstrated that scalp EEG signals are not merely an attenuation of large amplitude cortical activity, that the appearance of scalp EEG signals is likely due to widespread synchronous activity in the brain, and that intracranial signals can have markedly different characteristics from one electrode to its neighboring electrode at only a millimeter of distance. In follow-up work ten years later, Pfurtscheller and Cooper (Pfurtscheller and Cooper 1975) reported that beta range frequencies are attenuated in scalp recordings as compared to cortical recordings as a result of phase cancellation. Very little work has been done with simultaneous intracranial and scalp EEG over the past three decades, likely because it became standard clinical practice to record from scalp EEG prior to the implantation of intracranial electrodes and to remove large sections of scalp during intracranial monitoring. Nonetheless, the data presented in Chapter IV of this dissertation are from concurrently recorded scalp and intracranial EEG. Independent component analysis of concurrently recorded iEEG and EEG demonstrates that sources from ICA decomposition include a wide range of sources: those that project predominantly to the implanted electrode array and minimally to scalp EEG, sources that project to both implanted and scalp electrodes, and sources that

predominant project to the scalp montage (Whitmer, Worrell et al. 2007; Whitmer, Lee et al. 2008; Whitmer, Worrell et al. 2008).

To summarize thus far, the methodologies for studying the relationships between brain and behavior from an electrophysiological perspective range from recordings of the action potentials of single neurons to the average electrical field generated over the entire brain. The advantage of studying single neurons is that we understand the precise biophysical mechanism of the measurement being made. Single unit studies, however, have the challenge of extrapolating to larger populations of neurons based on such sparse sampling. At the opposite end of the spectrum, EEG recordings of the whole brain blur together many different underlying processes and fail to detect fields produced by many current sources due to cancellation of dipoles. Acquisition of intracranial recordings at an intermediate spatial scale is limited to clinical settings and clinical criteria for determining the numbers and placement of electrodes. A critical research direction in neuroscience will be to understand the relationships between these different scales of measurement. The work that follows spans the range from local field potentials in rat hippocampus to widespread oscillations over square centimeters of human cerebral cortex.

1.2. Mammalian Brain Rhythms

Oscillations in the brain have been apparent since the earliest EEG recordings, when Hans Berger noted a prominent 10 Hz rhythm in EEG recordings (Berger 1929). Since that time, electroencephalographic signals have been classified into a standardized set of frequency bands as follows: delta: < 4 Hz, theta: 4-8 Hz, alpha: 8-12 Hz, beta: 13-25 Hz, and gamma: above 25 Hz. It is worth exploring each of these rhythms in detail as background for later thesis chapters that discuss results from signals in all of these frequency bands.

Alpha (8-12 Hz)

The alpha rhythm, a widespread 10 Hz oscillation, was the most salient oscillatory signal observed in the first EEG recordings by Hans Berger (1929). This spontaneous oscillation is apparent over occipital cortex during the subject's resting state with eyes closed and is attenuated or blocked with eyes opening and/or during attention and mental effort (Niedermeyer 1999). During drowsiness at the onset of sleep, the alpha rhythm is replaced by low voltage slow activity, a phenomenon known as "alpha dropout" (Niedermeyer 1999). Alpha has been shown to represent an idling rhythm of the brain (Adrian 1934), with some evidence of its role as a thalamic pacemaker (Bishop 1936; Andersen 1968). In the past couple of decades, a resurgence of research on the alpha rhythm have demonstrated that alpha is not merely a unitary process. A variety of studies have demonstrated that alpha is a set of distributed dynamical processes in overlapping frequency bands, with a multiplicity of functions and different topographical manifestations (Nunez 1995; Klimesch 1999; Nunez, Wingeier et al. 2001). To

summarize a large body of work, changes in an alpha rhythm have been associated with memory (Basar 1992; Klimesch 1997; Klimesch, Doppelmayr et al. 1997; Schurmann and Basar 2001; Slotnick, Moo et al. 2002), sensory processing (Basar 1992; Schurmann and Basar 2001), attention (Klimesch, Doppelmayr et al. 1998; Palva 2007), mental calculations (Shaw 1999; Palva, Palva et al. 2005), conscious perception (Palva 2007), and movement (Pfurtscheller and Aranibar 1980; Pfurtscheller and Neuper 1992; Crone, Miglioretti et al. 1998; Babiloni 1999). The movement-related aspect of alpha is a special rhythm called the "mu rhythm" During some of the earliest EEG recordings (Jasper 1949), this salient 10 Hz oscillation was apparent over rolandic cortex and would disappear during voluntary movement and tactile stimulation. The movement-induced cessation of mu rhythm, called "mu blocking," (Pfurtscheller 1981; Pfurtscheller and Neuper 1994) is a robust phenomenon observed with EEG, MEG, and intracranial EEG, during movements of the tongue, hand, arm, leg, and foot (Pfurtscheller, Neuper et al. 1997). The mu rhythm will be discussed in further detail in Section 1.4 of this chapter and in Chapter IV.

Beta (13-25 Hz)

The beta rhythm, an oscillatory signal between 13 Hz and 25 Hz, was identified by Hans Berger at the same time that he first observed the alpha rhythm. Like alpha oscillations, beta range oscillations also contribute spectrally to the mu rhythm (Pfurtscheller 1981; Pfurtscheller and Neuper 1994; Crone, Miglioretti et al. 1998). Beta power decreases are therefore associated with tactile stimulation (Jasper 1938; Pfurtscheller, Krausz et al. 2001), with movement (Jasper & Penfield, 1949), and with

imagined movement (Pfurtscheller et al., 2005). A rebound (increase) in beta has been shown to follow movements (Pfurtscheller, Stancak et al. 1996; Pfurtscheller, Zalaudek et al. 1998; Pfurtscheller, Woertz et al. 2003; Pfurtscheller, Neuper et al. 2005).

The extent beta's role in sensorimotor processing is made evident by coherence calculations. Numerous studies demonstrate that beta band (~20 Hz) oscillations in motor cortex are coherent with contralateral muscle activity although alpha (~10 Hz) oscillations are not (Baker 2003). This had encouraged researchers to propose that beta oscillations represent a cortical state that allows for maintenance of ongoing motor activity (Gilbertson, Lalo et al. 2005). However, beta is not merely a motor signal. Beta oscillations in primary somatosensory cortex and posterior parietal cortex are stronger than those in primary motor cortex (Witham and Baker 2007). Furthermore, beta oscillations in sensory cortex are coherent with motor cortex (Witham, Wang et al. 2007). A variety of experimental results (reviewed in (Baker 2008) suggest the possibility that beta plays a role in providing sensory afference information to the motor system.

There is evidence to suggest that the functional role of beta extends beyond its relationship with sensorimotor processing. For example, EEG studies demonstrate a consistent hemispheric asymmetry in beta oscillations in response to emotional and cognitive processes (Ray and Cole 1985). During a face recognition paradigm, the amplitude of beta oscillations on frontal electrodes was higher during the recognition of a familiar face as compared to an unfamiliar face (Ozgoren, Basar-Eroglu et al. 2005). A recent study demonstrated multi-focal beta band oscillations in prefrontal and posterior cortical areas concomitant with a state of expectation-based attention (Basile 2007). Finally, beta oscillations have been implicated in semantic processing. Von Stein and

colleagues (von Stein 1999) reported beta band synchronization between neighboring temporal and parietal cortex during multi-modal semantic processing of objects conveyed as either spoken words, written words, or pictures.

Gamma (Above 25 Hz)

It is well established that fast cortical oscillations in the gamma band represent ensembles of synchronously firing neurons. The earliest observation of what came to be known as "gamma," was 30-40 Hz waves in the olfactory bulb of the hedgehog in response to olfactory stimuli (Adrian 1942). Measurements of gamma oscillations during olfaction were subsequently repeated in the rat, cat, and rabbit (Freeman 1959; Freeman 1975; Bressler and Freeman 1980), setting a precedent for gamma as a hypothesized mechanism for sensory representation. Seminal experiments on the cat visual system demonstrated that spikes burst at a gamma rate and that synchronous gamma band firing in visual cortex represents specific features of visual stimuli (Eckhorn, Bauer et al. 1988; Gray, Konig et al. 1989; Gray and Singer 1989). Recent studies using intracranial depth probes have explored a gamma response to more complex visual stimuli than the classical moving bars of early experiments. Event-related increases in gamma power were observed in response to faces in the fusiform gyrus (Klopp, Halgren et al. 1999; Lachaux, George et al. 2005), ventrolateral prefrontal (Klopp, Halgren et al. 1999), along with the lateral occipital gyrus and intraparietal sulcus (Lachaux, George et al. 2005).

Widespread, diffuse gamma band oscillations are also apparent in response to sensory stimuli with EEG recordings. Transient low (~40 Hz) gamma responses can be seen in response to auditory stimuli (Galambos, Makeig et al. 1981; Pantev 1995), flashes

of light (Pantev 1995), and evoked somatosensory responses from stimulation of the medial nerve (Pantev 1995).

In addition to encoding stimulus features, gamma band oscillations play a role in attention, both at the level of single units and at the level of wide scale brain signals EEG recordings. Single unit studies show that cortical neurons activated by attended visual stimuli fire with increased gamma frequency synchronization as compared to those activated by unattended stimuli (Fries, Reynolds et al. 2001; Treue 2001). Single units from secondary somatosensory cortex demonstrate increased synchrony in response to somatosensory attention (Steinmetz, Roy et al. 2000). Additionally, gamma band EEG oscillations between parietal and prefrontal areas are transiently phase-locked in a somatic attention task (Desmedt and Tomberg 1994). Gamma oscillations are observed in frontal and central areas in response to attention to auditory stimuli (Tiitinen, Sinkkonen et al. 1993) and in frontal areas in response to a specific percept in from an ambiguous (multistable) visual stimulus (Basar-Eroglu, Struber et al. 1996). A clever EEG study by Tallon-Baudry, Betrand et al. (Tallon-Baudry, Bertrand et al. 1997) disambiguated perceptual binding of features ("bottom-up processing") from attentional mechanisms ("top-down processing") and demonstrated that both of these processes were demonstrably modulated by changes in gamma power, but at different latencies with respect to the time of stimulus presentation. Von Stein and Sarnthein (von Stein and Sarnthein 2000) demonstrated that, in the case of visual processing, power changes in the gamma band of EEG in response to visual stimuli of moving bars, results from an increase in coherence (a phase code) rather than an increased in the active population of neurons (an amplitude code).

There is convergent evidence from single neurons in primates, human intracranial EEG, and human scalp EEG, that gamma oscillations play a role in memory. Sustained gamma synchronization occurs in frontal regions during the maintenance period of a working memory paradigm, both for spatial working memory (Pesaran, Pezaris et al. 2002) and visual working memory (Tallon-Baudry, Bertrand et al. 1998; Howard, Rizzuto et al. 2003). Gamma has also been associated with long-term memory. For example, the degree of gamma synchrony between hippocampal and rhinal cortical areas (Fell, Klaver et al. 2001) and over wide spread cortical areas (Sederberg, Kahana et al. 2003) predict the successful encoding of long-term memory. Premotor cortex also shows differential gamma band activation to identical stimuli that elicit either a spatial attention/working memory task or a motor planning task (Brovelli, Lachaux et al. 2005).

To summarize the role of gamma, oscillations in this band are associated with the representation of sensory features, attention, and both short and long-term memory. The precise relationship between populations of units, and large-scale EEG, is not yet understood, but both exhibit changes in gamma frequency associated with cognitive and perceptual processing.

Theta (4-8 Hz)

The theta rhythm, a 4-8 Hz oscillation, is the most salient oscillatory signal in the rat brain, predominantly apparent in the hippocampus during voluntary motor behaviors including locomotion, swimming, orienting, and sniffing (Green and Arduini 1954; Vanderwolf 1969; Vanderwolf and Robinson 1981). Hippocampal theta has been classified into two types: type 1 which occurs during movement, and type 2 with a

slightly lower spectral peak that occurs during immobile but alert animals presented with sensory stimuli (Bland 1985; Bland 1986). Chapter III of this dissertation will explore the role of theta in the whisker movements of the rat vibrissa system.

In addition to its role in motor behaviors, the theta rhythm has been associated with learning, spatial cognition. Place cells are single units in the rat hippocampus that fire when a rat enters a specific location within an environment (O'Keefe and Dostrovsky 1971; O'Keefe 1976). The theta rhythm has been found to define an envelope at which the bursting of place cells is modulated (O'Keefe and Recce 1993). Furthermore, the phase of the theta cycle at which an individual neuron fires shifts earlier as rats traverse the place field (O'Keefe and Recce 1993).Theta has been associated with learning at the fundamental cellular level of Hebbian plasticity. Long-term potentiation (LTP) is preferentially induced at theta frequency (Greenstein, Pavlides et al. 1988), and hippocampal cells are sensitive to the phase of the theta cycle, with LTP more likely to occur during the peak and long-term depression (LTD) more likely during a theta trough (Hoschler, Anwyl et al. 1997).

The relationships between hippocampal theta recorded as local field potentials in the rat, and widespread cortical theta recorded from the scalp of humans, are not very well understood, although both seem to play a role in cognitive processing. In both rats and humans, there is strong evidence that the theta rhythm plays a key role in working memory. In the rat, hippocampal theta becomes phase-locked to stimuli in working memory condition but not in a control condition, although the baseline level of theta activity is the equivalent across conditions (Givens 1996). In the human, frontal midline theta increases in power with increased working memory load (Gevins, Smith et al.

1997), and an increase in theta power is associated with the encoding of new information for subsequent memory retrieval (Klimesch 1999). Additionally, theta oscillations in non-hippocampal areas of cortex in human intracranial EEG have exhibited task dependence during maze navigation (Kahana, Sekuler et al. 1999). Furthermore, episodic memory is associated with synchronization in the theta band; an increase in theta power at the time of word presentation was predictive of later performance in recall (Klimesch, Schimke et al. 1994; Klimesch, Doppelmayr et al. 1996). Researchers speculate that hippocampal-neocortical feedback loops might provide a mechanism for hippocampal to induce scalp-recordable theta oscillations (Klimesch 1996). Researchers also propose a "gating" role for theta for processing non-spatial working memory. Intracranial recordings during a verbal memory task demonstrate that theta oscillates increase in amplitude at multiple locations through the duration of a trial, suggesting that theta might help organize working memory (Raghavachari, Kahana et al. 2001).

Delta (< 4 Hz)

Finally, we consider the delta rhythm, which is the lowest frequency band observed with field potential recordings. Delta band oscillations, occurring from 1 Hz to 4 Hz, have primarily been associated with slow wave sleep during stages 3 and 4 of deep sleep, prominent over anterior regions. There is also evidence of an increase in delta activity during the performance of short-term memory tasks and mental calculations (Vogel, Broverman et al. 1968; Harmony, Fernandez et al. 1996), in addition to in response to an auditory oddball paradigm (Basar-Eroglu, Basar et al. 1992).

Delta band activity can also be seen in pathological brain signals. Frontal intermittent rhythmic delta activity (FIRDA) is an example of a clinically defined, non-specific, pathological rhythm seen in EEG recordings (Niedermeyer 1999; Niedermeyer 2003). FIRDA is associated with a variety of conditions including toxic, metabolic, neurodegenerative, inflammatory, traumatic, vascular, and neoplastic disorders, and will be explored further in Chapter IV of this work. Temporal intermittent rhythmic delta activity (TIRDA) is another pathological signal in the delta band, but with more clinical diagnostic power than FIRDA. TIRDA is associated with epilepsy and can help lateralize/localize the epileptogenic zone (Gennaro 2003).

Role of oscillations

To summarize this section, brain oscillations are apparent in a wide range of frequency bands from less than 1 Hz to the upper limits of physiological recordings based on sampling frequency and play a fundamental role in the "neural code." Slower oscillations (delta through beta) are a result of dynamic large-scale synchronous activity, whereas gamma band oscillations are correlated with the firing rate of individual neurons. In the theta through gamma bands, oscillations in many cases represent the "bottom-up" encoding of sensory stimulus features (Eckhorn, Bauer et al. 1988; Gray and Singer 1989). On the other end of the cognitive spectrum, oscillations have been shown to represent "top-down" processing, for example by providing a mechanism for attention (Lakatos, Karmos et al. 2008) and expectation (Engel, Fries et al. 2001). Bottom-up and top-down processing are not mutually exclusive, but likely work in concert within the same task (Tallon-Baudry, Bertrand et al. 1997; Karakas, Basar-Eroglu et al. 2001).

A fundamental open question in the neuroscience of consciousness is how different features of a single object are combined for the experience of a single percept. The synchrony of oscillations representing the individual features has been hypothesized as a fundamental mechanism to enable feature binding (Singer 1994; Buzsaki and Chrobak 1995; Singer and Gray 1995; Engel, Roelfsema et al. 1997; Singer 1999; Engel and Singer 2001). A similar hypothesis of Fries (Fries 2005) proposes that neuronal communication is enabled through dynamic coherently oscillating neuronal groups. Fries hypothesizes that synchrony allows for time windows within which communication can occur within a particular subset of neurons within a population.

Finally, recent research findings have uncovered evidence that the role of some oscillations is to modulate other oscillations. Functional relationships exist between oscillations in different frequency bands on a task-driven basis (Palva, Palva et al. 2005; Lakatos, Karmos et al. 2008). For example, the phase of theta oscillations can modulate gamma power on a basis of a word recognition working memory task (Mormann, Fell et al. 2005), a language-related auditory target detection task (Canolty, Edwards et al. 2006), and in recall of long-term memories (Lisman and Buzsaki 2008).

1.3. Review of Rat Vibrissa System

The rat vibrissa system is a model system for studying sensorimotor processing because of its simple and well-described organization relative to other mammalian sensory systems. The whiskers on the face of the rat form a two-dimensional array of sensors that are represented topographically through each level of the afferent pathway. A single sensory nerve ending wraps around the base of each whisker. These neurons project in a one-to-one arrangement to topographically organized neurons in the brainstem, which project to the thalamus, and finally to sensory cortex within which a cortical whisker "barrel" (patch of cortex) is devoted to each whisker. Because of the preservation of topography and the discrete representation of individual whiskers, the vibrissa system lends itself easily to electrophysiology recordings within functionally connected circuits.

Unlike the whiskers of many mammalian species that behave merely as passive sensors, the rodent vibrissa system is an active sensorimotor system. Rats sweep their whiskers back and forth in a behavior referred to as "whisking," both in air while the animal is exploring its environment and also when the animal makes contact with and palpates objects (Berg and Kleinfeld 2003).

Early behavioral experiments with rats demonstrated the ethological importance of the whisker system. For example, rats are deficient in their ability to path-find through mazes when both their vision and vibrissa systems are lesioned (Vincent 1912). Furthermore, when faced with competing visual and sensory information about the distance to a lower platform in an illusory cliff experiment, tactile information from the vibrissa system overrides visual information (Schiffman, Lore et al. 1970). Rats will

make decisions about crossing a gap in front of them using their vibrissae in the absence of all other sensory cues and only with the complete vibrissa system intact from the whisker to the barrel cortex (Hutson and Masterton 1986). More recent behavioral studies have demonstrated that rats can make judgments about object position not only in the rostral-caudal direction, but also in the medial-lateral direction (Krupa, Matell et al. 2001). Rats can determine the relative distance to walls on the side of its head and discriminate between wide and narrow gaps (Krupa, Matell et al. 2001; Shuler, Krupa et al. 2002).

These experiments suggest a functional role of the vibrissa system to help the animal determine *where* objects are in space and to make decisions based on these assessments. Recent research has uncovered another role of the vibrissa system: to make judgments about *what* stimuli are present in a rat's environment. For example, by using only the microvibrissae on the snout, the rat can differentiate between different shapes and sizes of cookies (Brecht, Preilowski et al. 1997). Rats can also make behavioral choices based on differentiating between textures by touching them with their whiskers (Guic-Robles, Valdivieso et al. 1989; Carvell and Simons 1990).

Both the "where" and the "what" role of the vibrissa raise questions about the coding strategy employed by the nervous system. The work in Chapter 2 of this thesis explores the use of vibrissa for object localization. To localize an object in three-dimensional space relative to the animal's own body, information from three different axes must be made available: the rostral-caudal axis, the medial-lateral axis, and the dorsal-ventral (azimuthal) axis. Location in both the dorsal-ventral direction could in theory be encoding by a "labeled line" code, in which the specific row of whiskers

making contact with the object activates a region in the topographically arranged cortex corresponding to those whiskers. This is also referred to as a "place code" and has been hypothesized to serve as a fundamental coding mechanism within the nervous system in general (Perkel and Bullock 1968) but has not been explicitly tested with behavioral measurements in the rat.

A labeled line code is not a viable strategy for determining the position of objects in the rostral-caudal direction because the whiskers are moving sensors. At least two pieces of information are necessary to disambiguate position in the direction along which the whiskers move. To determine the position of a single object (as opposed to the relative position of two different objects), information about where the whisker is relative to the animal must be made available to the nervous system. Many sensory systems accomplish this standard problem with the use of proprioceptors. Proprioceptors are specialized sensory neurons that convey information about the position of particular muscle relative to the rest of the body. There is currently no evidence for proprioceptors in the rat vibrissa system. A reasonable coding strategy would be for the phase of a whisker oscillation to serve as a reference signal about the whisker's position, which can be compared to the phase or position of the whisker at the time that it makes contact with an object.

At the time that the work in Chapter II was undertaken, it was unknown whether rats could use the motion of their vibrissae to determine the position of objects in the horizontal plane, although there was speculation about the algorithm by which this could be accomplished (Ahissar, Haidarliu et al. 1997; Fee, Mitra et al. 1997; Diamond 2000; Ahissar and Arieli 2001; Ahissar and Kleinfeld 2003) based on evidence for a

"reference" signal in vibrissa cortex (Fee, Mitra et al. 1997) as well as in the trigeminal ganglion which is the first neuron in afferent pathway (Szwed, Bagdasarian et al. 2003). We therefore set out to test the rat's ability to locate objects in the rostral-caudal direction, and to determine whether object localization could be accomplished with a single vibrissa, which would provide strong evidence for a code for object location based on the phase of the whisking cycle.

The motor aspects of the vibrissa system are not as well characterized as the sensory aspects. In Chapter III, we seek to understand a potential oscillatory signal that might drive rhythmic vibrissa movements. It is known that the motor cortex plays a critical role in whisking, and that the local field potentials of primary motor cortex are coherent with whisker movements on a cycle by cycle basis, even in the absence of sensory input (Ahrens and Kleinfeld 2004). However, motor cortex is not critical for whisker movements: decorticated rats still whisk (Welker 1964). There is strong behavioral evidence for a central pattern generator (CPG) in the vibrissa system (Gao, Bermejo et al. 2001), but the location and mechanism of the CPG is not known (Brecht, Grinevich et al. 2006). Researchers speculate that the serotonergic neurons that provide input to the whisking motor neurons in the facial nucleus in the brainstem may provide the pattern generation of whisking (Brecht, Grinevich et al. 2006). Because the rat hippocampus exhibits strong oscillations in the same frequency band as whisking, we will measure the coherence between hippocampal theta and whisking, to test whether the hippocampus plays a role in regulating oscillatory whisking.

1.4. Sensorimotor Processing of Primate Finger Movements

The sensorimotor system of primate hand and finger movements is significantly more complicated than the rat vibrissa system. Whereas whisking movement has two degrees of freedom (amplitude and phase), there are many degrees of freedom in movements of the hand and wrist. Additionally, although there is somatotopic representation of the fingers within sensory cortex, the representation is overlapping and redundant (Hlustik, Solodkin et al. 2001), rather than discrete like the rat vibrissa system. Cortical areas representing individual finger movements in primary motor cortex (M1) are also overlapping (Hlustik, Solodkin et al. 2001) and redundant (Schieber and Hibbard 1993), demonstrated from both single unit recordings from M1 (Schieber and Hibbard 1993) and by fMRI studies (Sanes, Donoghue et al. 1995).

What is the cortical signature of hand and finger movements, and which brain areas are involved? The answers to these questions are largely dependent on the specific type of movement being exerted. Primary motor cortex (M1), supplementary motor cortex (SMA), and primary sensory cortex (S1) all play a role in sequential finger movements (Shibasaki, Sadato et al. 1993), although supplementary motor cortex plays less of a role for simpler tasks in which all the fingers are moved together (Rao, Binder et al. 1993). Self-paced finger movements activate motor areas differently than cued finger movements do. Some premotor neurons are responsive only before cued movements and but not before self-paced finger movements (Rao, Binder et al. 1993). Additionally, SMA neurons show earlier responses to self-paced movements than to triggered movements (Okano and Tanji 1987). Grasping movements have specialized circuitry within motor cortex (Fogassi, Gallese et al. 2001; Culham, Danckert et al. 2004). For example, single

unit studies demonstrate that area F5 of ventral premotor cortex has neurons that are responsive to specific finger configurations necessary to facilitate grasping behavior (Rizzolatti, Luppino et al. 1988). Moreover, a different population of neurons within the M1 hand area is activated for a "power grip" than is activated for fine control of fingertips (Napier 1980).

The specific areas of the brain associated with an actively versus passively moved hand are different. Studies by Mima and colleagues (Mima, Sadato et al. 1999) demonstrate that active movement is associated with activation of primary sensorimotor cortex, premotor cortex, supplementary motor area (SMA), secondary somatosensory areas, basal ganglia, and cerebellum. By contrast, only primary and secondary somatosensory areas are activated by passive hand movements (Mountcastle, Lynch et al. 1975; Mima, Sadato et al. 1999).

The cortical dynamics associated with hand and finger movements vary with the scale of measurement. However, single unite studies from primates and EEG studies from humans converge with regard to the frequency bands in which movement-related oscillations occur. Primate LFP measurements during visually guided wrist and digit movements demonstrated that oscillations in the beta and gamma (15-50 Hz) of primary motor areas and premotor areas play a fundamental role (Sanes and Donoghue 1993). In this study, oscillations were synchronous between primary and premotor recording sites, preceded movements suggestive, and ceased during movements, suggestive of a movement preparatory signal (Sanes and Donoghue 1993).

As mentioned earlier in this chapter, the mu rhythm is a central EEG rhythm first described by Japser & Penfield (1938) as a "precentral alpha rhythm," and then more

specifically defined by its temporal features of a sharp, spiky negative phase followed by a rounded positive phase, by Gastaut (Gastaut 1952). The cessation of the mu rhythm during movements, "mu blocking," is its most salient characteristic. Spectral decomposition reveals components in both the alpha and beta frequency bands, and there is evidence that the beta component arises from motor cortex while the alphoid component is attributed to sensory cortex (Salmelin and Hari 1994).

The spectral manifestation of the mu rhythm have been described as event-related desynchronization (ERDs), purportedly due to a phase resetting of ongoing brain oscillations (Pfurtscheller and Aranibar 1977), and have been demonstrated in the 8-12 Hz alpha band (Pfurtscheller, Aranibar et al. 1980) and subsequently in the beta (12-28 Hz) frequency band (Pfurtscheller 1981) during repeated manual squeezing of a rubber ball. Alpha and beta power decreases locked to movement are a robust phenomenon observed during rhythmic hand contractions (Arroyo, Lesser et al. 1993), sustained muscle contractions (Crone, Miglioretti et al. 1998; Crone, Miglioretti et al. 1998), self-paced finger movements (Ohara, Ikeda et al. 2000), cued finger movements (Pfurtscheller and Neuper 1997; Klopp, Marinkovic et al. 2001), and complex visuomotor tasks of the hand (Aoki, Fetz et al. 1999). An absence of event-related potentials (ERP) (Klopp, Marinkovic et al. 2001) and an absence of inter-trial coherence suggest that mu-related power decreases reflect time-locked but not phase-locked signal changes.

The observation of gamma power increases in the 40 Hz band concomitant with finger movement was first observed in scalp EEG over primary sensorimotor cortex (Pfurtscheller, Neuper et al. 1993). Subsequent studies performed at higher sampling rates demonstrate power increases in the gamma band up to 200 Hz during movement,

that event-locked spectral changes in higher frequency bands are more focal than that of the alpha and beta frequency bands (Crone, Miglioretti et al. 1998; Crone, Sinai et al. 2006; Miller, Leuthardt et al. 2007), and that gamma power increases occur over primary but not supplementary motor areas (Ohara, Ikeda et al. 2000).

The rat vibrissa and primate hand sensorimotor systems are markedly different. Although motor cortex plays the pivotal role in driving whisker movements, whisking behavior is predominantly driven by a central pattern generator. As a result, the mystacial pad muscles are innervated by the facial motor nucleus of the brainstem in addition to direct connections from motor cortex. The muscles involved in finger and hand movements are innervated directly by motor cortex; therefore, the lesioning of M1 results in severe motor impairments for the voluntary movements of the hand and fingers.

Despite these differences, the same sets of issues associated with any sensorimotor system pertain to both the rodent vibrissa system and primate hand movements. A primary issues that researchers strive to resolve is the question of how sensory input from active movements can be differentiated from passive sources. In the primate hand and finger sensory motor system, proprioceptors convey kinesthetic information about the relative positions and movements of limbs to the central nervous system. Chapter II addresses this question for the rat vibrissa system indirectly by examining decision-making in rats from sensory cues during whisker movements. A quest of researchers is to determine the cortical signals necessary and sufficient for movement. Chapters III and IV address this question in two different model systems. Chapter III specifically asks whether the theta rhythm of the rat hippocampus is necessary to drive exploratory whisking. Chapter IV strives to parse out the source

signals underlying cortical dynamics seen at the sensor level during human finger movements.

REFERENCES

1. Abeles, M., H. Bergman, et al. (1993). "Spatiotemporal firing patterns in the frontal cortex of behaving monkeys." J Neurophysiol **70**(4): 1629-38.

2. Abraham, K. and C. A. Marsan (1958). "Patterns of cortical discharges and their relation to routine scalp electroencephalography." Electroencephalogr Clin Neurophysiol **10**(3): 447-61.

3. Adrian, E. D. (1942). "Olfactory reactions in the brain of the hedgehog." J Physiol **100**: 459-473.

4. Adrian, E. D. a. M. B. H. C. (1934). "The Berger rhythm: potential changes from the occipital lobes in man." Brain **57**: 355-385.

5. Ahissar, E. and A. Arieli (2001). "Figuring space by time." Neuron **32**(2): 185-201.

6. Ahissar, E., S. Haidarliu, et al. (1997). "Decoding temporally encoded sensory input by cortical oscillations and thalamic phase comparators." Proc Natl Acad Sci U S A **94**(21): 11633-8.

7. Ahissar, E. and D. Kleinfeld (2003). "Closed-loop neuronal computations: focus on vibrissa somatosensation in rat." Cereb Cortex **13**(1): 53-62.

8. Ahrens, K. F. and D. Kleinfeld (2004). "Current flow in vibrissa motor cortex can phase-lock with exploratory rhythmic whisking in rat." J Neurophysiol **92**(3): 1700-7.

9. Andersen, P. a. A., S.A. (1968). Physiological basis of the alpha rhythm. New York, Appleton-Century-Crofts.

10. Aoki, F., E. E. Fetz, et al. (1999). "Increased gamma-range activity in human sensorimotor cortex during performance of visuomotor tasks." Clin Neurophysiol **110**(3): 524-37.

11. Arroyo, S., R. P. Lesser, et al. (1993). "Functional significance of the mu rhythm of human cortex: an electrophysiologic study with subdural electrodes." Electroencephalogr Clin Neurophysiol **87**(3): 76-87.

12. Ary, J.P., S.A. Klein, et al., (1981). "Location of sources of evoked scalp potentials: corrections for skull and scalp thicknesses." IEEE Trans Biomed Eng 28(6): 446-52.

13. Babiloni, C., Carducci, F., Cincotti, F., Rossini, P.M., Neuper, C., Pfurtscheller, G.,

14. Babiloni, F. (1999). "Human movement-related potentials vs desynchronization of EEG alpha rhythm: a high-resolution EEG study." Neuroimage **10**(6): 658-665.

15. Baillet, S., Mosher, J.C., Leahy, R.M. (2001). "Electromagnetic brain mapping." Signal Processing Magazine, IEEE **18**(6).

16. Baker, S. N. (2008). "Oscillatory interactions between sensorimotor cortex and the periphery." Current Opinion in Neurobiology **17**(6): 649-655.

17. Baker, S. N., Pinches, E.M., Lemon, R.N. (2003). "Synchronization in monkey motor cortex during a precision grip task. II. effect of oscillatory activity on corticospinal output." J Neurophysiol **89**(4): 1941-1953.

18. Barlow, H. B. (1953). "Action potentials from the frog's retina." J Physiol **119**(1): 58-68.

19. Basar, E., Basar-Eroglu, C., Parnefjord, R., Rahn, E. and Schurmann, M. (1992). Evoked potentials: ensembles of brain induced rhythmicities in the alpha, theta and gamma ranges. Induced Rhythms in the Brain. E. a. B. Basar, T.H. Boston, Birkhauser.

20. Basar-Eroglu, C., E. Basar, et al. (1992). "P300-response: possible psychophysiological correlates in delta and theta frequency channels. A review." Int J Psychophysiol **13**(2): 161-79.

21. Basar-Eroglu, C., D. Struber, et al. (1996). "Frontal gamma-band enhancement during multistable visual perception." Int J Psychophysiol **24**(1-2): 113-25.

22. Basile, L. F. (2007). "Complex, multifocal, individual-specific attention-related cortical functional circuits." Biol Res **40**(4): 451-70.

23. Becker, M. C., Frank, K., and Nelson, P.G. (1959). Preparation and testing of microelectrodes. Handbook used in Laboratory of Neurophysiology, National Institutes of Health.

24. Bell, A. J. and T. J. Sejnowski (1995). "An information-maximization approach to blind separation and blind deconvolution." Neural Comput **7**(6): 1129-59.

25. Berg, R. W. and D. Kleinfeld (2003). "Rhythmic whisking by rat: retraction as well as protraction of the vibrissae is under active muscular control." J Neurophysiol **89**(1): 104-17.

26. Berger, H. (1929). "Uber das Elektrenkephalogram des Menschen." Arch Psychiat. Nervenkr. **87**: 527-570.

27. Bishop, G. H., O'Leary, J. (1936). "Component of the electrical response of the optic cortex of the rabbit." American Journal of Physiology **117**: 292-308.

28. Bland, B. H. (1985). Behavioral correlates and afferent control of hippocampal theta cell discharges. Electrical Activity of the Archicortex. G. a. V. Buzsaki, C.H. Budapest, Akademiai Kiado**:** 125-142.

29. Bland, B. H. (1986). "The physiology and pharmacology of hippocampal formation theta rhythms." Prog Neurobiol **26**: 1-54.

30. Brecht, M., V. Grinevich, et al. (2006). "Cellular mechanisms of motor control in the vibrissal system." Pflugers Arch **453**(3): 269-81.

31. Brecht, M., B. Preilowski, et al. (1997). "Functional architecture of the mystacial vibrissae." Behav Brain Res **84**(1-2): 81-97.

32. Bressler, S. L. and W. J. Freeman (1980). "Frequency analysis of olfactory system EEG in cat, rabbit, and rat." Electroencephalogr Clin Neurophysiol **50**(1-2): 19-24.

33. Brovelli, A., J. P. Lachaux, et al. (2005). "High gamma frequency oscillatory activity dissociates attention from intention in the human premotor cortex." Neuroimage **28**(1): 154-64.

34. Bullock, T. H., M. C. McClune, et al. (1995). "EEG coherence has structure in the millimeter domain: subdural and hippocampal recordings from epileptic patients." Electroencephalogr Clin Neurophysiol **95**(3): 161-77.

35. Buzsaki, G. and J. J. Chrobak (1995). "Temporal structure in spatially organized neuronal ensembles: a role for interneuronal networks." Curr Opin Neurobiol **5**(4): 504-10.

36. Cameron, K. A., S. Yashar, et al. (2001). "Human hippocampal neurons predict how well word pairs will be remembered." Neuron **30**(1): 289-98.

37. Canolty, R. T., E. Edwards, et al. (2006). "High gamma power is phase-locked to theta oscillations in human neocortex." Science **313**(5793): 1626-8.

38. Carvell, G. E. and D. J. Simons (1990). "Biometric analyses of vibrissal tactile discrimination in the rat." J Neurosci **10**(8): 2638-48.

39. Cole, K. S. a. C., H.J. (1939). "Electric impedance of the squid giant axon during activity." J. Gen. Physiol. **22**: 649-670.

40. Cooper, R., A. L. Winter, et al. (1965). "Comparison of Subcortical, Cortical and Scalp Activity Using Chronically Indwelling Electrodes in Man." Electroencephalogr Clin Neurophysiol **18**: 217-28.

41. Crone, N. E., D. L. Miglioretti, et al. (1998). "Functional mapping of human sensorimotor cortex with electrocorticographic spectral analysis. II. Event-related synchronization in the gamma band." Brain **121 (Pt 12)**: 2301-15.

42. Crone, N. E., D. L. Miglioretti, et al. (1998). "Functional mapping of human sensorimotor cortex with electrocorticographic spectral analysis. I. Alpha and beta event-related desynchronization." Brain **121 (Pt 12)**: 2271-99.

43. Crone, N. E., A. Sinai, et al. (2006). "High-frequency gamma oscillations and human brain mapping with electrocorticography." Prog Brain Res **159**: 275-95.

44. Culham, J. C., S. L. Danckert, et al. (2004). "Visually guided grasping produces fMRI activation in dorsal but not ventral stream brain areas." Exp Brain Res. **153**(2): 180-189.

45. Davies, P. W. (1956). "Chamber for microelectrode studies in the cerebral cortex." Science **124**(3213): 179-80.

46. de Munck, J. C. (1988). "The potential distribution in a layered anisotropic spheroidal volume conductor." Journal of Applied Physics **64**: 464.

47. Debener, S., S. Makeig, et al. (2005). "What is novel in the novelty oddball paradigm? Functional significance of the novelty P3 event-related potential as revealed by independent component analysis." Brain Res Cogn Brain Res **22**(3): 309-21.

48. Desmedt, J. E. and C. Tomberg (1994). "Transient phase-locking of 40 Hz electrical oscillations in prefrontal and parietal human cortex reflects the process of conscious somatic perception." Neurosci Lett **168**(1-2): 126-9.

49. Diamond, M. E. (2000). "Neurobiology: Parallel sensing." Nature **406**: 245-247.

50. Ebersole, J. S. (1997). "Defining epileptogenic foci: past, present, future." J Clin Neurophysiol **14**(6): 470-83.

51. Eckhorn, R., R. Bauer, et al. (1988). "Coherent oscillations: a mechanism of feature linking in the visual cortex? Multiple electrode and correlation analyses in the cat." Biol Cybern **60**(2): 121-30.

52. Engel, A. K., P. Fries, et al. (2001). "Dynamic predictions: oscillations and synchrony in top-down processing." Nat Rev Neurosci **2**(10): 704-16.

53. Engel, A. K., C. K. Moll, et al. (2005). "Invasive recordings from the human brain: clinical insights and beyond." Nat Rev Neurosci **6**(1): 35-47.

54. Engel, A. K., P. R. Roelfsema, et al. (1997). "Role of the temporal domain for response selection and perceptual binding." Cereb Cortex **7**(6): 571-82.

55. Engel, A. K. and W. Singer (2001). "Temporal binding and the neural correlates of sensory awareness." Trends Cogn Sci **5**(1): 16-25.

56. Engel, J. (1996). "Surgery for Seizures." New England Journal of Medicine **334**(10): 647-653.

57. Engel, J., Jr. and P. H. Crandall (1987). "Intensive neurodiagnostic monitoring with intracranial electrodes." Adv Neurol **46**: 85-106.

58. Fee, M. S., P. P. Mitra, et al. (1996). "Automatic sorting of multiple unit neuronal signals in the presence of anisotropic and non-Gaussian variability." J Neurosci Methods **69**(2): 175-88.

59. Fee, M. S., P. P. Mitra, et al. (1997). "Central versus peripheral determinants of patterned spike activity in rat vibrissa cortex during whisking." J Neurophysiol **78**(2): 1144-9.

60. Fell, J., P. Klaver, et al. (2001). "Human memory formation is accompanied by rhinal-hippocampal coupling and decoupling." Nat Neurosci **4**(12): 1259-64.

61. Fogassi, L., V. Gallese, et al. (2001). "Cortical mechanism for the visual guidance of hand grasping movements in the monkey: a reversible in activation study." Brain **124**(3): 571-586.

62. Forbes, A. a. T., C (1920). "Amplification of action currents with the electron tube in recording with the string galvanometer." American Journal of Physiology **52**(3): 409-471.

63. Freeman, W. J. (1959). "Distribution in time and space of prepyriform electrical activity." J Neurophysiol **22**: 644-65.

64. Freeman, W. J. (1975). Mass Action in the Nervous System. New York, Academic Press.

65. Freeman, W. J., M. D. Holmes, et al. (2006). "Fine spatiotemporal structure of phase in human intracranial EEG." Clin Neurophysiol **117**(6): 1228-43.

66. Fries, P. (2005). "A mechanism for cognitive dynamics: neuronal communication through neuronal coherence." Trends Cogn Sci **9**(10): 474-80.

67. Fries, P., J. H. Reynolds, et al. (2001). "Modulation of oscillatory neuronal synchronization by selective visual attention." Science **291**(5508): 1560-3.

68. Fuentemilla, L., J. Marco-Pallares, et al. (2006). "Modulation of spectral power and of phase resetting of EEG contributes differentially to the generation of auditory event-related potentials." Neuroimage **30**(3): 909-16.

69. Galambos, R., S. Makeig, et al. (1981). "A 40-Hz auditory potential recorded from the human scalp." Proc Natl Acad Sci U S A **78**(4): 2643-7.

70. Gao, P., R. Bermejo, et al. (2001). "Whisker deafferentation and rodent whisking patterns: behavioral evidence for a central pattern generator." J Neurosci **21**(14): 5374-80.

71. Gastaut, H. (1952). "Etude electrocorticographique de la reactivite des rythmes rolandiques." Rev. Neurol. **87**: 176-743.

72. Gennaro, D. (2003). "Localizing significance of temporal intermittent rhythmic delta activity (TIRDA) in drug-resistant focal epilepsy." Clinical Neurophysiology **114**(1): 70-78.

73. Georgopoulos, A. P., J. F. Kalaska, et al. (1982). "On the relations between the direction of two-dimensional arm movements and cell discharge in primate motor cortex." J Neurosci **2**(11): 1527-37.

74. Georgopoulos, A. P., A. B. Schwartz, et al. (1986). "Neuronal population coding of movement direction." Science **233**(4771): 1416-9.

75. Gevins, A., M. E. Smith, et al. (1997). "High-resolution EEG mapping of cortical activation related to working memory: effects of task difficulty, type of processing, and practice." Cereb Cortex **7**(4): 374-85.

76. Gilbertson, T., E. Lalo, et al. (2005). "Existing motor state is favored at the expense of new movement during 13-35 Hz oscillatory synchrony in the human corticospinal system." J Neurosci **25**(34): 7771-9.

77. Givens, B. (1996). "Stimulus-evoked resetting of the dentate theta rhythm: relation to working memory." Neuroreport **8**(1): 159-63.

78. Gray, C. M., P. Konig, et al. (1989). "Oscillatory responses in cat visual cortex exhibit inter-columnar synchronization which reflects global stimulus properties." Nature **338**(6213): 334-7.

79. Gray, C. M. and W. Singer (1989). "Stimulus-specific neuronal oscillations in orientation columns of cat visual cortex." Proc Natl Acad Sci U S A **86**(5): 1698-702.

80. Green, J. D. and A. A. Arduini (1954). "Hippocampal electrical activity in arousal." J Neurophysiol **17**(6): 533-57.

81. Greenstein, Y. J., C. Pavlides, et al. (1988). "Long-term potentiation in the dentate gyrus is preferentially induced at theta rhythm periodicity." Brain Res **438**(1-2): 331-4.

82. Guic-Robles, E., C. Valdivieso, et al. (1989). "Rats can learn a roughness discrimination using only their vibrissal system." Behav Brain Res **31**(3): 285-9.

83. Halgren, E. (2004). "How can intracranial recordings assist MEG source localization?" Neurol Clin Neurophysiol **2004**: 86.

84. Halgren, E. (2008). Brain states measured as the P3, Multimodal Imaging Laboratory, UC San Diego.

85. Halgren, E., P. Baudena, et al. (1994). "Spatio-temporal stages in face and word processing. 2. Depth-recorded potentials in the human frontal and Rolandic cortices." J Physiol Paris **88**(1): 51-80.

86. Halgren, E., P. Baudena, et al. (1994). "Spatio-temporal stages in face and word processing. I. Depth-recorded potentials in the human occipital, temporal and parietal lobes [corrected]." J Physiol Paris **88**(1): 1-50.

87. Hamalainen, M., Hari, R., Ilmoniemi, R.J., Knuutila, J., Lounasmaa, O.V. (1993). Review of Modern Physics **65**: 413-497.

88. Harmony, T., T. Fernandez, et al. (1996). "EEG delta activity: an indicator of attention to internal processing during performance of mental tasks." Int J Psychophysiol **24**(1-2): 161-71.

89. Hlustik, P., A. Solodkin, et al. (2001). "Somototopy in human primary motor and somatosensory hand representations revisited." Cereb Cortex **11**(4): 312-321.

90. Hoschler, C., R. Anwyl, et al. (1997). "Stimulation on the positive phase of hippocampal theta rhythm induces long-term potentiation that can be depotentiated by stimulation on the negative phase in area CA1 in vivo." J Neurosci **17**: 6470-6477.

91. Howard, M. W., D. S. Rizzuto, et al. (2003). "Gamma oscillations correlate with working memory load in humans." Cereb Cortex **13**(12): 1369-74.

92. Hubel, D. H. (1959). "Single unit activity in striate cortex of unrestrained cats." J Physiol **147**: 226-38.

93. Hubel, D. H. (1960). "Single unit activity in lateral geniculate body and optic tract of unrestrained cats." J Physiol **150**: 91-104.

94. Hubel, D. H. and T. N. Wiesel (1959). "Receptive fields of single neurones in the cat's striate cortex." J Physiol **148**: 574-91.

95. Hutson, K. A. and R. B. Masterton (1986). "The sensory contribution of a single vibrissa's cortical barrel." J Neurophysiol **56**: 1196-1222.

96. Jasper, H. a. P., W (1949). "Electrocorticograms in man: effect of voluntary movement upon the electrical activity of the precentral gyrus." Arch f Psychiatr Nervenk **183**: 162-174.

97. Jasper, H. H. a. A., H.L. (1938). "Brain potentials and voluntary muscle activity in man." J Neurophysiol **1**: 87-100.

98. Kaas, J. H. (1997). "Topographic maps are fundamental to sensory processing." Brain Res Bull **44**(2): 107-12.

99. Kahana, M. J., J. B. Caplan, et al. (1999). "Using intracranial recordings to study thetaResponse to J. O'Keefe and N. Burgess (1999)." Trends Cogn Sci **3**(11): 406-407.

100. Kahana, M. J., R. Sekuler, et al. (1999). "Human theta oscillations exhibit task dependence during virtual maze navigation." Nature **399**(6738): 781-4.

101. Karakas, S., C. Basar-Eroglu, et al. (2001). "Gamma response of the brain: a multifunctional oscillation that represents bottom-up with top-down processing." International Journal of Psychophysiology **39**(2-3): 137-150.

102.Klimesch, W. (1996). "Memory processes, brain oscillations and EEG synchronization." Int J Psychophysiol **24**(1-2): 61-100.

103. Klimesch, W. (1997). "EEG-alpha rhythms and memory processes." Int J Psychophysiol **26**(1-3): 319-40.

104. Klimesch, W. (1999). "EEG alpha and theta oscillations reflect cognitive and memory performance: a review and analysis." Brain Res Brain Res Rev **29**(2-3): 169-95.

105.Klimesch, W., M. Doppelmayr, et al. (1997). "Brain oscillations and human memory: EEG correlates in the upper alpha and theta band." Neurosci Lett **238**(1-2): 9-12.

106. Klimesch, W., M. Doppelmayr, et al. (1996). "Theta band power in the human scalp EEG and the encoding of new information." Neuroreport **7**(7): 1235-40.

107. Klimesch, W., M. Doppelmayr, et al. (1998). "Induced alpha band power changes in the human EEG and attention." Neurosci Lett **244**(2): 73-6.

108. Klimesch, W., H. Schimke, et al. (1994). "Episodic and semantic memory: an analysis in the EEG theta and alpha band." Electroencephalogr Clin Neurophysiol **91**(6): 428-41.

109. Klopp, J., E. Halgren, et al. (1999). "Face-selective spectral changes in the human fusiform gyrus." Clin Neurophysiol **110**(4): 676-82.

110. Klopp, J., K. Marinkovic, et al. (2001). "Timing and localization of movement-related spectral changes in the human peri-Rolandic cortex: intracranial recordings." Neuroimage **14**(2): 391-405.

111. Kraskov, A., R. Q. Quiroga, et al. (2007). "Local field potentials and spikes in the human medial temporal lobe are selective to image category." J Cogn Neurosci **19**(3): 479-92.

112. Kreiman, G., Fried, I. & Koch, C. (2002). "Single-neuron correlates of subjective vision in the human medial temporal lobe." Proc Natl Acad Sci U S A **99**: 8378-8383.

113. Kreiman, G., C. Koch, et al. (2000). "Category-specific visual responses of single neurons in the human medial temporal lobe." Nat Neurosci **3**(9): 946-53.

114. Kruger, J. (1983). "Simultaneous individual recordings from many cerebral neurons: techniques and results." Rev Physiol Biochem Pharmacol **98**: 177-233.

115. Krupa, D. J., M. S. Matell, et al. (2001). "Behavioral properties of the trigeminal somatosensory system in rats performing whisker-dependent tactile discriminations." J Neurosci **21**(15): 5752-63.

116. Kuffler, S. W. (1953). "Discharge patterns and functional organization of mammalian retina." J Neurophysiol **16**(1): 37-68.

117. Lachaux, J. P., N. George, et al. (2005). "The many faces of the gamma band response to complex visual stimuli." Neuroimage **25**(2): 491-501.

118. Lachaux, J. P., E. Rodriguez, et al. (1999). "Measuring phase synchrony in brain signals." Hum Brain Mapp **8**(4): 194-208.

119. Lachaux, J. P., D. Rudrauf, et al. (2003). "Intracranial EEG and human brain mapping." J Physiol Paris **97**(4-6): 613-28.

120. Lakatos, P., G. Karmos, et al. (2008). "Entrainment of neuronal oscillations as a mechanism of attentional selection." Science **320**(5872): 110-113.

121. Le Van Quyen, M., Foucher, J., Lachaux, J-P., Rodriguez, E., Lutz, A., Martinerie, J., Varela, F.J. (2001). "Comparison of Hilbert transform and wavelet methods for the analysis of neuronal synchrony." Journal of Neuroscience Methods **111**(2): 83-98.

122. Lewicki, M. S. (1998). "A review of methods for spike sorting: the detection and classification of neural action potentials." Network: Computation in Neural Systems **9**: R53-R78.

123. Li, C. L. and H. Jasper (1953). "Microelectrode studies of the electrical activity of the cerebral cortex in the cat." J Physiol **121**(1): 117-40.

124. Liddell, E. G. T. a. S., C. (1924). "Reflexes in response to stretch (myotactic reflexes)." Proceedings of the Royal Society of London. Series B, Containing Papers of a Biological Character **96**(675): 212-242.

125. Lisman, J. and G. Buzsaki (2008). "A neural coding scheme formed by the combined function of gamma and theta oscillations." Schizophr Bull **34**(5): 974-80.

126. Lopes da Silva, F. H. (1973). "Organization of thalamic and cortical alpha rhythms: spectra and coherences." Electroencephalogr Clin Neurophysiol **35**: 626-639.

127. Luders, H., I. Awad, et al. (1992). "Subdural electrodes in the presurgical evaluation for surgery of epilepsy." Epilepsy Res Suppl **5**: 147-56.

128. Mainen, Z. F. and T. J. Sejnowski (1995). "Reliability of spike timing in neocortical neurons." Science **268**(5216): 1503-6.

129. Makeig, S. (2002). "Dynamic brain sources of visual evoked responses (vol 295, pg 690, 2002)." Science **295**(5559): 1466-1466.

130. Makeig, S., L. AnlloVento, et al. (1996). "Independent component analysis of event-related potentials during a selective attention task." Psychophysiology **33**: S58-S58.

131. Menon, V., W. J. Freeman, et al. (1996). "Spatio-temporal correlations in human gamma band electrocorticograms." Electroencephalogr Clin Neurophysiol **98**(2): 89-102.

132. Miller, K. J., E. C. Leuthardt, et al. (2007). "Spectral changes in cortical surface potentials during motor movement." J Neurosci **27**(9): 2424-32.

133. Mima, T., N. Sadato, et al. (1999). "Brain structures related to active and passive finger movements in man." Brain **122 (Pt 10)**: 1989-97.

134. Mitzdorf, U. (1985). "Current source-density method and application in cat cerebral cortex: investigation of evoked potentials and EEG phenomena." Physiol Rev **65**(1): 37-100.

135. Mormann, F., J. Fell, et al. (2005). "Phase/amplitude reset and theta-gamma interaction in the human medial temporal lobe during a continuous word recognition memory task." Hippocampus **15**(7): 890-900.

136. Mosher, J. C., R. M. Leahy, et al. (1999). "EEG and MEG: forward solutions for inverse methods." IEEE Trans Biomed Eng **46**(3): 245-59.

137. Mountcastle, V. B. (1957). "Modality and topographic properties of single neurons of cat's somatic sensory cortex." J Neurophysiol **20**(4): 408-34.

138. Mountcastle, V. B., Berman, A.L., Davies, P.W. (1955). "Topographic organization and modality representation in first somatic area of cat's cerebral cortex by method of single unit analysis." American Journal of Physiology **183**: 646.

139. Mountcastle, V. B., J. C. Lynch, et al. (1975). "Posterior parietal association cortex of the monkey: command functions for operations within extrapersonal space." J Neurophysiol **38**(4): 871-908.

140. Nam, H., T. G. Yim, et al. (2002). "Independent component analysis of ictal EEG in medial temporal lobe epilepsy." Epilepsia **43**(2): 160-4.

141. Napier, J. R. (1980). Hands. London, George Allen & Unwin.

142. Nicholson, C. and J. A. Freeman (1975). "Theory of current source-density analysis and determination of conductivity tensor for anuran cerebellum." J Neurophysiol **38**(2): 356-68.

143. Nicolelis, M. A. and S. Ribeiro (2002). "Multielectrode recordings: the next steps." Curr Opin Neurobiol **12**(5): 602-6.

144. Niedermeyer, E. (2003). "The clinical relevance of EEG interpretation." Clin Electroencephalogr **34**(3): 93-8.

145. Niedermeyer, E. a. L. D. S., F. (1999). Electroencephalography: Basic principles, clinical applications, and related fields. Baltimore, Williams & Wilkins.

146. Nir, Y., L. Fisch, et al. (2007). "Coupling between neuronal firing rate, gamma LFP, and BOLD fMRI is related to interneuronal correlations." Curr Biol **17**(15): 1275-85.

147. Nunez, P. L. (1995). Neocortical Dynamics and Human EEG Rhythms. New York, Oxford University Press.

148. Nunez, P. L., Srinivasan, R. (2006). Electric Fields of the Brain: The Neurophysics of EEG. New York, Oxford University Press.

149. Nunez, P. L., B. M. Wingeier, et al. (2001). "Spatial-temporal structures of human alpha rhythms: theory, microcurrent sources, multiscale measurements, and global binding of local networks." Hum Brain Mapp **13**(3): 125-64.

150. O'Keefe, J. (1976). "Place units in the hippocampus of the freely moving rat." Exp Neurol **51**(1): 78-109.

151. O'Keefe, J. and J. Dostrovsky (1971). "The hippocampus as a spatial map. Preliminary evidence from unit activity in the freely-moving rat." Brain Res **34**(1): 171-5.

152. O'Keefe, J. and M. L. Recce (1993). "Phase relationship between hippocampal place units and the EEG theta rhythm." Hippocampus **3**(3): 317-30.

153. Ohara, S., A. Ikeda, et al. (2000). "Movement-related change of electrocorticographic activity in human supplementary motor area proper." Brain **123 (Pt 6)**: 1203-15.

154. Ojemann, G. A., I. Fried, et al. (1989). "Electrocorticographic (ECoG) correlates of language. I. Desynchronization in temporal language cortex during object naming." Electroencephalogr Clin Neurophysiol **73**(5): 453-63.

155. Ojemann, G. a. S.-M., J. (1999). "Activity of neurons in human temporal cortex during identification and memory for names and words." Journal of Neuroscience **19**: 5674-5682.

156. Okano, K. and J. Tanji (1987). "Neuronal activities in the primate motor fields of the agranular frontal cortex preceding visually triggered and self-paced movement." Experimental Brain Research **66**(1): 1432-1106.

157. Onton, J., A. Delorme, et al. (2005). "Frontal midline EEG dynamics during working memory." Neuroimage **27**(2): 341-56.

158. Ozgoren, M., C. Basar-Eroglu, et al. (2005). "Beta oscillations in face recognition." Int J Psychophysiol **55**(1): 51-9.

159. Palva, J. M., S. Palva, et al. (2005). "Phase synchrony among neuronal oscillations in the human cortex." J Neurosci **25**(15): 3962-72.

160. Palva, S. a. P., J.M. (2007). "New vistas for alpha-frequency band oscillations." Trends in Neurosciences **30**(4): 150-158.

161. Pantev, C. (1995). "Evoked and induced gamma-band activity of the human cortex." Brain Topogr **7**(4): 321-30.

162. Perkel, D. H. and T. H. Bullock (1968). "Neural Coding: A Report Based on an NRP Work Session." Neurosciences Research Program Bulletin **6**(3): 221-348.

163. Pesaran, B., J. S. Pezaris, et al. (2002). "Temporal structure in neuronal activity during working memory in macaque parietal cortex." Nature Neuroscience **5**(8): 805-811.

164. Pfurtscheller, G. (1981). "Central beta rhythm during sensorimotor activities in man." Electroencephalogr Clin Neurophysiol **51**(3): 253-64.

165.Pfurtscheller, G. (1992). "Event-related synchronization (ERS): an electrophysiological correlate of cortical areas at rest." Electroencephalogr Clin Neurophysiol **83**(1): 62-9.

166. Pfurtscheller, G. and A. Aranibar (1977). "Event-related cortical desynchronization detected by power measurements of scalp EEG." Electroencephalogr Clin Neurophysiol **42**(6): 817-26.

167. Pfurtscheller, G. and A. Aranibar (1980). "Changes in central EEG activity in relation to voluntary movement. I. Normal subjects." Prog Brain Res **54**: 225-31.

168. Pfurtscheller, G., A. Aranibar, et al. (1980). "Changes in central EEG activity in relation to voluntary movement. II. Hemiplegic patients." Prog Brain Res **54**: 491-5.

169. Pfurtscheller, G. and R. Cooper (1975). "Frequency dependence of the transmission of the EEG from cortex to scalp." Electroencephalogr Clin Neurophysiol **38**(1): 93-6.

170. Pfurtscheller, G., G. Krausz, et al. (2001). "Mechanical stimulation of the fingertip can induce bursts of beta oscillations in sensorimotor areas." J Clin Neurophysiol **18**(6): 559-64.

171.Pfurtscheller, G. and C. Neuper (1992). "Simultaneous EEG 10 Hz desynchronization and 40 Hz synchronization during finger movements." Neuroreport **3**(12): 1057-60.

172. Pfurtscheller, G. and C. Neuper (1994). "Event-related synchronization of mu rhythm in the EEG over the cortical hand area in man." Neurosci Lett **174**(1): 93-6.

173. Pfurtscheller, G. and C. Neuper (1997). "Motor imagery activates primary sensorimotor area in humans." Neurosci Lett **239**(2-3): 65-8.

174. Pfurtscheller, G., C. Neuper, et al. (1997). "Foot and hand area mu rhythms." Int J Psychophysiol **26**(1-3): 121-35

175. Pfurtscheller, G., C. Neuper, et al. (2005). "Beta rebound after different types of motor imagery in man." Neurosci Lett **378**(3): 156-9.

176. Pfurtscheller, G., C. Neuper, et al. (1993). "40-Hz oscillations during motor behavior in man." Neurosci Lett **164**(1-2): 179-82.

177. Pfurtscheller, G., A. Stancak, Jr., et al. (1996). "Post-movement beta synchronization. A correlate of an idling motor area?" Electroencephalogr Clin Neurophysiol **98**(4): 281-93.

178. Pfurtscheller, G., M. Woertz, et al. (2003). "Early onset of post-movement beta electroencephalogram synchronization in the supplementary motor area during self-paced finger movement in man." Neurosci Lett **339**(2): 111-4.

179. Pfurtscheller, G., K. Zalaudek, et al. (1998). "Event-related beta synchronization after wrist, finger and thumb movement." Electroencephalogr Clin Neurophysiol **109**(2): 154-60.

180. Pitts, W. (1952). Investigation on synaptic transmission. Cybernetics, Trans. 9th Conf., New York: Josish Macy Found.

181. Raghavachari, S., M. J. Kahana, et al. (2001). "Gating of human theta oscillations by a working memory task." J Neurosci **21**(9): 3175-83.

182. Rao, S. M., J. R. Binder, et al. (1993). "Functional magnetic resonance imaging of complex human movements." Neurology **43**: 2311-2318.

183. Ray, S., E. Niebur, et al. (2008). "High-frequency gamma activity (80-150Hz) is increased in human cortex during selective attention." Clin Neurophysiol **119**(1): 116-33.

184. Ray, W. J. and H. W. Cole (1985). "EEG alpha activity reflects attentional demands, and beta activity reflects emotional and cognitive processes." Science **228**(4700): 750-2.

185. Renshaw, B., Forbes, A., and Morrison, B. (1940). "Activity of isocortex and hippocampus: Electrical studies with micro-electrodes." J Neurophysiol **3**: 74-105.

186. Rieke, F., Warland, D., de Ruyter van Steveninck, R., Bialek, W. (1997). Spikes: Exploring the neural code. Cambridge, MA, The MIT Press.

187. Rizzolatti, G., G. Luppino, et al. (1988). "The organization of the cortical motor system: new concepts." Electroencephalogr Clin Neurophysiol **106**(4): 283-296.

188. Salmelin, R. and R. Hari (1994). "Spatiotemporal characteristics of sensorimotor neuromagnetic rhythms related to thumb movement." Neuroscience **60**(2): 537-50.

189. Sanes, J. N. and J. P. Donoghue (1993). "Oscillations in local field potentials of the primate motor cortex during voluntary movement." Proc Natl Acad Sci U S A **90**(10): 4470-4.

190. Sanes, J. N., J. P. Donoghue, et al. (1995). "Shared neural substrates controlling hand movements in human motor cortex." Science **268**(5218): 1775-1777.

191. Schieber, M. L. and L. S. Hibbard (1993). "How somatotopic is the motor cortex hand area?" Science **261**(5120): 489-492.

192. Schiffman, H. R., R. Lore, et al. (1970). "Role of vibrissae for depth perception in the rat (rattus norvegicus)." Animal Behav. **18**: 290-292.

193. Schmidt, E. M. (1984). "Computer separation of multi-unit neuroelectric data: a review." J Neurosci Methods **12**(2): 95-111.

194. Schurmann, M. and E. Basar (2001). "Functional aspects of alpha oscillations in the EEG." Int J Psychophysiol **39**(2-3): 151-8.

195. Sederberg, P. B., M. J. Kahana, et al. (2003). "Theta and gamma oscillations during encoding predict subsequent recall." J Neurosci **23**(34): 10809-14.

196. Shaw, J. C. (1999). "Intention as a component of the alpha-rhythm response to mental activity." International Journal of Psychophysiology **24**(1-2): 7-23.

197. Shibasaki, H., N. Sadato, et al. (1993). "Both primary motor cortex and supplementary motor area play an important role in complex finger movement." Brain **116**(6): 1387-1398.

198. Shuler, M. G., D. J. Krupa, et al. (2002). "Integration of bilateral whisker stimuli in rats: role of the whisker barrel cortices." Cereb Cortex **12**(1): 86-97.

199. Singer, W. (1994). "Coherence as an organizing principle of cortical functions." Int Rev Neurobiol **37**: 153-83; discussion 203-7.

200. Singer, W. (1999). "Neuronal synchrony: a versatile code for the definition of relations?" Neuron **24**(1): 49-65, 111-25.

201. Singer, W. and C. M. Gray (1995). "Visual feature integration and the temporal correlation hypothesis." Annu Rev Neurosci **18**: 555-86.

202. Singer, W., A. K. Kreiter, et al. (1996). "Precise timing of neuronal discharge within and across cortical areas: implications for synaptic transmission." J Physiol Paris **90**(3-4): 221-2.

203. Slotnick, S. D., L. R. Moo, et al. (2002). "Interactions between thalamic and cortical rhythms during semantic memory recall in human." Proc Natl Acad Sci U S A **99**(9): 6440-3.

204. Steinmetz, P. N., A. Roy, et al. (2000). "Attention modulates synchronized neuronal firing in primate somatosensory cortex." Nature **404**(6774): 187-190.

205. Szwed, M., K. Bagdasarian, et al. (2003). "Encoding of vibrissal active touch."Neuron **40**(3): 621-30.

206. Tallon-Baudry, C., O. Bertrand, et al. (1997). "Oscillatory gamma-band (30-70 Hz) activity induced by a visual search task in humans." J Neurosci **17**(2): 722-34.

207. Tallon-Baudry, C., O. Bertrand, et al. (1998). "Induced gamma-band activity during the delay of a visual short-term memory task in humans." J Neurosci **18**(11): 4244-54.

208. Tiitinen, H., J. Sinkkonen, et al. (1993). "Selective attention enhances the auditory 40-Hz transient response in humans." Nature **364**(6432): 59-60.

209. Treue, S. (2001). "Neural correlates of attention in primate visual cortex." Trends Neurosci **24**(5): 295-300.

210. Usrey, W. M. and R. C. Reid (1999). "Synchronous activity in the visual system." Annu Rev Physiol **61**: 435-56.

211. Vaadia, E., I. Haalman, et al. (1995). "Dynamics of neuronal interactions in monkey cortex in relation to behavioural events." Nature **373**(6514): 515-8.

212. Vanderwolf, C. H. (1969). "Hippocampal electrical activity and voluntary movement in the rat." Electroencephalogr Clin Neurophysiol **26**: 407-418.

213. Vanderwolf, C. H. and T. Robinson (1981). "Retino-cortical activity and behavior: A critique of the arousal theory and a new synthesis." Behav. Brain Sci. **4**: 459-514.

214. Vincent, S. B. (1912). "The function of vibrissae in the behavior of the white rat." Behavior Monogr **1**: 1-81.

215. Vogel, W., D. M. Broverman, et al. (1968). "EEG and mental abilities." Electroencephalogr Clin Neurophysiol **24**: 166-175.

216. von Stein, A., Rappelsberger, P., Sarnthein, J., Petsche, H. (1999). "Synchronization between temporal and parietal cortex during multimodal object processing in man." Cereb Cortex **9**(2): 137-150.

217. von Stein, A. and J. Sarnthein (2000). "Different frequencies for different scales of cortical integration: from local gamma to long range alpha/theta synchronization." International Journal of Psychophysiology **38**(3): 301-313.

218. Welker, W. I. (1964). "Analysis of sniffing of the albino rat." Behaviour **22**: 223-244.

219. Whitmer, D., I. K. Lee, et al. (2008). Multi-scale investigation of scalp and intracranial EEG with independent component analysis.

220. Whitmer, D., G. Worrell, et al. (2007). Cortical mapping based on independent analysis and spectral changes in the electrocorticogram. Abstract for Human Brain Mapping, Chicago, IL.

221. Whitmer, D., G. Worrell, et al. (2008). Dynamics of Visually-Cued Finger Movements based on Independent Component Analysis of Electrocorticogram (ECoG) and EEG.

222. Wilson, M. A. and B. L. McNaughton (1993). "Dynamics of the hippocampal ensemble code for space." Science **261**(5124): 1055-8.

223. Witham, C. L. and S. N. Baker (2007). "Network oscillations and intrinsic spiking rhythmicity do not covary in monkey sensorimotor areas." J Physiol **580**(Pt.3): 801-14.

224. Witham, C. L., M. Wang, et al. (2007). "Cells in somatosensory areas show synchrony with beta oscillations in monkey motor cortex." Eur J Neurosci **26**(9): 2677-86.

225. Wolters, C. H., M. Kuhn, et al. (2002). "A parallel algebraic multigrid solver for finite element method based source localization in the human brain." Comput. Visual Sci. **5**: 165-177.

226. Woolsey, T. A. and H. Van der Loos (1970). "The structural organization of layer IV in the somatosensory region (SI) of mouse cerebral cortex. The description of a cortical field composed of discrete cytoarchitectonic units." Brain Res **17**(2): 205-42.

227. Worrell, G. A., A. B. Gardner, et al. (2008). "High-frequency oscillations in human temporal lobe: simultaneous microwire and clinical macroelectrode recordings." Brain **131**(Pt 4): 928-37.

Chapter II. Active Spatial Perception in the Vibrissa Scanning Sensorimotor System

Haptic perception is an active process that provides an awareness of objects that are encountered as an organism scans its environment. In contrast to the sensation of touch produced by contact with an object, the perception of object location arises from the interpretation of tactile signals in the context of the changing configuration of the body. A discrete sensory representation and a low number of degrees of freedom in the motor plant make the ethologically prominent rat vibrissa system an ideal model for the study of the neuronal computations that underlie this perception. We found that rats with only a single vibrissa can combine touch and movement to distinguish the location of objects that vary in angle along the sweep of vibrissa motion. The patterns of this motion and of the corresponding behavioral responses show that rats can scan potential locations and decide which location contains a stimulus within 150 ms. This interval is consistent with just one to two whisk cycles and provides constraints on the underlying perceptual computation. Our data argue against strategies that do not require the integration of sensory and motor modalities. The ability to judge angular position with a single vibrissa thus connects previously described, motion-sensitive neurophysiological signals to perception in the behaving animal.

2.1 Introduction

"Neurophysiologists…have been reluctant to face up to [changes in anatomy from moment to moment] in explaining perception, for they know more about the anatomy of

the eyes, ears, and skin than they do about the physiology of looking, listening, and touching" – J. J. Gibson [1].

The noted psychologist J. J. Gibson argued forty years ago [1] that the sensations produced by feed-forward transformation of inputs from neuronal exteroreceptors are distinct from the dynamic perception of the environment derived from the "neural loops of an active perceptual system". Gibson's thesis was that the perception of the location of a contacted object, for example, is fundamentally different from the sense impressions that arise from skin mechanotransduction. Perception requires an integration of information across sensory and motor modalities that is not necessarily derived from successive transformations of the touch data alone. Studies in systems from posture control [2,3] to eye movement [4] have elucidated principles of such "neural loops" when used in motor systems with explicit sensory feedback. The work described here addresses the complementary case of positional context in a sensory system with explicit motor drive [5,6].

The rat vibrissa system, with its tactile hairs and their associated neuronal architecture, provides our prototype for this sensorimotor model. For nearly a century, researchers have compiled behavioral evidence that the vibrissae are both sensors and effectors in a complex sensory system that is able to identify and locate objects [7]. Although recent insights into the mechanical properties of the vibrissae [8,9] may explain the processing of qualities such as texture [10–13], few experiments, to our knowledge, have explicitly characterized the spatial information available from the vibrissae. Early work indicated that rats use this system for the detection of surfaces during navigation

[14], and more recent studies have shown that the vibrissae provide information about object distance [15,16], shape [17], and orientation [18,19]. Few of these behaviors inherently engaged the sensorimotor nature of the system, and rats are known to perform some tasks, such as vibration [20] and bilateral distance [21] discrimination, with only passive vibrissa contacts. The system as a whole, in contrast, is fundamentally active. Whereas nearly all mammalian species have vibrissae [22], rats and related rodent species have specifically evolved the ability to sweep their vibrissae for dynamic exploration of the environment [23]. This ability leads us to question whether touch and motion are used in concert, in the spirit of Gibson, to form an "active perceptual system."

Neurophysiologically, the sensory and motor processes are tightly interwoven. A nested series of loops, at levels from brainstem to cortex, connect the vibrissa sensory stream to a hierarchical motor drive that ordinarily produces a rhythmic rostrocaudal movement known as exploratory whisking [24]. Sensory inputs feed back onto motor areas at all levels and can alter motor output at even the lowest-order brainstem loops [25]. The information flow is bidirectional, however, and electrophysiological recordings have found neurons, again at levels from the brainstem to cortex, that encode the changing position of the vibrissae even in the absence of contact with an external object [26–29]. These cells complement somatosensory neurons that encode the qualities of contact and could provide the brain with an internal reference as self-generated motion modulates the external location that corresponds to contact.

The existence of position-sensitive signals does not prove that they are actually used for spatial perception. What has been lacking in the study of the neural

computations that underlie the fusion of these touch and motion signals is a vibrissa-mediated behavior that requires sensorimotor integration. One such task would ask if a rat can use its vibrissae to differentiate between objects that differ only in rostrocaudal angle, i.e., azimuthal angle or angle along the rostrocaudal sweep of the vibrissae. However, the nervous system could in principle ignore motor information and solve this problem using the topography of the vibrissa array. When the motion of the vibrissae is comparable to their separation, the rostrocaudal position of an object can be judged from the peripheral origin of the touch signal (Figure 2.1A), in an encoding scheme known as a labeled-line scheme [30]. In this representation, the topographic identity of the cortical region activated by contact corresponds to object location, because each region of space is only scanned by a single sensor. An animal could thus use its vibrissa array to discriminate object angle if it used large-amplitude, exploratory motion to detect an object and switched to smaller motion for localization.

In the more typical exploratory whisking motion [31–34], vibrissa sweeps overlap, and the angular location that corresponds to contact requires information beyond the identity of the contacting vibrissa (Figure 2.1B). In this case, the presence of position-sensitive neurons suggests that the position of the vibrissae at the time of contact could provide context to clarify the contact event [35,36]. This sensorimotor approach falls under the rubric of haptic perception, as it is based on the awareness of the position of "an object relative to the body and the body relative to an object" [1]. Other algorithms derived from the touch sensation, such as duration of contact [28], are possible if different object positions result in reproducible differences in the structure of the contact event [37]. These approaches share the common feature that they do not depend on

vibrissa identity and, therefore, unlike the labeled-line scheme, could be performed with a single vibrissa. To differentiate between these possibilities for spatial encoding and relating known sensorimotor physiological signals to a sensorimotor behavior, we thus ask if behaving rats are able to discriminate between objects at different rostrocaudal angles when restricted to the use of a single vibrissa.

2.2 Results

We tested 14 rats in an angle-based spatial discrimination task by using an apparatus designed for semi-automated training (Figure 2.2). Briefly, each animal was assigned two stimulus positions whose rostrocaudal angles differed by 15 °. One of these positions was designated the rewarded, or ***S***+*,* stimulus, and the other position was designated unrewarded, or ***S***_. The animal performed a series of trials in which it maintained a fixed head position while presented with a thin rod at one of these two positions. Under a go/no-go paradigm with a fixed ratio reinforcement schedule [38], the animal was required to respond to the ***S***+ position with a block of L lever presses within T seconds after stimulus presentation to obtain a fluid reward (see Methods); we used $T = 8$ s. Lever presses in the ***S***_ condition were recorded but had no consequences. An animal was considered to discriminate between the two positions when multiple consecutive sessions showed a statistically significant difference between ***S***+ and ***S***_ trials in the latency to complete this block response. We trained animals on this task with their full complement of vibrissae and then tested them while removing vibrissae, first down to a single row and finally to a single vibrissa.

We considered it likely that a typical rat has the perceptual ability to perform this single vibrissa discrimination, despite the fact that only five of our initial 14 animals showed consistent behavioral differences between ***S***+ and ***S***_ trials when tested with a single vibrissa (Figure 2.3). This attrition was largely due to a weakness in the behavioral measure used early in the study. The majority of the animals who did not progress to the single vibrissa condition were tested with a minimal lever press response requirement, $L = 1$ (Figure 2.3; animals outside the dashed box did not succeed in the single vibrissa task and animals with numbers in gray were tested with $L = 1$). The lack of demonstrated discrimination for these animals was likely because the low response requirement did not discourage animals from responding when they were able to predict that no reward would be forthcoming [38]. We thus raised the response requirement on L for later animals until differences in ***S***+ and ***S***_ responses were seen ($L = 4$–6), and we then reliably measured discrimination for testing with all vibrissa intact (Figure 2.3; animals with numbers in black). This large increase in training success rate suggests that the measurements were limited by our ability to motivate the desired behavior rather than the animals' perceptual abilities.

Time Scale of Single Vibrissa Discrimination

We compared the pattern of lever presses between ***S***+ and ***S***_ trials to estimate the time required to form a behavioral decision. In our analysis, we considered only the first L responses in each trial, because the presence or absence of a reward after L lever presses could be used to distinguish the two stimulus conditions (Figure 2.4A). The cumulative response count, averaged separately for ***S***+ and ***S***_ trials, quantified this time course for a given session (Figure 2.4B). ***S***+ trials resulted both in a higher response rate

and in a lower latency to response onset relative to ***S***_ trials. In a typical session for the animal with the fastest responses (Rat number 20), the average response counts for the two conditions began to diverge approximately 250 ms after the start of a trial, and the 95% confidence regions became permanently nonoverlapping after 500 ms (Figure 2.4B; gray arrows). Thus, we could confidently measure a difference in the average response to ***S***+ and ***S***_ stimuli for this animal within 0.5 s of stimulus delivery.

The time in which these two response profiles diverge included the intervals needed both to form a sensory percept and to emit at least one lever press, i.e., $t_{\text{diverge}} = t_{\text{perception}} + t_{\text{motor}}$. To place an upper bound on the interval $t_{\text{perception}}$ needed for active sensing alone, we estimated the minimum time t_{motor} required for the motor act of pressing the lever from two observations. First, the slope of the linear part of the cumulative response for ***S***+ trials gave the mean response rate during sustained responding. This rate was roughly 2.5 lever presses per second, or 400 ms per average lever press (e.g., Figure 2.4B). Second, the shortest time taken by any animal to reach L = 5 lever presses was roughly 1.5 s (e.g., Figure 2.4C). Because few responses occurred in the first 250 ms of a trial (e.g., Figure 2.4A), this left 1.25 s for five lever presses, or 250 ms per lever press in the fastest cases. Both measures were based on blocks of lever presses that did not require further decision-making by the animal, and thus isolate the time t_{motor} to be 400 ms for typical responses and 250 ms for the fastest responses. Given t_{diverge} = 500 ms and using $t_{\text{motor}} \geq 250$ ms, these data demonstrate that the complete interval $t_{\text{perception}}$ required to detect the stimulus and form a percept of stimulus position is less than 250 ms.

Variability across Sessions and Animals

The latency to reach the total required number of responses L in each trial served as our primary measure of behavioral discrimination (Figures 2.4C and 2.5A). A given session was considered to demonstrate stimulus discrimination when the $\boldsymbol{S}+$ and $\boldsymbol{S}\_$ latency distributions significantly differed, as measured by a two-sided Kolmogorov-Smirnov (K-S) test. Consistent with the lack of an overt penalty in $\boldsymbol{S}\_$ trials, we observed many more false-positive (type I) errors—where an animal completed L lever presses with short latency during an $\boldsymbol{S}\_$ trial—than false-negative (type II) errors (Figures 2.4C, 2.5A, and 2.5B). Because the K-S statistic does not provide information about the types of errors, we confirmed consistent performance over multiple sessions by plotting receiver operating characteristic curves [39] for the detection of the $\boldsymbol{S}+$ stimulus (Figure 2.4D). Each receiver operating characteristic curve shows the dependency between false positive trials, i.e., $\boldsymbol{S}\_$ trials with latencies shorter than a threshold _, and true positive trials, i.e., $\boldsymbol{S}+$ trials with latencies shorter than _, as the latency threshold t is varied. Loosely, a steep slope near the left side of the graph indicates few type I errors, whereas a shallow slope near the right side of the graph indicates few type II errors; the integrated distance to the diagonal is a measure of the overall discriminability of the two distributions. The numbers of type I and type II errors fluctuated between sessions, but all animals showed a tendency for false-positive errors.

Further, although the bimodal nature of the latencies (Figure 2.4C) was consistent for all five animals in the single vibrissa task, the time at which $\boldsymbol{S}+$ and $\boldsymbol{S}\_$ responses diverged fluctuated across sessions and animals. Each of the three animals that passed all controls, as described below, performed sessions in which the average $\boldsymbol{S}+$ and $\boldsymbol{S}\_$

responses diverged within 650 ms. The remaining two animals took longer, i.e., greater than 1,000 ms, due to the head-turning behavior that is described below. These response times are consistent with an estimate of 250 ms for time needed for spatial discrimination.

Finally, the experimenter-defined association of stimulus position with reward condition varied across these five animals. Although all single vibrissa trials were performed at an angular separation of 15 °, the animals were tested on different absolute stimulus positions. For example, rat number 20 was tested with vibrissa C1 for ***S***+ set to +15 ° and ***S***_ set to 0 °, whereas rat number 9 was tested with vibrissa C2 for ***S***+ = _7.5 ° and ***S***_ = +7.5 °. In total, two animals had rostral ***S***+ assignments, whereas three had caudal ***S***+ assignments. We did not find any gross differences in training time or performance correlated with these parameters, which suggests that the absolute position of the ***S***+ and ***S***_ stimuli did not play a critical role in the discrimination.

Controls

For the five animals that succeeded in the single vibrissa task over multiple sessions, we carried out three controls to verify that discrimination derived solely from vibrissa-mediated tactile cues. We first tested for visual cues. Although behavioral testing occurred in a dark chamber, a high-intensity infrared lamp with a peak wavelength of 850 nm was used for videography. We considered it possible, though unlikely [40], that residual visible light from this lamp was available to the animals. We thus tested performance in sessions for which the lamp was turned off, as illustrated by the data of

Figure 2.5B. None of the five tested animals lost the ability to perform the task in the absence of the infrared illumination.

We next tested for a contribution from head movements. Stimuli were delivered after an animal fixed its head position in the nose poke and were retracted when fixation was lost (Figures 2.7C and 2.7D); but mechanical lags created approximately a 150-ms window after an animal left the nose poke during which the stimulus was not fully retracted. Video observation showed that two of the five animals that succeeded in discrimination with a single vibrissa habitually probed the stimuli with their snouts after making vibrissa contact. It was not clear whether this movement was needed to aid stimulus localization, or whether it occurred as a reflex motion after the location had already been judged. Because we could not rule out the former possibility, we considered these cases ambiguous (Figure 2.3; half-shaded circles).

We finally tested the remaining three animals for the use of auditory and vibrational cues. The pistons used to deliver the stimuli were damped to reduce vibrations, and testing was carried out in the presence of an audio mask to interfere with any sound differences in ***S***+ and ***S***_ stimulus delivery. To confirm that discrimination was not based on residual indirect cues arising from stimulus motion, each animal was tested in a session where the pistons functioned as usual but the stimulus pins were absent. A resulting degradation in performance indicated that tactile contact with the vibrissa was required (see Figure 2.5C and the orange line in Figure 2.4D). None of the three tested animals showed significant discrimination in these control sessions.

In several sessions, we were able to further control for vibration cues by restricting our attention to trials in which the animal broke fixation less than 250 ms after the start of a trial. In these cases, the stimulus was retracted before it fully entered the vibrissa field. This allowed the pistons to travel over nearly their entire range but left insufficient time for the vibrissae to encounter the stimuli. In sessions with sufficient numbers of these "jump-the-gun" trials, we verified that discrimination performance was at or near chance with this limited opportunity for vibrissa contact, as seen in Figure 2.5D.

Whisking Strategies

To characterize the formation of the spatial percept in the interval $t_{\text{perception}}$ preceding the motor response, we made high-speed infrared video recordings of vibrissa motion for two of the three animals that passed all of the controls, i.e., rat number 9 and rat number 20 (Figure 2.6A, 2.6B, 2.6D, and 2.6E). Vibrissae positions estimated from these recordings typically showed a slow drift until approximately 100 ms into the trial, followed by larger-amplitude, but often non-sinusoidal, vibrissa motion on a changing baseline (Figure 2.6C and 2.6F). This interval reflects the delay after the stimulus begins to descend before the animal realizes that a trial has begun. Thus, further subdividing $t_{\text{perception}} = t_{\text{delay-to-start-of-search}} + t_{\text{active-sensing}}$ yields an estimate for the average time required to actively scan for a stimulus as $t_{\text{active-sensing}} \approx 150$ ms.

Constraints on sensorimotor algorithms can be obtained from a more detailed analysis of patterns in the vibrissa motion. An animal could adopt a purely motor strategy by repeatedly positioning its vibrissa in the expected location of one of the stimuli and

then simply detecting contact. To rule out this approach, we examined the distribution of all vibrissa positions in the first 250 ms of the trials, an interval chosen because it included few stimulus contacts. This distribution was, in all cases, centered between the two stimuli, indicating that vibrissa positions spanned both potential locations rather than habitually preferring one (Figure 2.6G). In a related strategy, an animal could center its vibrissa between the ***S***+ and ***S***_ stimulus locations and then associate contact during protraction with the more rostral stimulus and contact during retraction with the more caudal stimulus. As a test of this directional bias, we calculated the velocity of the vibrissa just before contact with ***S***+ and ***S***_ stimuli. Contact at each location occurs during both protracting and retracting movements, so that the direction of contact does not encode stimulus location (Figure 2.6H). This is consistent with the further observation that the distribution of vibrissa positions in the first 250 ms of the trials extends beyond the location of the two stimuli (Figure 2.6G), so that contacts can occur in both movement directions.

Another class of algorithms that does not require integration of positional and contact information depends on the duration of vibrissa contact [28,37,41]. For periodic vibrissa motion, the time between contact onset and offset could be transformed into object position. Such a scheme might be accomplished more generally for any vibrissa motion in which contact duration is a monotonic function of vibrissa angle. We thus asked if the distribution of contact event durations was different for ***S***+ and ***S***_ trials. These contacts were largely brief events of less than 50 ms, although extended contacts of greater than 300 ms occasionally occurred (Figure 2.6I). This overall distribution of contact durations is consistent with earlier measurements (Figure 3A from Sachdev et al.

[42]) but the precise times varied broadly from trial to trial. Thus, for all animals, the variability of contact duration was large relative to any separation between the peaks of the distributions for the ***S***+ and ***S***_ conditions. In light of this variability, we consider an algorithm based on the duration of contact unlikely to account for the observed behavioral performance.

2.3 Discussion

We have demonstrated that rats with a single vibrissa can respond to differences in the position of external objects that differ only in angle along the direction of vibrissa motion. A rat with a full array of vibrissa could in principle perform this task by limiting vibrissa motion to nonoverlapping fields and by using the collection of vibrissa columns, or arcs, as a spatial sensory array to test multiple locations in parallel (Figure 2.1A). The ability of animals to identify spatial angle when restricted to a single vibrissa argues that this sensorimotor system is able to determine the position of an object contact while serially scanning a single sensor. While the animal is performing this task, vibrissa motion spanned both stimulus locations before contact (Figure 2.6G), made contact during both protraction and retraction (Figure 2.6H), and remained in contact with both ***S***+ and ***S***_ stimuli for similar durations (Figure 2.6I). Although these experiments did not focus on discrimination using multiple vibrissae, we note that animals did not show any marked change in strategy or accuracy as they transitioned from single row to single vibrissa testing. This suggests that animals used the scanning strategy with multiple

vibrissae as well, but the large variability in performance may have obscured indications of subtle changes in strategy.

The time scale for tactile search was estimated from the measured behavior. Animals could selectively initiate a motor response in as little as 250 ms after the start of an ***S***+ trial (Figures 2.4B and 2.4C). In this short interval, we typically observed delays of 100 ms from the start of a trial before the vibrissa started a large amplitude scanning motion (Figure 2.6C and 2.6F). Taken together, these intervals imply that the time $t_{\text{active-sensing}}$ including the entire sensorimotor process of motor scanning, object detection, and spatial categorization can be as short as 150 ms. Given a typical frequency of exploratory whisking in the range of 7–15 Hz [33], this suggests that no more than one to two whisk cycles were sufficient to judge position. Although the animals in our study often did not show the highly sinusoidal vibrissa motion found in other studies [33,43], perhaps due to the physical restriction of the nose poke, the observed time scale of vibrissa motion here is consistent with these frequencies.

Neural Algorithms

Earlier studies have suggested the calculation of dorsoventral angle from the identity of the contacting row [41,44] and demonstrated discrimination of distance from contact with multiple vibrissae, even in the absence of active whisking [21]. We focused here on the decoding of angle along the axis of vibrissa motion because of the confound arising due to that motion, i.e., the environmental meaning of exteroceptive tactile signals changes as an animal moves its vibrissae. Given that this computation can be

accomplished using the information associated with a single moving sensor, we consider the algorithms that might be used to transform a contact signal into a spatial position.

A purely motor strategy could have taken advantage of the fixed stimulus locations in our task design. Because only two positions were possible, an animal might learn to focus its now sparse sensory apparatus on one of these two positions and use the presence or absence of a contact event to detect the ***S***+ (or equivalently, ***S***_) condition without considering both sensory and motor cues. This is a single vibrissa approximation of a labeled-line strategy (Figure 2.1A), which requires motor control sufficient to hold a lone sensor near an expected target. This approach was ruled out by the motion patterns of the vibrissa; in both animals for which we tracked vibrissa position, the scanning motion was not restricted to the region of a single stimulus (Figure 2.6G). At the opposite extreme, the wealth of sensory information available from the vibrissa follicle suggests a purely sensory strategy that might arise from differences in the nature of contact as a function of position. The existence of separate on- and off-contact touch signals [28] allows for the possibility that the nervous system determines the duration of a contact and converts it into a spatial position, for cases such as sinusoidal motion where different positions result in characteristic contact durations. This temporal delay scheme is contraindicated by the similarity of the measured contact durations (Figure 2.6I). Finally, a strategy that uses both sensory and motor signals, but with low resolution, would be to position a vibrissa such that it approaches the two stimulus positions from different directions, e.g., during protraction versus retraction. The measured broad heterogeneity of velocity approaching contact (Figure 2.6H) makes it unlikely that such gross directional cues encoded stimulus position.

The most parsimonious remaining explanation for the computation needed to derive spatial position from a contact event is the integration of touch with kinesthetic information about the location of the vibrissa at the time of contact. Although there is no evidence of proprioceptive muscle spindles in the mystacial pad [45], physiological studies have shown that a reafferent motor signal from the pad is present at levels from the trigeminal ganglion [28,46] to thalamic nuclei [47] to primary somatosensory cortex [26,29,48,49]. The evidence described here argues that this positional information can be used behaviorally as a reference against which to interpret sensory contact, informing spatial perception of objects near the head. Preliminary electrophysiological data show how the fusion of these two signals can occur in the brain [50].

Previous theoretical studies have taken advantage of the rhythmic nature of exploratory whisking to suggest neuronal circuits that might compute spatial location given periodic spike trains representing both contact and vibrissa motion [36,51–53]. The mathematical formulation of this class of algorithm, however, requires multiple rhythmic whisk cycles to establish a phase reference. The animals in our study and another study with head-restrained animals trained to touch objects with their vibrissae [54] do not appear to precede contact with periodic whisking (Figure 2.6C and 2.6F) (Figure 3A of Sachdev et al. [54]). This ability to form a spatial percept from oscillatory but irregular vibrissa motion, within one to two cycles after whisking onset, argues against mechanisms that depend on periodicity. A more-direct circuit that performs the same computation would compare spiking in contact-sensitive and position-sensitive cells of varying preferred position. Ongoing physiological studies characterizing these neuronal interactions suggest that this comparison can in fact integrate tactile and haptic streams

[50]. Finally, a last constraint on any proposed neuronal implementation of a spatial decoding algorithm should at least account for resolution sufficient to distinguish contacts separated by 15 °. Directed studies of the threshold for absolute angular discrimination are required to establish the psychophysical limits of spatial acuity, as has been done for the bilateral comparison of distance [21] and angle [55].

The Vibrissa System and Sensorimotor Integration

Our behavioral task was designed to isolate a sensory process that is ordinarily used in concert with other behaviors. Earlier studies involving spatial behaviors support the notion that the vibrissae serve as binary detectors in freely exploring animals [20], and this may be the ethologically more typical usage when an animal can orient its head following contact. Indeed, upon detection of the salient and asymmetric stimulus used in this study, some animals in our study reflexively oriented to explore the stimulus further, perhaps bringing their microvibrissae to bear. Although we could not determine whether those animals had judged stimulus position before orienting, we note that refined rostrocaudal information is necessary if a rat is to orient rapidly following contact without further search. Although the current study does not attempt to characterize the role of angular perception during natural activity, we note that the vibrissae are involved in activities with complex spatial demands, such as navigation [14,44], aggression [56], and swimming [57] (for a general review, see Gustafson and Felbain-Keramidas [7]). This ubiquitous role suggests that these sensorimotor organs paint a richer picture of the tactile world than would be possible from binary detection alone. When taken with recent

work on the role of the vibrissae in the transduction of fine texture [10–13], the proportionally large neural territory given to vibrissa processing emerges as the potential locus of integration for multiple modalities.

A practical advantage to the study of integration processes in the vibrissa system lies in the large body of work on the plasticity, anatomy, and sensory response properties [36,58–62] related to the vibrissa primary somatosensory or barrel cortex. A variety of recent studies take advantage of this growing body of literature and use the vibrissa system to develop modern experimental methodologies [63–65]. In recognition of the requirements of these techniques, our choice of a go/no-go paradigm, rather than a two-alternative forced choice design [66], was in part motivated by the hope of eventually measuring behavior in animals head-fixed for imaging or intracellular studies [29,63,67–69]. The present work demonstrates that rats can use this popular model system to integrate feed-forward sensory events with motor feedback to inform their model of the external world. The elucidation of the circuitry that performs this computation will bring us a step closer to understanding how sensorimotor loops derive the perception of space from the sensation of touch.

2.4 Methods

Our initial cohort of behavioral subjects consisted of 24 Long-Evans rats, 14 of which reached the stimulus training stage of the study (Figure 2.3). All of these animals were females of 100–200-g mass at the start of training. All procedures involving animals conformed to National Institutes of Health guidelines and were approved by the

Institutional Animal Care and Use Committee at the University of California at San Diego (La Jolla, California, United States).

Training apparatus

Animals were trained and tested in a custom operant arena (Figure 2.2A). The arena was contained in an enclosure 760 mm _ 500 mm _ 420 mm (not shown in Figure 2.2) made of 0.635-cm acrylic and padded with skinned polyether foam (2.54 cm; NRC 0.8, McMaster-Carr, 5692T49 [http://www.mcmaster.com/]) to dampen external sound and light. The enclosure contained a speaker to deliver sound cues, an auditory white-noise mask, a SecuraCam infrared camera (Swann [http://www.swann.com.au/]) for monitoring by the trainer, and a low-flow gas line to ensure breathable air. The area available to the animal consisted of an acrylic vestibule, 200 mm on a side, and a 200-mm long _ 57-mm inner diameter tunnel, both placed on an acrylic shelf elevated 60 mm above the floor of the external enclosure. Motion through the tunnel was registered by an 880-nm infrared photodiode (Photonic-Devices, PDI-E802 [http://www.photonicdevicesinc.com])/phototransistor (DigiKey, QSE156-ND [http://www.digikey.com/]) pair to signal the presence of a rat. The end of the tunnel was fitted with a U-shaped restraint bar that allowed free movement of the head and paws while preventing escape (Figure 2.2B).

Behavioral output was measured through a water-sealed lever of 25-g activating force (Cherry E73-series switch, DigiKey, CH566-ND), affixed with a plastic crossbar, and placed at the end of the tunnel (Figure 2.2B). Animals typically rested on the

crossbar and activated the lever by briefly raising their paws; early in training, a small spring was often placed to aid this motion. Fluid rewards were delivered to a sip cup cut into a stainless steel dispenser, placed ~ 60 mm from the end of the tunnel and designed with inflow and outflow ports to control the timing of fluid delivery. Fluid was delivered in 50-µl aliquots through a miniature directional control solenoid valve (Parker-Hannifin, 004-0008-900 [http://www.parker.com/]) with a custom timer circuit (University of California at San Diego Physics Electronics Shop) to gate flow from a reservoir and then removed by a similarly controlled solenoid gating a vacuum line. A bright yellow light-emitting diode (587 nm, 1,900 mcd, Radio Shack 276-351 [http://www.radioshack.com]) was wired in parallel with the reward timer to indicate reward availability and interfere with visual dark-adaptation to any residual light in the chamber, e.g., from the camera illumination lamp. This entire fluid delivery system was flushed with enzymatic detergent (MaxiZyme, Henry Schein, #10-7410 [http://www.hsa.ca/]) after each training session to prevent build-up of organic solids. This cleaning step was particularly necessary early in the training when chocolate milk was sometimes used as a liquid reward.

Rat head position was fixed by a 13-mm outer diameter brass nose poke cone, painted black to minimize stray reflections, with an analog reflective infrared sensor (940 nm, DigiKey, QRD1114-ND), whose output was taken to an analog comparator (LM319N, DigiKey, 497-1577-5-ND). The comparator was wired as a Schmitt trigger and referenced to a potentiometer adjusted to control nose poke sensitivity. The nose poke was placed close to the fluid dispenser and fixed relative to the stimulus with an aluminum bracket (not shown in Figure 2.2). This system allowed some positional

ambiguity, as an animal could roll its snout freely while maintaining fixation. However, translational position was reproducibly constrained (Figures 2.6B and 2.6E).

Digital inputs taken from the lever, tunnel sensor, and nose poke sensor were sampled at 16 Hz by a multifunction digital input/output board (National Instruments, AT-MIO-16DE [http://www.ni.com/]) in a personal computer running custom LabVIEW software (National Instruments). The software logged the inputs, implemented training logic, and supplied digital control signals for the reward, vacuum, and stimulus valves.

Tactile stimuli

The stimuli for the spatial task were 0.86-mm steel rods translated into and out of the vibrissa field by a custom air-piston and guide assembly. Two paired Lexan guide blocks were aligned on Teflon-coated shafts (15.24 cm long _ 0.630 cm deep, McMaster-Carr, 7875K11). The floor of the bottom guide rested on plastic legs 110 mm above the floor of the tunnel. These legs, the top-guide, and the alignment shafts were left out of Figure 2.2A for clarity. A carriage block with a captured linear bearing was free to slide on the two rostral shafts, and a mirror-image block traveled along the two caudal shafts. Two stainless-steel air cylinders (spring-return, 5.08 cm travel, McMaster-Carr, 6498K27) were fixed to the top block, each with its piston bolted to one of the carriage blocks. Air at 20 psi was delivered to the pistons through a pair of three-way miniature solenoid valves (Parker-Hannifin, 004-0008-900) that were placed outside of the enclosure to minimize noise. These valves were connected to 12 V of direct current supplies via power transistors (Mouser, 610-2N6387 [http://www.mouser.com/]) for

digital control. Inflowing air was passed through a restriction valve, common to both stimuli, which was adjusted to slow piston descent and minimize vibration during stimulus delivery. Outflowing air was similarly restricted, and silicone bumpers were placed between the carriage and guide blocks to damp vibration from the sudden deceleration at the ends of travel. The resulting stimulus descent and ascent took ~250 ms and ~150 ms, respectively, for the full 5.08 cm travel, including an approximate 30-ms delay in both cases for computer processing, solenoid switching, and the build-up of a sufficient change in air pressure. The white-noise audio mask was played continuously in the box to confound any auditory differences between the stimuli.

Both carriage blocks and the bottom guide block were drilled with matching hole patterns on a circle of 25-mm diameter with either 15 ° or 7.5 ° spacing. The nose poke was bolted to the bottom guide block and positioned such that a line connecting the caudal edges of both mystacial pads would approximately coincide with the center of this circle. A backstop was constructed by gluing 18-gauge hypodermic tubing to the back of 90-mm lengths of the 0.86-mm diameter stimulus rods. The backstops rested above the stimulus carriage blocks and allowed the stimuli to travel with the carriage blocks, extending from 10–61 mm below the floor of the bottom guide block. This arrangement allowed the angular location of the stimuli to be rapidly adjusted for each animal and was intrinsically safer for the animals, as the stimuli dropped due to gravity rather than direct piston drive. Our typical configuration fixed potential locations for the stimuli at 3.75 + n7.5 (where n is an integer between _5 and 5), measured relative to a line through the center of the circle described above and perpendicular to the animal's midline. In all

cases, one stimulus was placed at a positive angle and another placed at a negative angle; the angular difference and offset were adjusted for each animal so that both rostral and caudal stimuli fell within the range of vibrissa motion (Figure 2.6A, 2.6B, 2.6D, and 2.6E).

Video imaging

High-speed videography was used to characterize the movement of the vibrissae once discrimination was established. An IEEE-1394 monochrome complimentary metal oxide semiconductor camera (Basler Vision Technologies, 602f [http://www.baslerweb.com/]) with infrared sensitivity was mounted under the elevated shelf in the training enclosure and focused on the plane of the nose poke using a television lens (f/0.95, 17 mm, JML Optical Industries, 71932 [http://www.jmloptical.com/]) and a 45 ° mirror under the stimuli (Figure 2.2A). Illumination was provided by an infrared lamp (The LED Light, 850 nm peak [http://www.theledlight.com/]), which was modified to double output power, while strobed and filtered at 850 nm to reduce leakage into the rat-visible spectrum. The camera was interfaced to a personal computer running custom LabVIEW software and typically acquired 360 _ 300 pixel images at 200 Hz with a 1.2-ms exposure. Images were read into a circular buffer, and 600 images were saved to disk 2.5 s after the start of each behavioral trial, so that 0.5 s of pre-trial video was included in each video sequence.

Video images were analyzed in MatLab (The Mathworks [http://www.mathworks.com/]). Gross head motion was extracted from the videos to control for cases in which animals were able to break fixation and reach the stimulus

before it could be fully withdrawn. Vibrissa motion was estimated from line-scan data extracted from an image column over multiple time points (Figure 2.6B and 2.6E). The median column over time was subtracted from each column to remove stationary objects, and custom segmentation and tracking algorithms (D. N. Hill and S.B. Mehta, unpublished data) were applied to estimate vibrissa position at each time point. This line-scan analysis was performed on image columns ten pixels to the left and right of the stimulus to avoid contamination from the motion of the stimulus itself, and vibrissa position in the vicinity of the stimulus was interpolated from a linear fit through these left and right position estimates. Over these short regions, vibrissae were well approximated with a linear fit; quadratic fits from three-point estimates showed negligible contributions from the second-order coefficient. For simplicity, line scans were used throughout rather than arcs, and the position of the vibrissa tracks along the vibrissa length varied slightly. In these tracks, the distance of the line-scan column from the mystacial pad at 30 ° was approximately 15% greater than the distance at 0 °. However, the placement of the stimuli was such that there was no systematic difference in the length at which a vibrissa contacted the rostral and caudal stimuli.

To identify potential contact events, the motion of the stimulus was also extracted from the video. Epochs were identified in which the vibrissa trajectory overlapped the stimulus position and showed a velocity of no more than four pixels per frame (Figure 2.6H). We used this heuristic because we lacked a bona fide detector for stimulus contact and because image overlap of the vibrissa with the stimulus did not necessarily correspond to physical contact in three dimensions. However, this estimate of vibrissa

contact was highly accurate, as verified by manual inspection of the video corresponding to a representative sample of contact events.

Operant shaping

The discrimination behavior was shaped in three stages through classical operant training techniques (Figure 2.7) [70]. A small number of parameters were varied in the behavioral program to increment task difficulty, and a large part of training occurred without further experimenter intervention. The parameters used in Figure 2.7 and in the description below are: *T,* trial length; *D,* delay between trials; *N,* duration of nose fixation; *P,* delay until audio prompt; and *L,* number of lever press responses required to obtain a reward. *P* and *L* were used in rewarded stimulus trials only.

The first stage defined the lever response and brought it under experimental control (Figure 2.7A). In this stage, animals were required to be in the tunnel without emitting lever press responses for an interval of *D* seconds to elicit an audio prompt, i.e., 300 ms at 2 kHz, which indicated the start of a trial. The first lever press response within *T* seconds following the prompt was rewarded with a 50-_l reward, signaled by a light-emitting diode indicator as described above. At the end of *T* seconds, the trial ended, and any water still in the dispenser was removed by vacuum. This schedule encouraged early responses relative to the audio prompt, because responses that were late but still within *T* seconds after the prompt afforded less time to drink. The trial length *T* was set here to 6 s, and the delay parameter *D* was increased from 0.25 s to 4 s. Human intervention was often necessary in the first several sessions to model the lever press response, but was minimal as *D* increased.

The second stage shaped the nose fixation behavior (Figure 2.7B). Here, the *D* parameter from stage 1 was increased from 4 s to 60 s, so that the audio prompt was more difficult to elicit by waiting alone. As before, the first lever press response within $T = 6$ s of the prompt was rewarded. A nose poke response of duration *N* seconds short-circuited this delay and immediately caused the start of a trial. The nose fixation duration *N* was increased from 0.063 s to 1.5 s in increments of 0.063 s. Acquisition of the basic nose poke behavior was assisted by increasing the sensitivity of the nose cone sensor and baiting the nose cone with water or chocolate milk; after this acquisition, little intervention was required as the fixation duration parameter *N* was increased.

The third training stage transferred the reward context from the audio prompt to one of the two stimuli in a go/no-go task (Figure 2.7D). Each animal was randomly and permanently assigned a relative position, either more rostral or more caudal. For each session, the tactile stimulus that occupied this relative angular position was designated ***S***+, as opposed to the ***S***_ stimulus at the second position. In this stage, trials could only be initiated by nose fixation. After a nose poke of $N = 1.5$ s, either the ***S***+ or the ***S***_ stimulus, chosen at random with equal probability, was delivered to indicate the start of a trial. For ***S***_ trials, lever press responses in the *T* seconds ($T = 6$ s) following stimulus delivery were unrewarded, and the audio prompt used in earlier stages was never presented. For ***S***+ trials, the first lever press in the *T* seconds ($T = 6$ s) after the start of the trial was rewarded, as before. In ***S***+ trials only, if no lever press response had occurred within *P* seconds after stimulus delivery, an audio prompt was presented to the animal. This delay *P* was increased from 0.125 s to *T* seconds and, as before, any unfinished reward was removed after the trial's end at *T* seconds. Thus, responses to the audio prompt resulted in

less time to drink than responses that used the ***S***+ stimulus as a predictor. In both ***S***+ and ***S***_ trials, the stimulus was removed from the vibrissa field if nose poke fixation was broken or the trial ended, whichever came first.

Acquisition of stimulus discrimination was indicated when the number of lever press responses in the first *P* seconds of a trial differed significantly between ***S***+ and ***S***_ trials. The first *P* seconds were used because an animal had access to additional information, in the form of the cue, after *P* seconds. At this point, the audio prompt was eliminated and performance was measured. For some animals, a final parameter was varied during this testing stage. The number of lever press responses *L* (Figure 2.7D) required to obtain a reward increased from one to five, and the trial length *T* was increased to 8 s to allow time for the longer behavioral response. This manipulation increased the effort necessary to complete a full response in the go/no-go task and discouraged the animal from responding if the stimulus did not predict a reward. The direct use of air puffs as negative reinforcement was unsuccessful at strengthening this asymmetry of response, as it tended to lower the total number trials rather than selectively suppressing ***S***_ responses.

Fluid restriction and training sessions

Animals initially acclimated to handling and to chocolate milk (Yoo-Hoo, Cadbury-Schweppes [http://www.cadburyschweppes.com/EN]) from the fluid dispenser in the behavioral chamber over a period of 2–3 wk. Animals were housed in pairs and maintained on a standard light/dark cycle, and both morning and evening training

sessions were used. We did not observe any significant effect of time of day or estrous cycle periodicity on behavioral performance. Further, although chocolate milk was used early in training, fluid-deprived animals appeared to perform equally well for water rewards, which were preferred for ease of delivery.

Upon reaching 230 g, animals entered a fluid restriction regimen in which water was removed from their home cage 16–23 h before training to increase motivation. Animals were allowed ad libitum fluid access two days a week, and weights were monitored daily. We used a variable restriction schedule for two reasons. First, the total duration of the training ranged from 6–12 mo, and the long-term health of the animals was a concern. Second, increased pretraining fluid deprivation did not correlate strongly with an increased number of trials per session. Further, the longest deprivation durations we tried, i.e., 24 h, at times caused animals to respond indiscriminately to both ***S***+ and ***S***_ stimuli. Restriction duration was thus tuned separately for each animal.

Daily training sessions were 20–30 min in duration. The physical proximity of the tactile stimulus and response apparatus allowed animals to perform a large number of trials in this amount of time; a total of 50 trials was typical in intermediate stages of training, and a total of 100 trials, of which approximately 50 were rewarded, was typical of well-trained animals on the full discrimination task. These large numbers of trials were needed to obtain statistical evidence of discrimination, and we thus required animals to perform at high rates. As such, five of the initial cohort of 24 rats were removed early in training, i.e., after fewer than 30 sessions, because they performed significantly fewer trials than their littermates. A further five animals were removed at intermediate stages,

i.e., after approximately 100 sessions, for performing small numbers of trials after the lever and nose poke were introduced. We did not consider these ten animals in the summary analysis shown in Figure 2.3, because they were not introduced to the stimulus.

For the remaining 14 animals, the number of sessions required to acquire the lever press response and nose fixation of 1.5 s ranged from 225 for our earliest animals to 61 for animals who started training later in the study. This large reduction in the number of sessions occurred as the training procedures described above were established, and the earlier numbers reflect our adjustments to these procedures rather than the intrinsic time needed to train these behaviors. Further, we chose relatively short session durations to facilitate the concurrent training of multiple animals as we developed the procedures described above. In many cases, however, animals would still be performing trials at the end of a session, albeit at a decreasing pace. It is thus likely that the use of our eventual protocol with longer sessions to obtain more trials per animal per day would have further decreased the training time necessary to achieve this level of behavioral performance.

The number of sessions required to learn the stimulus task was more variable, ranging from 17 to 75, and did not reliably decrease over the course of the study. Further, this measure did not appear correlated with eventual performance as the vibrissae were trimmed.

Vibrissa trimming

Animals that successfully discriminated their assigned ***S***+ and ***S***_ stimuli in the absence of the audio prompt (Figure 2.7D) in multiple consecutive sessions were then

trained with only a single vibrissae row intact. At least once per week, animals at this stage were lightly anesthetized on isoflurane for vibrissa trimming. All vibrissae on the left side and all vibrissae on the right side except for the C row were cut. Animals continued training with a single row until they again demonstrated successful discrimination in multiple consecutive sessions, at which point their vibrissae were further trimmed to leave only a single vibrissa intact. This vibrissa was required to be sufficiently long to reach the stimuli and was thus typically chosen to be C1. Animals that performed successfully with a single intact vibrissa were recorded on video as described above and finally challenged with a series of controls.

2.5 Acknowledgments

Chapter II is a reprint, in full, of the material as it appears in *PLoS Biology*, 2007 Feb;5(2):e15. The dissertation author is the second author on this paper from work completed in the Kleinfeld lab. I would like to thank the first author, Samar Mehta, for his mentoring and collaboration on this project, co-author Rodolfo Figueroa for his teamwork in the acquisition of behavioral data, co-author Professor Ben Williams, and senior author Professor David Kleinfeld.

Figure 2.1 Two Localization Algorithms: Topographic Labeled-Line and Haptic-Sensing

Each cartoon depicts an animal contacting a small object (black circle) and an idealization of the resulting neural streams (dashed arrows) afferent to the vibrissa somatosensory cortex.

(A) A labeled-line strategy. During small motion, the location of an object is encoded in the identity of the vibrissa that contacts it. For clarity, only one row of vibrissae is shown; additional rows do not directly aid localization.

(B) A sensorimotor strategy. During large motion, contact on a given vibrissa leaves object position ambiguous. Information about the position of that vibrissa at the time of contact resolves the confound. This scheme does not require multiple vibrissae.

(C) Rat with only the C row intact. The _ stradler is shown contacting the caudal stimulus. The red arrows point to the location of contact. This stimulus is 30 ° caudal to the stimulus shown in (B).

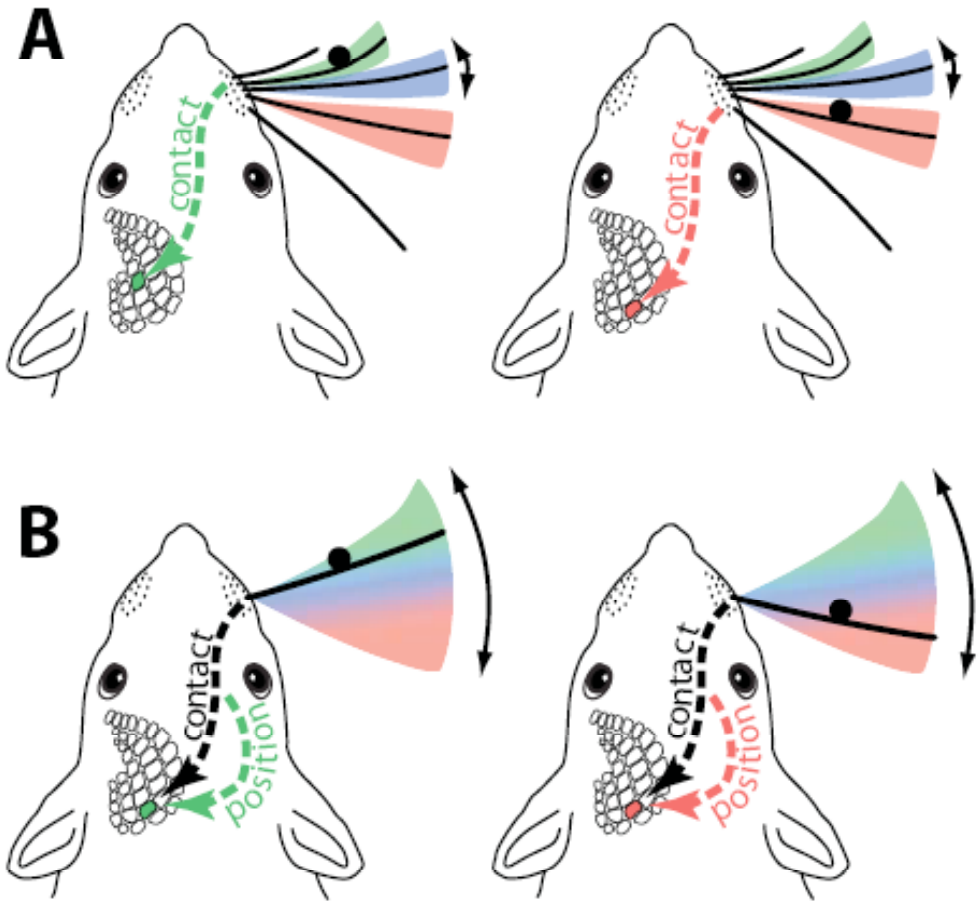
A
contact
contact
B
contact
position
contact
position

Figure 2.2 Apparatus for Behavioral Testing and Training

(A) View of training arena. Animals were placed in the vestibule at the start of a session, and their position was monitored through infrared sensors. The U-shaped restraint bar blocked the tunnel while allowing access to the operant lever and nose poke. Discrimination trials started when an animal interrupted the nose poke sensor, causing either the rostral or caudal stimulus pin to descend into the vibrissa field. The stimuli were translated by air-driven pistons and positioned through a circular guide fixed relative to the nose poke (supporting parts omitted for clarity). Lever presses in response to the ***S***+ stimulus, either rostral or caudal for each animal, were rewarded with a drop of water in the fluid dispenser. Any remaining fluid was withdrawn by vacuum at the end of the trial. An infrared lamp provided backlit contrast of the head and vibrissa for the camera recording the ventral view shown in (C). The entire arena was enclosed in a darkened, sound-attenuated chamber (not shown).

(B) Detail of stimulus area from (A).

(C) View of stimulus area from (A), as seen by the camera. The nose poke allowed reproducible positioning of the stimuli in head-centered coordinates (see also Figures 2.6A, 2.6B, 2.6D, and 2.6E).

[Original artwork: Jenny Groisman]

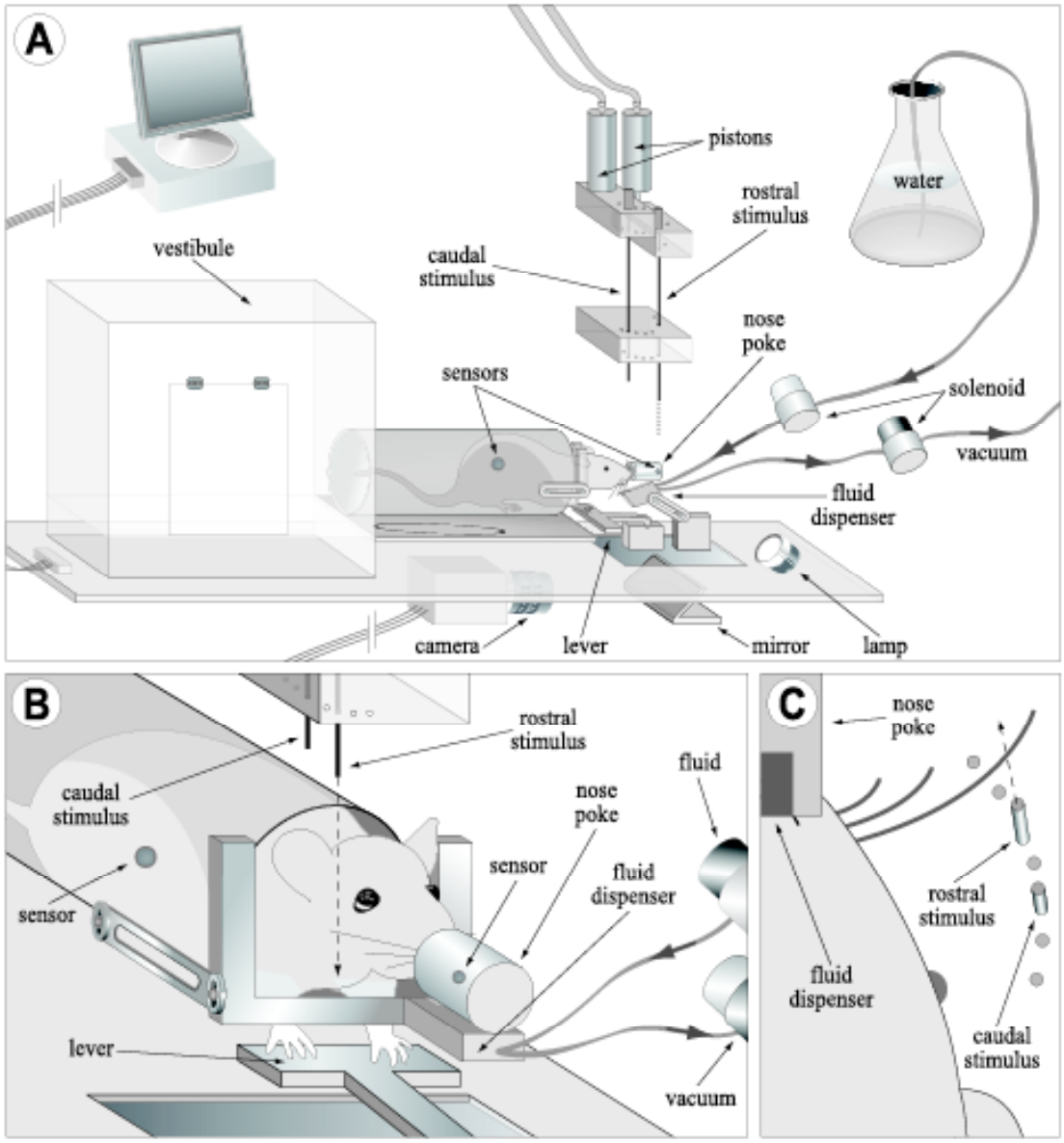
A
pistons
water
rostral stimulus
vestibule
caudal stimulus
nose poke
sensors
solenoid
vacuum
fluid dispenser
camera
lever
mirror
lamp
B
rostral stimulus
caudal stimulus
fluid
nose poke
sensor
fluid dispenser
sensor
lever
vacuum
C
nose poke
rostral stimulus
fluid dispenser
caudal stimulus

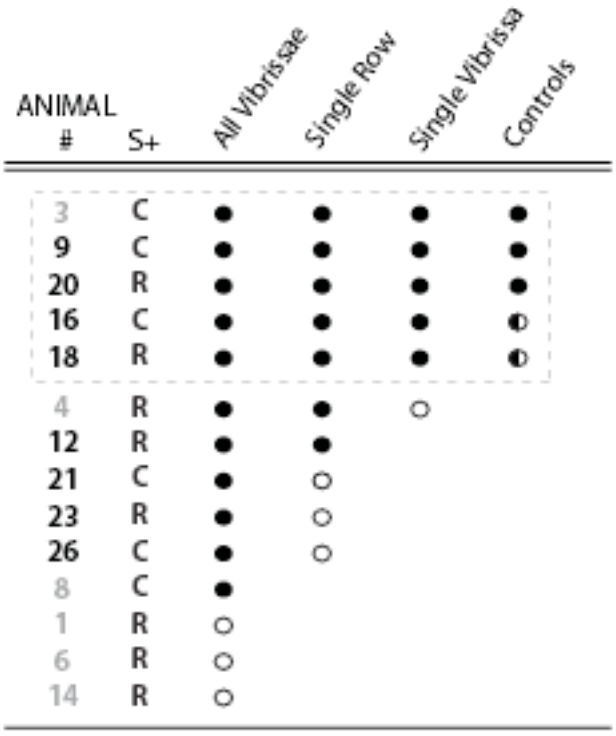

Figure 2.3 Summary of Performance Levels Achieved for All Animals

Each row represents one of 14 rats tested on the spatial discrimination task. The first column gives an identifying number, and the second column gives the corresponding ***S***+ stimulus assignment (R for rostral and C for caudal). Animals with gray numbers were tested with response requirement *L* (Figure 2.7D) set to 1, and the remaining animals were tested with *L* = 4–6. The next three columns summarize performance as the number of intact vibrissae decreased. Filled circles indicate stable performance at a given level, whereas open circles imply that an animal was tested but did not achieve stable performance. "Stable performance" is defined here as statistically significant differences in ***S***+ and ***S***_ responses over multiple sessions. In two cases, rat number 8 and rat number 12, external circumstances caused the end of testing despite success at all attempted stages. The final column describes testing under various control conditions, and filled circles here indicate that a given animal passed all controls. The dashed box highlights those animals that succeeded in the task when limited to a single vibrissa. Among these rats, those that habitually sampled the stimuli with their head are shown with half-filled circles in the control column, because it was unclear whether this movement was involved in forming a spatial percept.

Figure 2.4 Temporal Profile of Behavioral Responses for One Session

(A) Lever press responses in a session by rat number 20 restricted to the right C1 vibrissa. The trial length *T* was 8 s and response requirement *L* (Figure 2.7D) was five lever presses. Each row shows the first five lever presses in one trial, with responses from ***S***+ trials in green and those from ***S***_ trials in red. The fifth response in an ***S***+ trial was followed by a reward. This session consisted of 58 ***S***+ trials and 56 ***S***_ trials over 30 min.

(B) Cumulative lever press counts from (A), averaged separately over ***S***+ and ***S***_ trials. The inset illustrates this data transformation. The green line and shaded region give the mean ± 2σ (standard error of mean) cumulative lever press counts for ***S***+ trials; equivalent data for ***S***_ trials are in red. The gray arrows at 0.5 s mark the time point after which the 2σ error regions remain nonoverlapping.

(C) Distribution of latencies from the start of a trial to the fifth lever press, for the trials shown in (A). Trials with fewer than five responses are shown at infinite latency. The bars and left ticks show numbers of trials as a function of latency, and the lines and right ticks show the same data as cumulative distributions. The ***S***+ and ***S***_ distributions are statistically distinct ($p < 0.001$, two-sided K-S test). Green indicates ***S***+ and red indicates ***S***_.

(D) Receiver operating characteristic curves summarizing differences between ***S***+ and ***S***_ latency distributions for multiple sessions. The fraction of ***S***+ trials with latencies below a threshold τ is plotted against the fraction of ***S***_ trials with latencies below the same τ; the curves are then constructed as τ varies parametrically. The result for the data from (C) is shown by the solid black line, where the heavy part of the line corresponds to the threshold τ having traversed the heavy parts of the lines in the inset data. The gray lines are from 12 subsequent single vibrissa sessions by the same animal (rat number 20). The orange line corresponds to the control session from Figure 2.5C. Identical ***S***+ and ***S***_ response distributions would yield the diagonal dashed line.

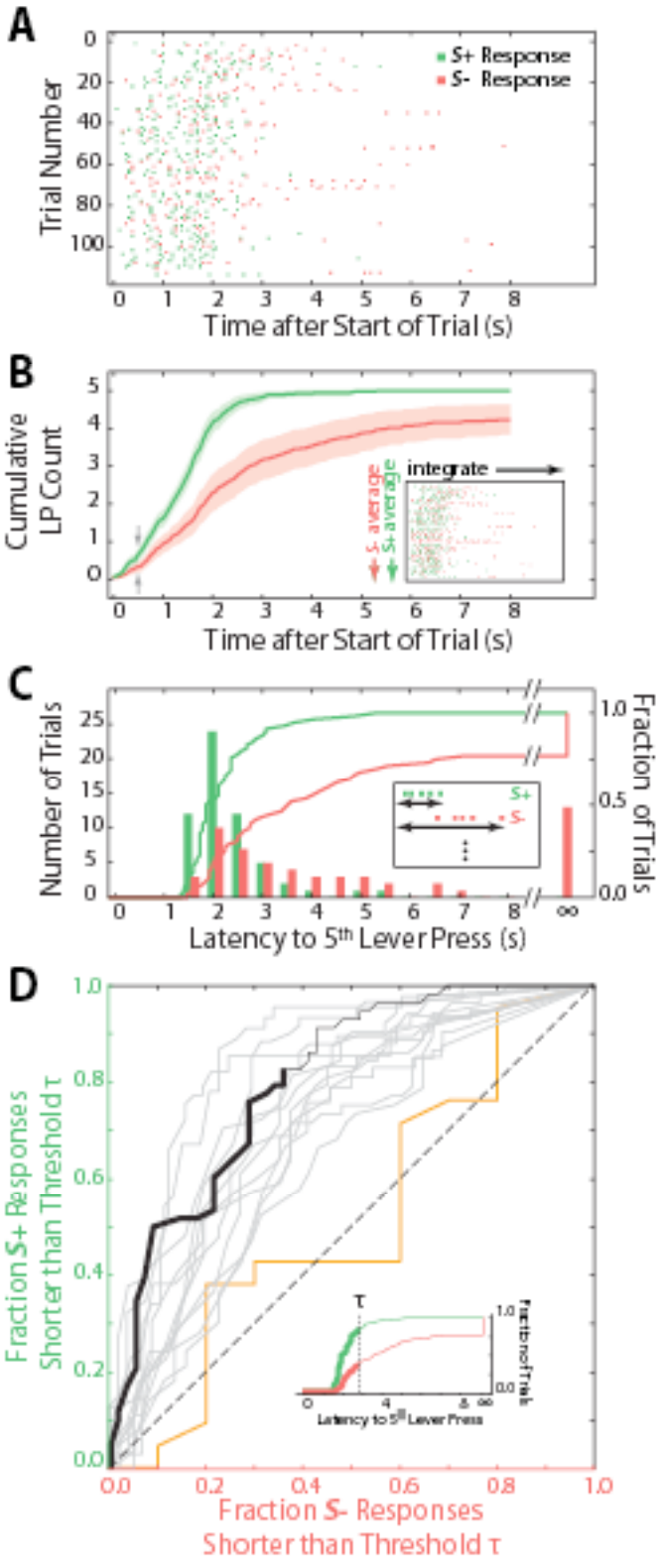
A
S+ Response
S- Response
Trial Number
Time after Start of Trial (s)
B
Cumulative LP Count
integrate
S- average
S+ average
Time after Start of Trial (s)
C
Number of Trials
Fraction of Trials
S+
S-
Latency to 5th Lever Press (s)
D
Fraction S+ Responses Shorter than Threshold τ
Fraction S- Responses Shorter than Threshold τ
τ

Figure 2.5 Controls for Extravibrissal Cues

(A) Latency distributions for a standard session, performed by rat number 20 and similar to Figure 2.4C. This session contained 54 ***S***+ trials and 51 ***S***_ trials and showed a significant difference in the latency to the completion of a five–lever press response requirement when comparing responses from ***S***+ and ***S***_ trials ($p < 0.001$, two-sided K-S test).

(B) A session performed without infrared (IR) illumination. This session contained 45 ***S***+ trials and 54 ***S***_ trials and showed a significant difference between ***S***+ and ***S***_ response latencies ($p < 0.001$, two-sided K-S test).

(C) A session in which the stimulus pins were absent. This session contained 21 ***S***+ trials and ten ***S***_ trials and showed no significant difference between ***S***+ and ***S***_ response latencies ($p > 0.1$, two-sided K-S test). The number of trials was smaller here because the animal performed trials at a lower rate in this condition, and because the session was short (15 min versus 30 min above) to prevent extinction of the discrimination behavior.

(D) Data from the session shown in (A) above, restricted to trials in which the animal broke fixation before the stimulus had fully extended. This condition included seven ***S***+ trials and ten ***S***_ trials and showed no significant difference between ***S***+ and ***S***_ response latencies ($p > 0.1$, two-sided K-S test).

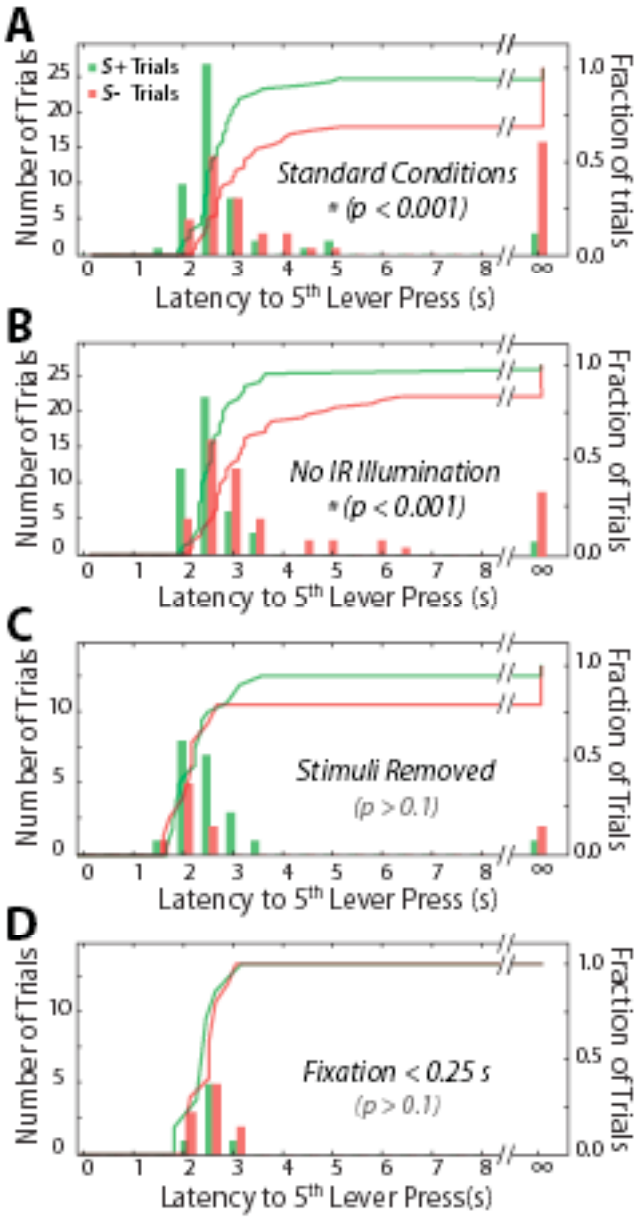
A
S+ Trials
S- Trials
Number of Trials
Fraction of trials
Standard Conditions
* (p < 0.001)
Latency to 5th Lever Press (s)
B
No IR Illumination
* (p < 0.001)
C
Stimuli Removed
(p > 0.1)
D
Fixation < 0.25 s
(p > 0.1)

Figure 2.6 Patterns of Vibrissa Motion during Discrimination

The data in (A) to (F) are from the session analyzed in Figure 2.4, with ***S***+ stimulus (rostral for rat number 20) at +15 ° and ***S***_ stimulus at 0 °. The scale bar in the photographs is equal to 4 mm.

(A) Projection of 400 frames from a single ***S***+ trial. This image shows the range of vibrissa positions in the interval from _0.5 to +1.5 s relative to the start of a trial; this range arises from whisking movements as well as small head motion and translations of the mystacial pad. The ***S***+ stimulus neighborhood is indicated by a green box, and the ***S***_ stimulus region is in red. The dark line in the green box is due to stimulus motion; compare to the green boxes in (B) and (E), which show fully extended and retracted positions, respectively. Stimulus displacement appears smaller than the true 5.08-cm travel because the motion was nearly normal to the focal plane (Figures 2.2A and 2.2C).

(B) Single frame in which the vibrissa contacted the ***S***+ stimulus, taken from the trial in (A). The blue rectangle indicates the region in which vibrissa position was estimated for (C).

(C) Vibrissa position as a function of time. The green and red bands correspond to the vertical extent of the similarly colored boxes in (A). The gray lines give position traces from 58 ***S***+ trials, and the black line highlights the trial shown in (A). The stimulus is not seen here, but both rostral and caudal stimuli started their descent at ~30 ms and reached full extension at ~300 ms. The stimuli were fully withdrawn within 150 ms of the end of nose poke fixation; this occurred at a median of 315 ms for ***S***+ trials and 530 ms for ***S***_ trials. The green arrow marks the ***S***+ contact in (B), and the dashed black line demonstrates the ~100-ms delay in the onset of whisking after the start of a trial. Breaks in the lines are due to tracking errors.

(D and E) Video images from an ***S***_ trial, analogous to (A) and (B).

(F)Vibrissa position traces for 56 ***S***_ trials, analogous to (C). The red arrow marks the ***S***_ contact in (E).

(G) Summary of all tracked vibrissa positions from 0–0.25 s after the start of each trial, including both ***S***+ and ***S***_ trials. The green and red bands correspond to the vertical extent of the corresponding regions in (A) and (C) and show that the vibrissa scanned both stimulus positions. The thick line is derived from the session analyzed in (A) through (F). The thin lines are taken from five more sessions by rat number 20 and four by rat number 9; these lines were scaled to align with the ***S***+ and ***S***_ bands drawn for the session represented by the thick line.

(H) Precontact vibrissa velocities. Bold lines show the distribution of angular velocities as the vibrissa approached the stimulus for all contacts from (C) and (F), excluding intervals in which the vibrissae were in contact with a stimulus and thus not appreciably moving (defined as a velocity ≤1 pixel per 5 ms frame). The thin lines are taken from the sessions considered in (G). In each case, the ***S***+ and ***S***_ stimuli are associated both with

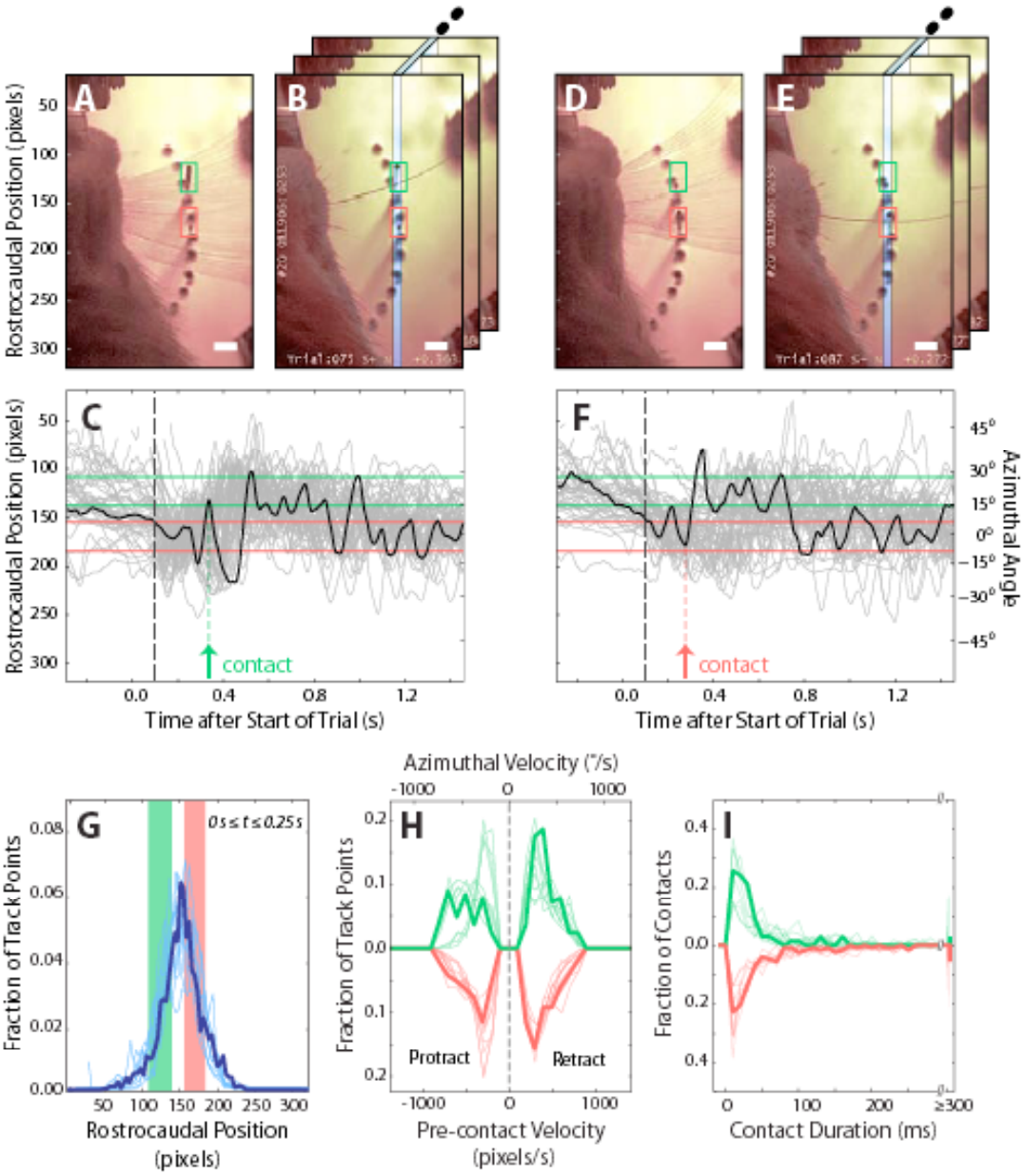
A
B
D
E
Rostrocaudal Position (pixels)
50
100
150
200
250
300
C
F
contact
contact
0.0
0.4
0.8
1.2
Time after Start of Trial (s)
Time after Start of Trial (s)
45°
30°
15°
0°
−15°
−30°
−45°
Azimuthal Angle
Azimuthal Velocity (°/s)
-1000
0
1000
G
0 s ≤ t ≤ 0.25 s
Fraction of Track Points
0.08
0.06
0.04
0.02
0.00
50 100 150 200 250 300
Rostrocaudal Position (pixels)
H
Protract
Retract
0.2
0.1
0.0
0.1
0.2
-1000
0
1000
Pre-contact Velocity (pixels/s)
I
Fraction of Contacts
0.4
0.2
0.0
0.2
0.4
0
100
200
≥300
Contact Duration (ms)

Figure 2.7 Behavioral Logic for Operant Training and Discrimination Testing

All diagrams use 0.5-s intervals here for clarity; the actual sampling rate was 16 Hz.

(A) Lever press response training. Animals that waited *D* seconds without emitting a lever press would elicit an audio prompt that signaled the start of a trial. The first lever press response in the following $T = 6$ s was rewarded with a drop of water. At the end of the trial, any remaining water was withdrawn. *D* was increased from 0.25 s to 4 s.

(B) Nose poke training. *D* was first increased from 4 to 60 s to decrease the frequency of trial initiated by waiting. Trials could alternatively be initiated if an animal placed its nose in the nose poke for *N* seconds. As this behavior was established, *N* was increased from 0.063 s to 1.5 s.

(C) Stimulus training. All trials in this stage were initiated by a 1.5-s nose poke. Each trial was randomly assigned as either ***S***+ or ***S***_, and the start of the trial was signaled by the descent of the corresponding stimulus pin. The pin remained in the vibrissa field until nose fixation was broken or until the trial ended. In ***S***+ trials, the first lever press response after the start of the trial resulted in a reward. If no response occurred within *P* seconds, an audio prompt sounded. *P* was increased from 0.125 s to 6 s. Lever presses were ignored in ***S***_ trials.

(D) Stimulus discrimination testing. The audio prompt was eliminated from ***S***+ trials. The number of lever press responses, *L,* required to obtain a reward in ***S***+ trials was increased until a difference between ***S***+ and ***S***_ responses was apparent. This value was typically $L = 5$ or 6; the example here illustrates $L = 2$. The structure of ***S***_ trials was unchanged.

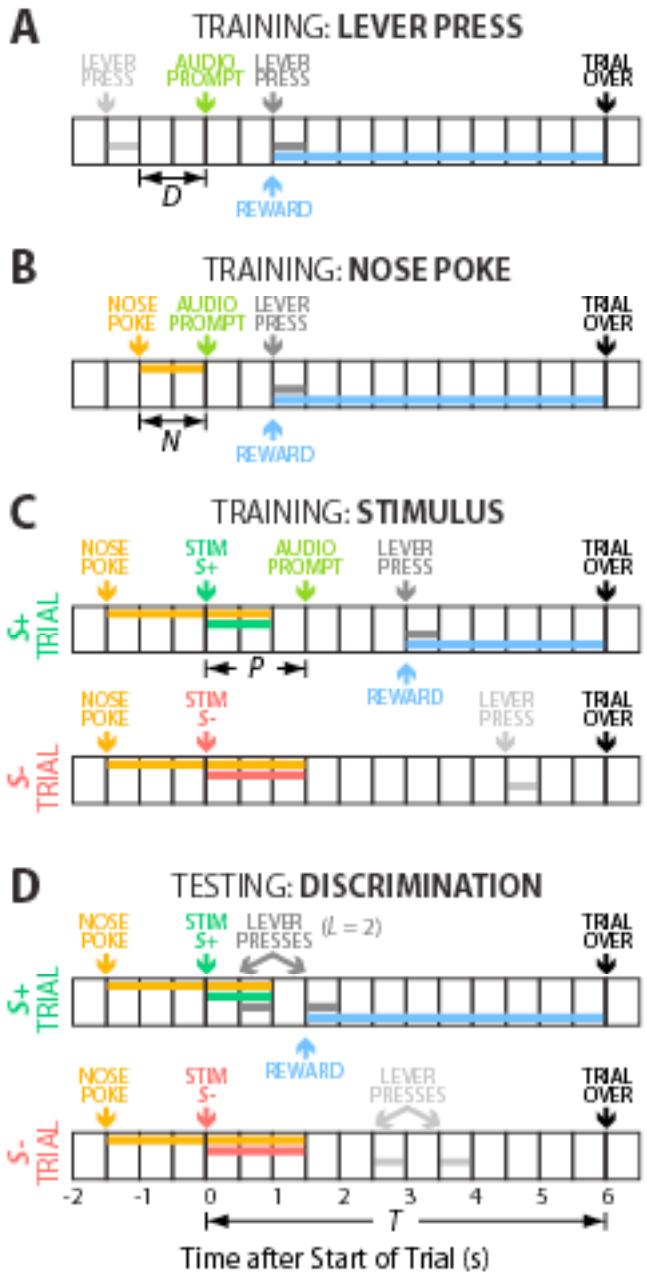
A
TRAINING: LEVER PRESS
LEVER PRESS
AUDIO PROMPT
LEVER PRESS
TRIAL OVER
D
REWARD
B
TRAINING: NOSE POKE
NOSE POKE
AUDIO PROMPT
LEVER PRESS
TRIAL OVER
N
REWARD
C
TRAINING: STIMULUS
NOSE POKE
STIM S+
AUDIO PROMPT
LEVER PRESS
TRIAL OVER
S+ TRIAL
P
REWARD
NOSE POKE
STIM S-
LEVER PRESS
TRIAL OVER
S- TRIAL
D
TESTING: DISCRIMINATION
NOSE POKE
STIM S+
LEVER PRESSES (L = 2)
TRIAL OVER
S+ TRIAL
REWARD
NOSE POKE
STIM S-
LEVER PRESSES
TRIAL OVER
S- TRIAL
-2
-1
0
1
2
3
4
5
6
T
Time after Start of Trial (s)

REFERENCES

1. Gibson JJ (1966) The senses considered as perceptual systems. Boston: Houghton Mifflin Company. 335 p.

2. Peterka RJ (2002) Sensorimotor integration in human postural control. J Neurophysiol 88: 1097–1118.

3. Deliagina TG, Orlovsky GN, Zelenin PV, and Beloozerova IN (2006) Neural bases of postural control. Physiology (Bethesda) 21: 216–225.

4. van Beers RJ, Wolpert DM, and Haggard P (2001) Sensorimotor integration compensates for visual localization errors during smooth pursuit eye movements. J Neurophysiol 85: 1914–1922.

5. Moss CF, Bohn K, Gilkenson H, and Surlykke A (2006) Active listening for spatial orientation in a complex auditory scene. PLoS Biol 4(4): e79. doi:10.1371/journal.pbio.0040079

6. Cullen KE and Roy JE (2004) Signal processing in the vestibular system during active versus passive head movements. J Neurophysiol 91: 1919–1933.

7. Gustafson JW and Felbain-Keramidas SL (1977) Behavioral and neural approaches to the function of the mystacial vibrissae. Psychol Bull 84: 477–488.

8. Neimark MA, Andermann ML, Hopfield JJ, and Moore CI (2003) Vibrissa resonance as a transduction mechanism for tactile encoding. J Neurosci 23: 6499–6509.

9. Hartmann MJ, Johnson NJ, Towal RB, and Assad C (2003) Mechanical characteristics of rat vibrissae: Resonant frequencies and damping in isolated whiskers and in the awake behaving animal. J Neurosci 23: 6510–6519.

10. Arabzadeh E, Zorzin E, and Diamond ME (2005) Neuronal encoding of texture in the whisker sensory pathway. PLoS Biol 3(1): e17. doi:10.1371/journal.pbio.0030017

11. Andermann ML, Ritt J, Neimark MA, and Moore CI (2004) Neural correlates of vibrissa resonance: Band-pass and somatotopic representation of high-frequency stimuli. Neuron 42: 451–463.

12. Hipp J, Arabzadeh E, Zorzin E, Conradt J, Kayser C, et al. (2006) Texture signals in whisker vibrations. J Neurophysiol 95: 1792–1799.

13. Moore C and Andermann ML (2005) The vibrissa resonance hypothesis. In: Ebner FF, editor. Neural plasticity in adult somatic sensory-motor systems. Boca Raton: Taylor & Francis.

14. Vincent SB (1912) The function of the vibrissae in the behavior of the white rat. Behavior Monographs 1: 7–81.

15. Shuler MG, Krupa DJ, and Nicolelis MA (2001) Bilateral integration of whisker information in the primary somatosensory cortex of rats. J Neurosci 21: 5251–5261.

16. Solomon JH and Hartmann MJ (2006) Biomechanics: Robotic whiskers used to sense features. Nature 443: 525.

17. Harvey MA, Bermejo R, and Zeigler HP (2001) Discriminative whisking in the head-fixed rat: Optoelectronic monitoring during tactile detection and discrimination tasks. Somatosens Mot Res 18: 211–222.

18. Polley DB, Rickert JL, and Frostig RD (2005) Whisker-based discrimination of object orientation determined with a rapid training paradigm. Neurobiol Learn Mem 83: 134–142.

19. Benison AM, Ard TD, Crosby AM, and Barth DS (2006) Temporal patterns of field potentials in vibrissa/barrel cortex reveal stimulus orientation and shape. J Neurophysiol 95: 2242–2251.

20. Hutson KA and Masterton RB (1986) The sensory contribution of a single vibrissa's cortical barrel. J Neurophysiol 56: 1196–1223.

21. Krupa DJ, Matell MS, Brisben AJ, Oliveira LM, and Nicolelis MAL (2001) Behavioral properties of the trigeminal somatosensory system in rats performing whisker-dependent tactile discriminations. J Neurosci 21: 5752–5763.

22. Ling JK (1966) The skin and hair of the southern elephant seal, *Mirounga leonina* (Linn.). Aust J Zool 14: 855–866.

23. Rice FL and Arvidsson J (1991) Central projections of primary sensory neurons innervating different parts of the vibrissae follicles and intervibrissal skin on the mystacial pad of the rat. J Comp Neurol 309: 1–16.

24. Kleinfeld D, Berg RW, and O'Connor SM (1999) Anatomical loops and their electrical dynamics in relation to whisking by rat. Somatosens Mot Res 16: 69–88.

25. Nguyen Q-T and Kleinfeld D (2005) Positive feedback in a brainstem tactile sensorimotor loop. Neuron 45: 447–457.

26. Fee MS, Mitra PP, and Kleinfeld D (1997) Central versus peripheral determinates of patterned spike activity in rat vibrissa cortex during whisking. J Neurophysiol 78: 1144–1149.

27. Yu C, Mutlu S, Selvaganapathy P, Mastrangelo CH, Svec F, et al. (2003) Flow control valves for analytical microfluidic chips without mechanical parts based on thermally responsive monolithic polymers. Anal Chem 75: 1958–1961.

28. Szwed M, Bagdasarian K, and Ahissar E (2003) Coding of vibrissal active touch. Neuron 40: 621–630.

29. Crochet S and Petersen CCH (2006) Correlating membrane potential with behaviour using whole-cell recordings from barrel cortex of awake mice. Nat Neurosci 9: 608–609.

30. Perkel DH and Bullock TH (1968) Neural coding. Neurosciences Research Program Bulletin 6: 223–344.

31. Carvell GE and Simons DJ (1990) Biometric analyses of vibrissal tactile discrimination in the rat. J Neurosci 10: 2638–2648.

32. Guic-Robles E, Valdivieso C, and Guajardo G (1989) Rats can learn a roughness discrimination using only their vibrissal system. Behav Brain Res 31: 285–289.

33. Berg RW and Kleinfeld D (2003) Rhythmic whisking by rat: Retraction as well as protraction of the vibrissae is under active muscular control. J Neurophysiol 89: 104–117.

34. Bermejo R and Zeigler HP (2000) “Real-time” monitoring of vibrissa contacts during rodent whisking. Somatosens Mot Res 17: 373–377.

35. Fee MS, Mitra PP, and Kleinfeld D (1996) Variability of extracellular spike waveforms of cortical neurons. J Neurophysiol 76: 3823–3833.

36. Kleinfeld D, Ahissar E, and Diamond ME (2006) Active sensation: Insights from the rodent vibrissa sensorimotor system. Curr Opin Neurobiol 16: 435–444.

37. Mehta SB and Kleinfeld D (2004) Frisking the whiskers: Patterned sensory input in the rat vibrissa system. Neuron 41: 181–184.

38. Williams BA (1971) Color alternation learning in the pigeon under fixed-ratio schedules of reinforcement. J Exp Anal Behav 15: 129–140.

39. Green D and Swets J (1966) Signal detection theory and psychophysics. New York: Wiley. 455 p.

40. Jacobs GH, Fenwick JA, and Williams GA (2001) Cone-based vision of rats for ultraviolet and visible lights. J Exp Biol 204: 2439–2446.

41. Derdikman D, Yu C, Haidarliu S, Bagdasarian K, Arieli A, et al. (2006) Layer-specific touch-dependent depression and facilitation in the somatosensory cortex during artificial active whisking. J Neurosci 26: 9538–9547.

42. Sachdev RHS, Sellien H, and Ebner FF (2001) Temporal organization of multi-whisker contact in rats. Somatosens Mot Res 18: 91–100.

43. Carvell GE, Simons DJ, Lichtenstein SH, and Bryant P (1991) Electromyographic activity of mystacial pad musculature during whisking behavior in the rat. Somatosens Mot Res 8: 159–164.

44. Brecht M, Preilowski B, and Merzenich MM (1997) Functional architecture of the mystacial vibrissae. Behav Brain Res 84: 81–97.

45. Rice FL, Fundin BT, Pfaller K, and Arvidsson J (1994) The innervation of the mystacial pad in the adult rat studied by anterograde transport of HRP conjugates. Exp Brain Res 99: 233–246.

46. Zucker E and Welker WI (1969) Coding of somatic sensory input by vibrissae neurons in the rat's trigeminal ganglion. Brain Res 12: 134–156.

47. Yu C, Derdikman D, Haidarliu S, and Ahissar E (2006) Parallel thalamic pathways for whisking and touch signals in the rat. PLoS Biol 4(5): e124. doi:10.1371/journal.pbio.0040124

48. O'Connor SM, Berg RW, and Kleinfeld D (2002) Coherent electrical activity along vibrissa sensorimotor loops during free whisking in rat. J Neurophysiol 87: 2137–2148.

49. Ganguly K and Kleinfeld D (2004) Goal-directed whisking behavior increases phase-locking between vibrissa movement and electrical activity in primary sensory cortex in rat. Proc Natl Acad Sci U S A 101: 12348–12353.

50. Curtis J and Kleinfeld D (2005) Cortical neurons that code vibrissa contact in face-centered coordinates. in Barrels.

51. Ahissar E (1998) Temporal-code to rate-code conversion by neuronal phase-locked loops. Neural Comput 10: 597–650.

52. Ahissar E, Haidarliu S, and Zackenhouse M (1997) Decoding temporally encoded sensory input by cortical oscillators and thalamic phase comparators. Proc Natl Acad Sci U S A 94: 11633–11638.

53. Ahissar E and Kleinfeld D (2003) Closed loop neuronal computations: Focus on vibrissa somatosensation in rat. Cereb Cortex 13: 53–61.

54. Sachdev RNS, Berg RW, Champney G, Kleinfeld D, and Ebner FF (2003) Unilateral vibrissa contact: Changes in amplitude but not timing of rhythmic whisking. Somatosens Mot Res 20: 162–169.

55. Knutsen PM, Pietr M, and Ahissar E (2006) Haptic object localization in the vibrissal system: Behavior and performance. J Neurosci 26: 8451–8464.

56. Thor DH and Ghiselli WB (1975) Vibrissal anesthesia and suppression of irritable fighting in rats: A temporary duration of effect in experienced fighters. Physiological Psychology 3: 1–3.

57. Griffiths WJ (1960) Responses of wild and domestic rats to forced swimming. Psychol Rep 6: 39–49.

58. Kleinfeld D (2005) Arithmetic with threshold elements and neuronal oscillators. Journal of Physics: solicited.

59. Feldman DE and Brecht M (2005) Map plasticity in somatosensory cortex. Science 310: 810–815.

60. Petersen CC, Grinvald A, and Sakmann B (2003) Spatiotemporal dynamics of sensory responses in layer 2/3 of rat barrel cortex measured in vivo by voltage-sensitive dye imaging combined with whole-cell voltage recordings and neuron reconstructions. J Neurosci 23: 1289–1309.

61. Moore CI, Nelson SB, and Sur M (1999) Dynamics of neuronal processing in rat somatosensory cortex. Trends Neurosci 86: 513–520.

62. Ebner FF and Armstrong-James MA (1990) Intracortical processes regulating the integration of sensory information. Prog Brain Res 11: 129–141.

63. Brecht M, Schneider M, Sakmann B, and Margrie T (2004) Whisker movements evoked by stimulation of single pyramidal cells in rat motor cortex. Nature 427: 704–710.

64. Kleinfeld D and Griesbeck O (2005) From art to engineering? The rise of in vivo mammalian electrophysiology via genetically targeted labeling and nonlinear imaging. PloS Biol 3(10): e355. doi:10.1371/journal.pbio.0030355

65. Ferezou I, Bolea S, and Petersen CCH (2006) Visualizing the cortical representation of whisker touch: Voltage-sensitive dye imaging in freely moving mice. Neuron 50: 617–629.

66. Shuler MG, Krupa DJ, and Nicolelis MA (2002) Integration of bilateral whisker stimuli in rats: Role of the whisker barrel cortices. Cereb Cortex 12: 86–97.

67. Sachdev RN, Sellien H, and Ebner FF (2000) Direct inhibition evoked by whisker stimulation in somatic sensory (S1) barrel field cortex of the awake rat. J Neurophysiol 84: 1497–1504.

68. Hentschke H, Haiss F, and Schwarz C (2006) Central signals rapidly switch tactile processing in rat barrel cortex during whisker movements. Cereb Cortex 16: 1142–1156.

69. Friedman WA, Jones LM, Cramer NP, Kwegyir-Afful EE, Zeigler HP, et al. (2006) Anticipatory activity of motor cortex in relation to rhythmic whisking. J Neurophysiol 95: 1274–1277.

70. Reynolds GS (1968) A primer of operant conditioning. Glenview, IL: Scott, Foresman and Company. 130 p.

Chapter III. Exploratory Whisking by Rat Is Not Phase-locked to the Hippocampal Theta Rhythm

3.1 Abstract

The rat has a strong 6 to 9 Hz rhythm of electrical activity in the hippocampus, known as the theta rhythm. Exploratory whisking, *i.e.*, the rhythmic movement of the rat's vibrissae to acquire tactile information, occurs within the same frequency range as the theta rhythm and provides a model system to examine the relationship between theta rhythm and active sensory movements. In particular, it has been postulated that these two rhythms are phase-locked as a means to synchronize sensory and hippocampal processing. We tested this hypothesis in rats trained to whisk in air. Theta activity was measured via field electrodes in the hippocampus and whisking was measured via the mystacial electromyogram. We calculated the spectral coherence between these two signals as a means to quantify phase-locking. First, we found that the fraction of epochs with high coherence is not significantly greater than that expected by chance (7 of 8 animals and as a population average). Second, we found that the trial averaged coherence is low ($|C| < 0.1$) and, as an average across all animals, statistically insignificant. We further asked if the strength of the theta rhythm correlated with that of whisking, independent of the lack of cycle-by-cycle coherence. We observe that the correlation is weak and insignificant (6 of 8 animals and as a population average). We conclude that there is no relation between the whisking and theta rhythms, at least as animals whisk in air.

3.2 Introduction

It is a matter of conjecture that oscillatory electrical dynamics in populations of hippocampal and cortical neurons serve a functionally relevant role (Buzsaki and Draguhn 2004). A large slow wave oscillation at 6 to 9 Hz, known as the theta rhythm, is one of the most salient electrophysiological properties of the hippocampus and is readily observable in many species. Investigators have been trying to elucidate the functional role of this rhythm. Numerous behavioral studies have demonstrated the coexistence of hippocampal theta rhythm and various voluntary motor patterns including locomotion, orienting, rearing (Vanderwolf 1969; Whishaw and Vanderwolf 1971), swimming (Whishaw and Vanderwolf 1971; Whishaw and Schallert 1977) and paradoxical sleep (Vanderwolf 1969; Winson 1974). Exploratory whisking is an active rhythmic movement of the rat's tactile sensory organs, the vibrissae, which occurs with the same frequency as the theta rhythm (Kleinfeld, Berg et al. 1999; Berg and Kleinfeld 2003) and occurs as a pattern with sniffing and head movements during exploration of novel objects (Welker 1964).

Whisking can occur in the absence of the theta rhythm, as demonstrated in experiments in which the medial septum was lesioned to abolish the theta rhythm (Gray 1971; Semba and Komisaruk 1984). While this establishes the independence of the oscillations, the precise relationship between theta rhythm and whisking is presently ambiguous. Komisaruk (Komisaruk 1970) describes a specific phase relationship between the hippocampal theta rhythm and whisking by rat. A similar claim holds for the relation between the hippocampal theta rhythm and sniffing by hamsters (Macrides 1975). In contrast to this result, Vanderwolf's (Vanderwolf 1969) simultaneous

recordings of hippocampal rhythm and the mystacial electromyogram (EMG), a surrogate of whisking (Carvell, Simons et al. 1991; Berg and Kleinfeld 2003), demonstrate that whisking co-occurs with the theta rhythm only when the rat is moving its head, and that hippocampal activity in an otherwise immobile rat is slow and irregular. Vanderwolf further demonstrates that the theta rhythm is absent in the hippocampus when vibrissae movement and sniffing co-occur in the absence of other movement (Whishaw and Vanderwolf 1971). Recordings from swimming rats also suggest the absence of a one-to-one relationship between whisking and theta (Whishaw and Schallert 1977). Thus, while past results point toward the presence of independent rhythmic generators for whisking and for the theta rhythm, there is a discordant view as to whether these generators can phase-lock. The importance of this issue is that locking can increase the reliability of synaptic transmission. This may provide a natural and efficient means to link the acquisition of new sensory information, such as that gleaned from vibrissa touch, with memories of past experiences and locations, whose storage and recall is dependent of hippocampal activity (Treves and Rolls 1994; Buzsaki 2002; Hasselmo 2005; Vertes 2005).

Here, we revisit the issue of coherence between whisking and the hippocampal theta rhythm. Our hypothesis is that the disparity in the early literature results largely from visual rather than analytical comparison of the measured time-series for whisking versus hippocampal activity. As a point of illustration, we consider the coherence between two rhythmic time-series with substantial overlap in their spectral power estimates (Figures 3.1A and 3.1B upper right). For the case in Panel A, the frequencies of the two signals co-drift and their spectral coherence, a measure of phase locking, is

high. For the case in panel B, the spectral content of the two signals is identical but they drift independently and thus are uncorrelated. The striking difference in coherence is unlikely to be found by visual comparison of the time-series. In the present study, we calculate the coherence between the mystacial EMG and the hippocampal theta rhythm and quantify the statistical significance of the measure across multiple whisking epochs and a cohort of animals.

3.3 Experimental Procedures

Our subjects were 8 female Long Evans rats, 200 to 300 g in mass. The mystacial EMG was recorded during whisking in air in free ranging animals on an elevated runway, as described (Berg and Kleinfeld 2003). These electrodes record motor unit activity from the intrinsic muscles. The signals from two electrodes that spanned mystacial pad were subtracted, high pass filtered, full wave rectified, and low pass filtered to form the measure of analysis which we denote ∇EMG; the gradient operator emphasizes that it is a spatially local measure of muscle activity. The local field potential (LFP) in hippocampus was recorded with a staggered triplet of Teflon coated tungsten microwires, as described (Berg, Friedman et al. 2005). The tips spanned a distance of 1 mm, with the upper and lower electrodes in the dentate gyrus and the central electrode in the CA3 region. The locations of the electrodes were verified *post hoc* from Nissl-stained histological sections, and by comparing the maximal amplitude of the theta rhythm with this in past studies (Robinson 1980). The signals from three electrodes were subtracted to form the discrete second spatial derivative, denoted ∇^2LFP, a measure of the current

source density. This electrical measurement provides a strictly local measure of hippocampal field activity, in this case current flow between the CA3 region and the dentate gyrus.

Each rat was gentled and acclimatized to the experimental environment over a period of 1 week prior to the surgical implantation of the electrodes. The animals recovered for five days upon completion of surgery, after which data was subsequently collected daily for a period of 14 d. Exploratory whisking was encouraged by introducing objects to the animal and by the dimming of lights. In one-half of the animals, the infraorbital branch of the trigeminal nerve (IoN) was lesioned, as described (Berg and Kleinfeld 2003), and data was collected for an additional 4 days. The care and all aspects of the experimental manipulation of our animals were reviewed and approved by the Institutional Animal Care and Use Committee at UCSD.

3.4 Analysis

For each whisking epoch, of T = 2 s, the spectral power of the mystacial ∇EMG and the hippocampal ∇^2LFP and the spectral coherence between these measures, denoted C, were calculated. The single-trial spectra were estimated as an average over K = 5 independent estimates using the multi-taper methods of Thomson (Thomson 1982; Percival and Walden 1993). The half bandwidth is Df = (2K-1)/T = 1.5 Hz. The center frequency for the whisking and theta rhythms were determined as the location of the respective peak in the power spectrum.

The confidence limit for the magnitude of the coherence across all frequencies was estimated from

$$|C|=\mathrm{SQRT}(\,1-P\hat{}[1/(NK-1)]) \qquad (1)$$

in which P = 0.05 represents the 95 % confidence limit, N is the number of trials or epochs, and NK is the number of degrees of freedom (Jarvis and Mitra 2001). The trial-averaged coherence at the whisking frequency was calculated as the mean of the complex-valued coherence. Lastly, the correlation coefficient between the normalized amplitude of the power in the whisking spectrum and that in the hippocampal spectrum, was computed on an epoch-by-epoch basis for each animal. Confidence intervals on the correlation coefficients were computed based on the correlation coefficient between 1000 shuffled and randomly trials.

3.5 Results

We analyzed 885 whisking epochs across 8 animals for which both rhythmic whisking and the hippocampal theta rhythm were within the range of 6 to 9 Hz. In a fraction of the trials, less than 10 % of total, the theta rhythm had marginal power and those trials were discarded. For the example data of Figure 3.2, the power spectra of the ∇EMG and the hippocampal ∇^2LFP were largely overlapping (right upper panels Figure 3.2 A and B). It is further evident that the two rhythms are locked to each other in some whisking epochs (Fig. 2a), but not in other epochs (Fig. 2b). The variability in the coherence across individual epochs illustrates how a limited data sets can be used to support the results of Vanderwolf (Vanderwolf 1969) versus Komisaruk (Komisaruk 1970). This variability does not depend on how closely the two spectral power peaks were aligned.

As a first means to establish the statistics of the coherence across individual epochs within each animal, the coherence between whisking and theta rhythm was computed for each epoch at the frequency of the peak in the whisking power spectrum as well as at the theta peak frequency. The magnitude of coherence between two unrelated processes will satisfy the null hypothesis for $|C| = 0.726$ (Eqn. 1 with $N = 1$, $K = 5$, and $P = 0.05$). The normalized distribution of coherence magnitudes across epochs for a representative animal (animal F9) shows that fewer than 5 % of the epochs exceed this level of coherence (Fig. 3A). This is particularly evident from the cumulative probability distribution, which crosses the 95 % line prior to reaching the significance value of $|C| = 0.726$ (Fig. 3B). As a population, the fraction of trials that had coherence magnitude above the line of significance was calculated at both the whisking frequency

and the theta frequency and compared across animals (Table 3.1). If this fraction was larger than 5 %, as expected by chance, the coherence between whisking and theta rhythm was significant. Seven out of 8 animals had insignificant coherence across trials, in that the cumulative distribution exceeded $|C| = 0.726$ for less than 5 % of the trails (Table 3.1). Critically, a composite analysis that includes all trials in all animals shows that this is insignificant at the $P < 0.05$ level (All, Table 3.1).

As a second means to establish the statistics of the coherence across individual epochs, we calculated the trial-averaged coherence for each animal. Consistent phase locking across epochs would be indicated by a statistically significant value of the magnitude of the coherence after averaging. Four out of eight subjects had insignificant trial-averaged coherence. The remaining four subjects had significant, albeit small, trial-averaged coherence (Table 3.1). Critically, a composite analysis that includes all trials across all animals shows that, on average, there is insignificant coherence (All, Table 3.1). In summary, we fail to reject the null hypothesis of no coherence between exploratory whisking and hippocampal rhythm.

Independent of frequency locking, it is possible that whisking and hippocampal theta rhythm activity can modulate each other on the second to seconds time-scale of individual epochs. To test this, we performed a linear regression analysis between the peak spectral power in the exploratory whisking band with that in the theta rhythm band to determine if the two signals were statistically correlated (Fig. 4A). Only one out of eight animals demonstrated a statistically significant correlation (Fig. 4B) at the $P < 0.05$ level. A composite across all epochs in all animals showed that the composite correlation

was insignificant ($r = -0.03$, $P = 0.013$). This result indicates that the amplitudes of the two rhythmic signals are independent of each other.

Finally, we revisit the issue of the independence of whisking and the theta rhythm in terms of a sensory lesion, rather than a lesion to the limbic tract (Gray 1971; Semba and Komisaruk 1984). Our analysis makes use of the known decrement in frequency of rhythmic whisking in response to lesion of the IoN to block sensory input (Welker 1964; Berg and Kleinfeld 2003). We asked if such a decrement occurs in the hippocampal rhythm as well during exploratory whisking. In agreement with past results, we observed a decrement in the frequency of whisking across 4 of 4 animals in which we lesioned the IoN (Table 3.2). In contrast, only one animal showed a systematic decrease in the frequency of the theta rhythm. This data further supports the independence of the two rhythms.

3.6 Discussion

The present study quantifies the coherence between the rhythmic movement (via the electromyogram) of the rat's vibrissae during exploratory whisking (Berg and Kleinfeld 2003), and the hippocampal theta rhythm. Overall, the two rhythms are not locked in a greater percentage of epochs than would be expected by chance (Table 3.1). This finding reconciles a long-standing disagreement in the literature.

The hippocampal theta rhythm and cortical desynchronization are considered hallmarks of arousal and alerted states (Komisaruk and Olds 1968; Moruzzi and Magoun 1995; Berg, Friedman et al. 2005). In pioneering work, Green and Arduini (Green and Arduini 1954) recorded from both anesthetized and awake but sessile animals and found that the theta rhythm occurred concomitantly with cortical desynchronization. The relationship between these rhythms appears less obvious in drowsy animals (Vanderwolf 1969). Studies of rhythmic activity in hippocampus during awake behavior were first provided by Grastyan *et al.* (Grastyan, Lissak et al. 1959) and Adey *et al.* (Adey, Dunlop et al. 1960), who recorded from cats as they performed learning tasks. Of direct relevance to the present work, Komisaruk and Olds (Komisaruk and Olds 1968) first reported on units in hippocampus that were active during bouts of exploratory vibrissa movements, suggesting a link between hippocampal activity and whisking. Further, the hippocampal theta activity and spontaneous vibrissa twitches during paradoxical sleep (Vanderwolf 1969) appear to be related on a cycle-by-cycle basis (Lerma and Garcia-Austt 1985).

The overlap in frequency range between exploratory whisking and the hippocampal theta frequency makes it tempting to speculate that the two rhythms phase-

lock during activity. Komisaruk (Komisaruk 1970) reported that a "one-to-one correlation was often observed between each vibrissa twitch and each beat of the theta rhythm", though their "rhythmicity are not always phase locked" (Figure 5 in Komisaruk (Komisaruk 1970)), a result later reaffirmed by Semba and Komisaruk (Semba and Komisaruk 1984). In complementary work with hamsters, potential coupling of exploratory sniffing with the theta rhythm was studied by Macrides and colleagues (Macrides 1975; Macrides, Eichenbaum et al. 1982), who found that "the mystacial musculature often appeared to be correlated with individual hippocampal slow waves at times" yet the timing of the theta rhythm "showed the timing of sniffs relative to peaks or troughs in the slow waves to be steadily drifting". Despite the stated caveats in past work, the notion of a one-to-one correlation between the two rhythms has gained undue acceptance. As quantified in this report, this acceptance is unfounded.

It is important to note that the phase relation between whisking and the theta rhythm may well depend on the state of the animal. First, recent work showed that the coherence between ongoing cortical activity and vibrissa motion triples when rats are engaged in a reward-based tasks (Ganguly and Kleinfeld 2004). Secondly, both past (Adey, Dunlop et al. 1960; Macrides, Eichenbaum et al. 1982) and recent (Jones and Wilson 2005) work suggests the hippocampal theta rhythm and ongoing cortical activity tend to phase-lock during a memory task. Thus it is possible that the theta rhythm and whisking will phase-lock under certain circumstances, such as when the rat learns to discriminate an object with the vibrissae, as opposed to whisk in air. For example, sniffing is locked to the theta rhythm during a reversal of odor contingency (Macrides

1975; Macrides, Eichenbaum et al. 1982), yet unlikely to be locked to the theta rhythm in the absence of novel odors (Kepecs, Uchida et al. 2005).

3.7 Acknowledgements

Chapter III is a reprint, in full, of the material as it appears as in the *Journal of Neuroscience*, 2006 Jun 14; 26(24):6518-22. The dissertation author is the second author on this paper from work performed in collaboration with first author Rune Berg while we were in the laboratory of senior author Professor David Kleinfeld.

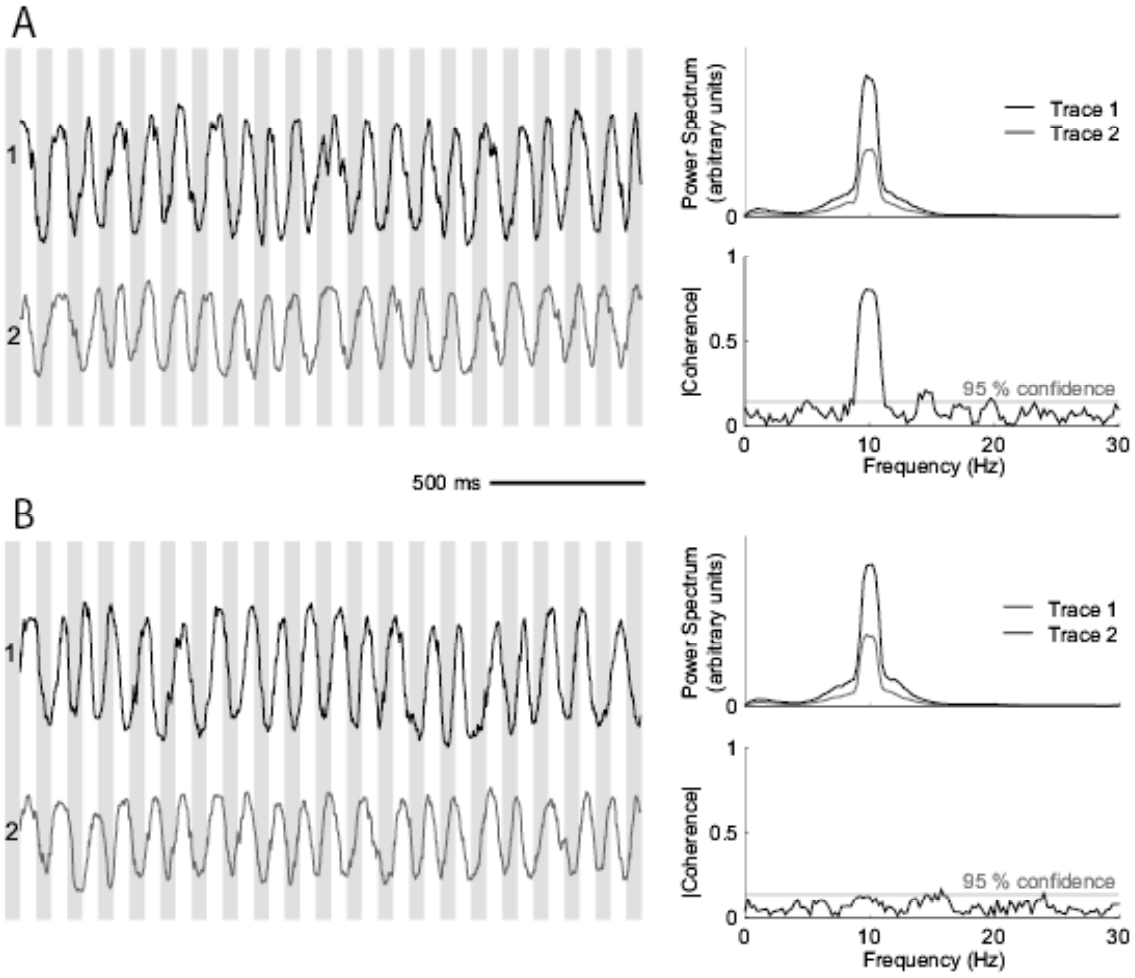

Figure 3.1 Illustration of Coherence Measurement between Two Rhythmic Traces

The time-series are based on simulated data that consists of sinusoids with added Gaussian amplitude noise, whose correlation time is 160 ms and standard deviation is 30 % of the sinusoidal amplitude, and added Gaussian phase noise, also with a 160 ms correlation time. The two time-series have the same frequency, but are modulated in frequency from trial-to-trial ($f = 10.0 \pm 0.3$ Hz). A. The two time-series co-drift; the bands on the left are to guide the eye. The upper right trace shows the two average power spectra of 50 samples, and the lower right trace is the magnitude of average coherence, which is high in the region of substantial overlap of the power spectra. The gray horizontal line represents the magnitude for which the coherence is significant at the $P < 0.05$. B. The two time-series drift independently. The peaks in the two power spectra overlap substantially, as shown to the upper right, but the magnitude of the coherence is low and insignificant at the overlap in frequency.

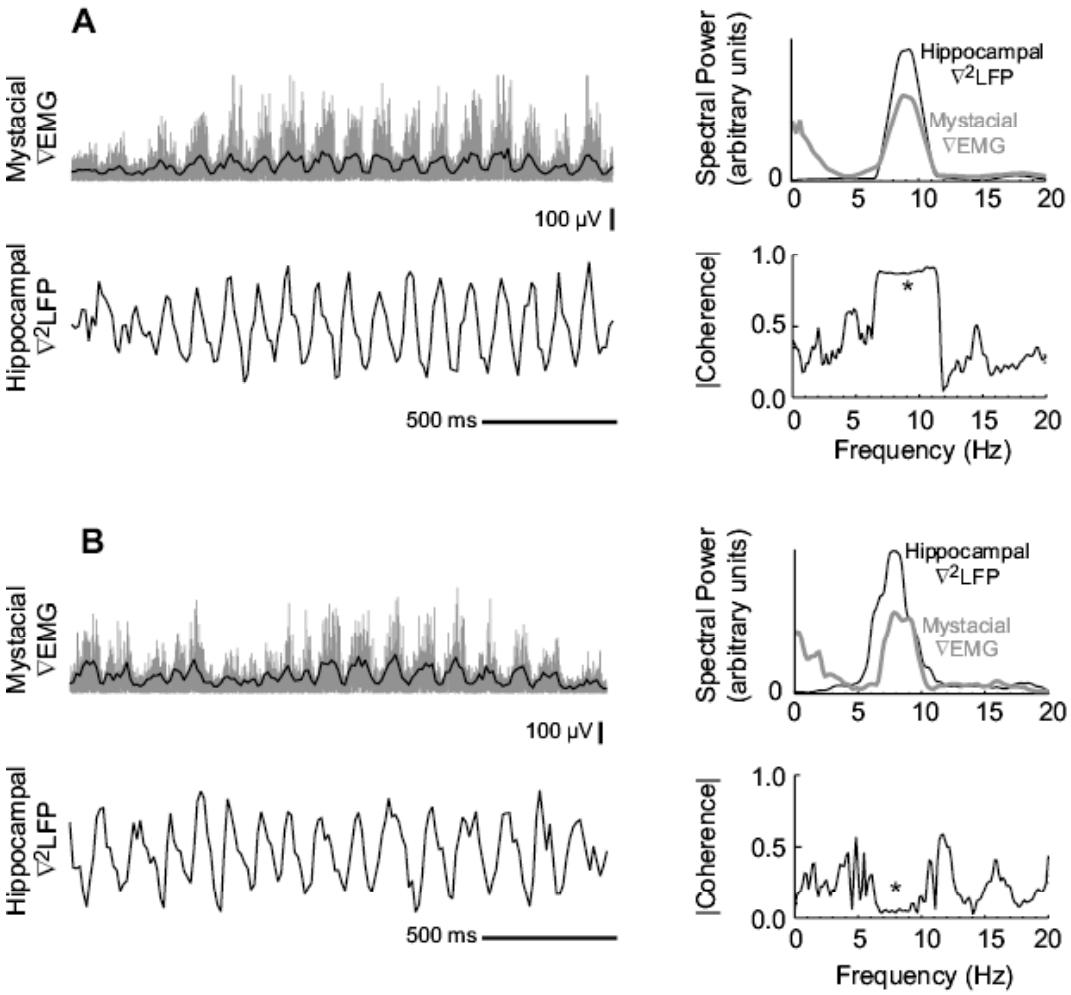

Figure 3.2 Spectral Measures of the Mystacial ∇EMG and the Hippocampal ∇2LFP in two, 2-s Whisking Epochs.

(A) Single epoch with overlapping power spectra and high coherence as indicated at the asterisk.
(B) Single epoch with overlapping power spectra and low coherence as indicated at the asterisk.

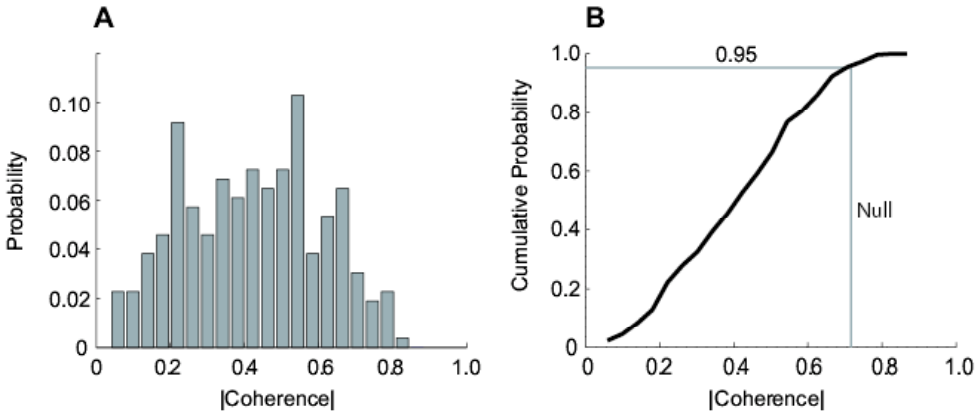

Figure 3.3 Trial-averaged Coherence between Whisking and the Theta Rhythm

(A) Probability density function (PDF) of coherence magnitudes for a sample animal (F9, n = 264).
(B) Cumulative density function (∫PDF) of coherence magnitudes for same animal. The significance line for a 95 % confidence interval is depicted as a horizontal line. Vertical line represents coherence magnitude that 5 % of epochs would be expected to exceed under null hypothesis. The ∫PDF would cross the vertical line at fewer than 95 % of the epochs if the number of coherent epochs were significant.

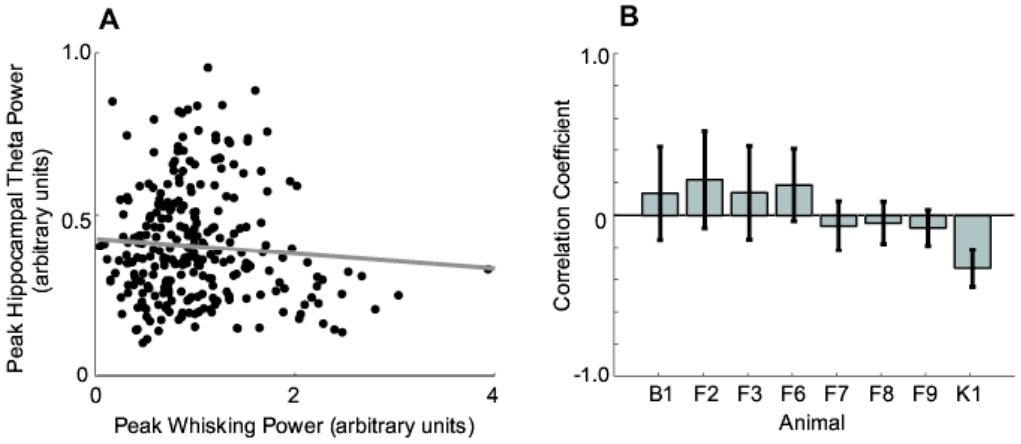

Figure 3.4 Lack of Amplitude Correlations between Whisking and the Theta Rhythm

(A) Peak power of whisking versus peak power of hippocampal signal for animal F9. Each dot represents a 2-second whisking epoch. Regression line demonstrates correlation is not statistically significant ($r = -0.08$ and $P = 0.06$).

(B) Correlation coefficient and 2-s error bars on relationship between peak power of whisking and peak power of hippocampus for each animal subject. There is a significant negative correlation for animal K1.

Table 3.1 Compendium of trail-by-trial coherence for all animals

Animal	Number of whisking epochs[1]	Trials with coherence above 95 % significance at $f = f_{whisk}$	Trials with coherence above 95 % significance at $f = f_{theta}$	Maximum value of trial averaged coherence, $\langle C(f) \rangle_{trials}$
B1	63	7.9 %	6.3 %	0.23
F2	45	0.0 % ✻	0.0 % ✻	0.09 ✻✻
F3	38	2.6 % ✻	2.6 % ✻	0.01 ✻✻
F6	103	2.9 % ✻	1.0 % ✻	0.09
F7	181	1.7 % ✻	1.7 % ✻	0.03 ✻✻
F8	100	1.0 % ✻	0.0 % ✻	0.12
F9	264	4.9 % ✻	4.6 % ✻	0.17
K1	91	1.1 % ✻	4.4 % ✻	0.05 ✻✻
All	885	3.1 % ✻	2.8 % ✻	0.07 ✻✻

1 – Each epoch is 2 s in duration with 6 Hz < f_{theta} < 9 Hz and 6 Hz < f_{whisk} < 9 Hz.

✻ Insignificant coherence, *i.e.*, the null hypothesis of significant coherence, based on $P < 0.05$, is rejected

✻✻ Insignificant coherence, *i.e.*, the null hypothesis of a significant trial-averaged coherence, based on $P < 0.05$, is rejected.

Table 3.2 Compendium of frequency changes after lesion of the IoN

Animal	Number of epochs before incision[1]	Number of epochs after incision[1]	Null hypothesis for equivalent distributions of whisking frequencies[2]	Null hypothesis for equivalent distributions of theta rhythm frequencies[2]
F7	408	343	Rejected ($P < 0.01$)	Not rejected ($P > 0.5$)
F8	215	179	Rejected ($P < 0.01$)	Not rejected ($P = 0.7$)
F9	419	295	Rejected ($P < 0.02$)	Not rejected ($P = 0.8$)
K1	139	114	Rejected ($P < 0.01$)	Rejected ($P < 0.01$)

REFERENCES

1. Adey WR, Dunlop W, Hendrix CED (1960) Hippocampal slow waves. Distribution and phase relationships in the course of approach learning. Archives Neurology 3:74-90.

2. Berg RW, Kleinfeld D (2003) Rhythmic whisking by rat: Retraction as well as protraction of the vibrissae is under active muscular control. Journal of Neurophysiology 89:104-117.

3. Berg RW, Friedman B, Schroeder LF, Kleinfeld D (2005) Activation of nucleus basalis facilitates cortical control of a brainstem motor program. Journal of Neurophysiology 94:699-711.

4. Buzsaki G (2002) Theta oscillations in the hippocampus. Neuron 33:325-340.

5. Buzsaki G, Draguhn A (2004) Neuronal oscillations in cortical networks. Science 304:1926-1929.

6. Carvell GE, Simons DJ, Lichtenstein SH, Bryant P (1991) Electromyographic activity of mystacial pad musculature during whisking behavior in the rat. Somatosensory and Motor Research 8:159-164.

7. Ganguly K, Kleinfeld D (2004) Goal-directed whisking behavior increases phase-locking between vibrissa movement and electrical activity in primary sensory cortex in rat. Proceedings of the National Academy of Sciences USA 101:12348-12353.

8. Grastyan E, Lissak K, Madarasz I, Donhoffer H (1959) Hippocampal electrical activity during the development of conditioned reflexes. Electroencephalography and Clinical Neurophysiology 11:409-430.

9. Gray JA (1971) Medial septal lesions, hippocampal theta rhythm and the control of vibrissa movement in freely moving rat. Electroencephalography and Clinical Neurophysiology 30:189-197.

10. Green JD, Arduini AA (1954) Hippocampal electrical activity in arousal. Journal of Neurophysiology 17:533-547.

11. Hasselmo ME (2005) What is the function of hippocampal theta rhythm? Linking behavioral data to phasic properties of field potential and unit recording data. Hippocampus 15:936-949.

12. Jarvis MR, Mitra PP (2001) Sampling properties of the spectrum and coherency of sequences of action potentials. Neural Computation 13:717-749.

13. Jones MW, Wilson MA (2005) Theta rhythms coordinate hippocampal–prefrontal interactions in a spatial memory task. PLoS Biology 3:e402.

14. Kepecs A, Uchida N, Mainen ZF (2005) The sniff as a unit of olfactory processing. Chemical Senses 31:167-179.

15. Kleinfeld D, Berg RW, O'Connor SM (1999) Anatomical loops and their electrical dynamics in relation to whisking by rat. Somatosensory and Motor Research 16:69-88.

16. Komisaruk BR (1970) Synchrony between limbic system theta activity and rhythmical behavior in rats. Journal of Comparative and Physiological Psychology 70:482-492.

17. Komisaruk BR, Olds J (1968) Neuronal correlates of behavior in freely moving rats. Science 161:810-813.

18. Lerma J, Garcia-Austt E (1985) Hippocampal theta rhythm during paradoxical sleep. Effects of afferent stimuli and phase relationships with phasic events. Electroencephalography and Clinical Neurophysiology 60:46-54.

19. Macrides F (1975) Temporal relationship between hippocampal slow waves and exploratory sniffing in hamsters. Behavioral Biology 14:295-308.

20. Macrides F, Eichenbaum HB, Forbes WB (1982) Temporal relationship between sniffing and the limbic theta rhythm during odor discrimination reversal learning. Journal of Neuroscience 12:1705-1717.

21. Moruzzi G, Magoun HW (1995) Brain stem reticular formation and activation of the EEG. 1949. Journal of Neuropsychiatry and Clinical Neurosciences 7:251-267.

22. Percival DB, Walden AT (1993) Spectral Analysis for Physical Applications: Multitaper and Conventional Univariate Techniques. Cambridge: Cambridge University Press.

23. Robinson TE (1980) Hippocampal rhythmic slow activity (RSA; theta): A critical analysis of selected studies and discussion of possible species-differences. Brain Research 203:69-101.

24. Semba K, Komisaruk BR (1984) Neural substrates of two different rhythmical vibrissal movements in the rat. Neuroscience 12:761-774.

25. Thomson DJ (1982) Spectral estimation and harmonic analysis. Proceedings of the IEEE 70:1055-1096.

26. Treves A, Rolls ET (1994) Computational analysis of the role of the hippocampus in memory. Hippocampus 4:374-391.

27. Vanderwolf CH (1969) Hippocampal electrical activity and voluntary movement in the rat. Electroencephalography and Clinical Neurophysiology 26:407-418.

28. Vertes RP (2005) Hippocampal theta rhythm: A tag for short-term memory. Hippocampus 15:923-935.

29. Welker WI (1964) Analysis of sniffing of the albino rat. Behaviour 12:223-244.

30. Whishaw IQ, Vanderwolf CH (1971) Hippocampal EEG and behavior: Effects of variation in body temperature and relation of EEG to vibrissae movement, swimming and shivering. Physiology and Behavior 6:391-397.

31. Whishaw IQ, Schallert T (1977) Hippocampal RSA (theta), apnea, bradycardia, and effects of atropine dunring underwater swimming in the rat. Electroencephalography and Clinical Neurophysiology 42:389-396.

32. Winson J (1974) Patterns of hippocampal theta rhythm in the freely moving rat. Electroencephalography in Clinical Neurophysiology 36:291-301.

Chapter IV. Utility of Independent Component Analysis for the Interpretation of Intracranial EEG

4.1 Abstract

Intracranial recordings from electrode arrays implanted in epilepsy patients are used for the localization of seizure foci and for cortical mapping of sensory and language areas prior to surgery. These clinical evaluations also provide a unique opportunity for cognitive neuroscience studies of language, motor activity, and perceptual processing. Analysis of intracranial EEG recordings is normally performed in the "channel domain," whereby EEG signals from individual implanted electrodes are examined separately. We postulate that intracranial EEG signals, like scalp EEG signals, are mixtures (superpositions) of local activity and volume-conducted activities of many sources. Independent component analysis (ICA) has aided the interpretation of scalp EEG by separating signal mixtures into independently generated source signals. Here, we apply ICA to intracranial data in an effort to better understand the composition of the field potentials recorded by intracranial electrodes. In this study, we use ICA to unmix model sources from intracranial EEG recorded from four epilepsy patients during a visually-cued finger movement task recorded in the presence of background interictal pathological brain activity. We demonstrate that the intracranial data channels are not independent as recorded, and verify that ICA decomposes the data into more independent signals. Further, many of the grid maps giving the pattern of projection of the independent components onto the channel grids are consistent with origins in synaptically connected brain regions. Finally, ICA identifies components exhibiting classic movement-related

dynamic patterns. The results suggest that ICA can be used to identify functionally linked networks of local field sources in intracranial data.

4.2 Introduction

The goal of cognitive neuroscience is to correlate cognition and behavior with brain function. While animal studies provide the opportunity to record neural activity directly, either at the level of single units or of local field potentials, human neuroscience is typically limited to non-invasive, whole-brain imaging techniques with limited spatial and/or temporal resolution. Electroencephalogram (EEG) recordings using electrodes placed on the scalp of humans is a technology for measuring electric fields generated by brain activity that bears the advantage of sub-millisecond temporal resolution. The spatial resolution of EEG, however, is both limited and ambiguous due to the multi-centimeter scale spacing of electrodes on the surface of the scalp, the linear mixing of electrical fields detected by the electrodes, and the difficulty of estimating source distributions on a highly folded brain surface from sparse measurements on the smooth and relatively distant scalp surface. The estimation of the locations of neurophysiological current sources that generate the electric fields recorded by EEG sensors is thus a mathematically underdetermined problem that requires brain modeling to achieve estimated solutions.

Independent component analysis (ICA) is a signal decomposition technique that finds a set of maximally independent signals that mix linearly to create the original data. The output of the ICA algorithm is an unmixing matrix with weights associated with each electrode, and a matrix of component time series. ICA has been instrumental in the interpretation of scalp EEG signals recorded during cognitive and perceptual tasks by finding independent brain signals that are modulated on an event-related basis (Makeig et

al., 1996; Makeig et al., 1997; for reviews, see Makeig, 2002; Makeig et al., 2004; Onton & Makeig, 2006). Additionally, many independent component maps created from projections of the mixing matrix onto the EEG electrode montage exhibit biologically plausible patterns that are consistent with fields generated by dipolar current sources, in the absence of any explicit localization constraints in the ICA model (Makeig et al., 1997; Makeig et al., 2004 PLoS). Although ICA has aided the interpretability of EEG recordings and has helped to localize current sources, neuroscientists continue to look to other brain imaging measures that exceed the limited spatial resolution of scalp EEG.

Intracranial EEG (iEEG) is a technique for invasively recording the electrical activity of the human brain, and is used for pre-surgical evaluation in patients with medically intractable partial epilepsy (Engel, 1996). Intracranial signals are recorded from surgically implanted subdural arrays or intraparyenchmal depth probes, typically 1-cm spaced electrodes with ~1 -10 mm^2 surface area, and are generally implicitly assumed to record activity from a local region of cortex (Bullock, McClune et al. 1995; Nunez 2006). Clinically, intracranial studies have been critical for the localization of seizure foci (Berger 1929; Jasper 1949; Wyler, Ojemann et al. 1984; Engel and Crandall 1987; Luders, Awad et al. 1992; Dewar, Passaro et al. 1996) and for cortical mapping of sensory, motor, and language areas prior to surgery (Penfield 1951; Penfield 1954; Ojemann 1982; Burchiel, Clarke et al. 1989; Luders, Dinner et al. 1995; Tharin and Golby 2007). In addition, intracranial recordings have also been utilized for cognitive neuroscience studies of language (Ojemann et al., 1983; Ojemann et al., 1989), motor activity (Arroyo, Lesser et al. 1993; Crone, Miglioretti et al. 1998; Crone, Miglioretti et al. 1998; Miller, Leuthardt et al. 2007; Ball, Demandt et al. 2008), visually guided

behaviors (Klopp, Marinkovic et al. 2001) (Klopp, Marinkovic et al. 2001), face recognition (Halgren, Baudena et al. 1994; Halgren, Baudena et al. 1994; Klopp, Marinkovic et al. 2000; Quiroga, Reddy et al. 2005), memory (Cameron, Yashar et al. 2001; Fell, Klaver et al. 2001; Rizzuto, Madsen et al. 2006), spatial cognition (Kahana, Caplan et al. 1999), and attention (Ray, Niebur et al. 2008).

The fact that intracranial recordings involve the implantation of electrodes directly on neocortex, and deep medial temporal structures amygdala and hippocampus provides advantages over scalp EEG of higher spatial resolution and frequency bandwidth. Intracranial EEG is therefore often treated as the "gold standard" to which clinical scalp EEG results are compared and the localization of sources verified (Cooper et al., 1965; Kobayashi et al., 2001; Dalal, 2008). It is generally agreed upon that intracranial recordings, like scalp EEG, are mixtures of volume-conducted activities of many current sources (Nunez, 2006). Despite this, the signals of each intracranial electrode are typically examined individually without the explicit application of un-mixing algorithms. Furthermore, because of volume conduction within the brain, signals recorded from clinical iEEG arrays or strips may include activities not generated near to the electrodes. Activity generated near to the electrode (or to the active reference electrode) may typically dominate the iEEG signal, but this domination need not be complete, as often assumed. Since volume conduction to both EEG and iEEG electrodes is linear and without appreciable delay (Nunez, 1995), we propose that ICA should work just as well for separating iEEG signal sources as for EEG sources.

That intracranial recordings are from epilepsy and other pre-surgical patients means that cognitive research is performed using brains with pathologies. Although

seizure episodes are not used in the analysis of cognitive experiments sometimes performed on these patients during implantation, ongoing pathological brain signals occur during interictal (between-seizure) periods. Thus, in data from cognitive iEEG experiments performed by epileptic patients, abnormal brain signals may be mixed with the task-relevant brain signals under inquiry, and ICA might separate the volume-conducted contributions of abnormal interictal activity from normal brain signals that may be generated near to adjacent iEEG electrodes. Similarly, ICA may be able to unmix normal brain activity from epileptic source activity, thereby revealing more about its location and temporal dynamics than visual inspection of the summed channel data themselves.

For these reasons, we propose that ICA may be useful in the interpretation of intracranial data, and the goal of this study is to test the utility of ICA on intracranial data. In this study, we use ICA to unmix independent sources of intracranial EEG data from four patients with medically intractable epilepsy who performed a visually-cued finger movement task. We first test whether the time series of intracranial recordings in the channel domain are themselves independent, or whether ICA finds in the data source signals having stronger independence. Next, we ask whether the grid projection maps associated with the independent iEEG components are organized in a way consistent with projections of compact, dipolar source regions or perhaps of sources including more than one anatomically connected brain area. Finally, we inquire whether independent components can better identify brain areas that are functionally linked. We make use of two types of well-characterized pathological signals and the well-known cortical

dynamics associated with motor tasks to determine whether ICA can identify and separate these signals.

4.3 Materials and Methods

Intracranial Recordings from Epilepsy Patients

Four patients with focal, medically intractable epilepsy participated in the study and gave informed consent with International Review Board approval. All patients had intracranial depth and/or grid electrodes (Adtech, Inc.) implanted according to standard pre-surgical evaluation protocol (Engel and Crandall 1987; Luders, Awad et al. 1992; Engel 1996), and simultaneous scalp EEG recordings. The intracranial electrode arrays are composed of 4mm diameter Platinum/Iridiumm (Pt/Ir) contacts separated by 10 mm center-to-center spacing.

Table 4.1 lists the locations and numbers of electrodes used from each of the participants of the study.

Data Acquisition and Preprocessing

For epilepsy monitoring, continuous video monitoring via scalp EEG and iEEG were recorded with a 128-channel, digital 12-bit, XLTEK system (XLTEK Inc.) with a sampling rate of 500 Hz. Patient 4 was recorded with a 128-channel, digital 24-bit, Neuralynx (Neuralynx Inc.), sampling at 32 kHz, and subsequently downsampled to 2 kHz. All recordings were obtained using a scalp suture reference or mastoid reference contralateral to the placement of the intracranial grid.

Channels with significant artifact or EEG signals indicating a bad electrical contact dominated by non-biological noise were removed from further analysis. The number of intracranial and scalp EEG channels used in the analysis of each patient dataset is indicated in Table 4.1.

Line noise (60 Hz noise) and its harmonics were removed on a single channel basis via harmonic analysis (Mitra and Pesaran 1999; Jarvis and Mitra 2001) using Matlab based software from http://www.chronux.org. Briefly, multi-taper spectral estimates (Thomson 1982) were performed on a 1-second sliding widow with 50% overlap. Five tapers were used for each estimate, and a zero padding factor of 2^10 to ensure high resolution in the frequency domain. A goodness-of-fit F-statistic (Thomson 1982) was used to determine which frequencies had statistically significant peaks, $p < 0.05$. The line noise for Patient 4 was statistically insignificant.

Visually-cued finger-movement task

Patients participated in a cued finger movement task for language and motor evaluation. The subject was presented with either the text of one finger name (“thumb”, “index”, etc.) among five fingers in one hand, or a picture of one hand with an arrow designating one finger (Figure 4.1). A patient was instructed to press one of five keys using the finger corresponding to the stimulus. Trials were time limited to 1.57 seconds, and a failure to respond within the allotted time was considered an incorrect trial. Auditory feedback was presented in the form of a beep 1.24 sec after the stimulus presentation. Two different audio tones were used for correct versus incorrect responses. Stimuli were presented in a block design (Figure 4.2) in order of left hand picture stimuli,

right hand picture stimuli, left-hand word stimuli, right-hand word stimuli, with the presentation of specific fingers in random order within a block. There were 400 trials in total for the task, consisting of 20 picture presentations and 20 text presentations for each finger. The task was performed twice for three of the patients (800 trials) and once for one of the patients. 400 (Patient 4) to 800 trials (Patients 1,2,3) were recorded, yielding recordings of 12.5 to 25.7 minutes in length.

Electrode Localization

Locations of implanted electrodes were approximated using the LOC software package developed and described in detail by Miller et al. (Miller, Makeig et al. 2007). In short, we estimated axes in a Talairach coordinate system from post-surgical lateral CT scans of the patient's brain using glabella and inion skull landmarks. Corresponding Brodmann areas were estimated from the Talairach coordinates using Talairach Daemon software (Lancaster, Woldorff et al. 2000).

4.4 Data Analysis

Independent Component Analysis

Infomax ICA (Bell and Sejnowski 1995) was performed on the data from each patient. In the ICA model, a set of recorded time series X(t), is the linear combination of a mixing matrix, A, and a set of source signals, S(t):

$$X(t) = A * S(t)$$

The solution to ICA is an unmixing matrix, W, that when multiplied by the original data produce a set of maximally independent time series "activations" U(t).

$$W * X(t) = U(t)$$

Multiplying both sides of the equation by the inverse of pseudo-inverse of W gives a description of the original data as the product of a mixing matrix and the component time series or activations matrix U(t):

$$X(t) = W^{(-1)} * U(t)$$

Note that the unmixing matrix $W^{(-1)}$ is the inverse of A when the activations U(t) are the underlying sources S(t). In practice, U and S may differ in the order of the components and/or in their polarities, since a reversed polarity of a component time signal in U(t) can be cancelled out by a reversed polarity of the component scalp map in the corresponding column of $W^{(-1)}$.

Pairwise Mutual Information

Mutual information based on differential entropy was computed between pairs of channels or pairs of components. Differential entropy, the extension of information entropy to continuous random variables, was used here in mutual information calculations because recorded voltages can take on continuous values. The equation for mutual information between two random variables X and Y based on differential entropy (Cover 2006) is:

$$I(X;Y) = h(X) + h(Y) - h(X,Y)$$

,where h(x) and h(y) are the marginal differential entropy for X and Y, respectively based on the marginal probability densities, and h(X,Y) is the joint differential entropy based on joint probability density p(x,y), using the following equation:

$$h(X) = -\sum_i p(x_i) \log p(x_i) \Delta x_i$$

Note that statistical independence can only be precisely determined on an infinite dataset. The marginal and joint probability densities were approximated in Matlab using Riemann sums:

$$p(x_i) = \frac{Ni}{N \Delta x_i}$$

, where N_i is the number of values in the ith bin, N is the total number of values, and delta-x is the bin size. The delta-x factor in the denominator ensures that the area under the probability density function sums to unity.

Differential entropy then becomes:

$$h(X) = -\sum_i \frac{Nx_i}{N \Delta x_i} \log \frac{Nx_i}{N \Delta x_i} \Delta x_i$$

When the above formulation for differential entropy is substituted into the equation for mutual information, the Δx and Δy cancel out, resulting the following equation:

$$I(X,Y) = -\sum_i \frac{Nx_i}{N} \log \frac{Nx_i}{N} - \sum_j \frac{Ny_j}{N} \log \frac{Ny_j}{N} + -\sum_i \sum_j \frac{Nx_i y_j}{N} \log \frac{Nx_i y_j}{N}$$

The time series data were divided into 100 bins for the entropy estimates of all channels and components, which was a bin size of 7.5 to 15.5 seconds depending on the length of the patient dataset.

Percent variance accounted for (pvaf)

The relationship between a channel's activity and the activity of independent components was quantified by percent variance. The percent variance of a channel's activity accounted for by a single component is computed as:

$$pvaf = (1 - \frac{\mathrm{var}(X_i(t) - \hat{X}_i(t)}{\mathrm{var}(X_i(t))}) * 100$$

,where X(t) is the time series for a single channel, and X^(t) is the back-projection of all components onto a given channel, absent the component of interest.

X^(t) is computed as

$$\hat{X}_i(t) = W^{(-1)}_{i,j} * U_j(t)$$

,where i is the channel index and j represents the indices of all but the excluded component.

Spectral Analysis

The time series of channels and independent components (depicted below in Figures 4.7 and 4.9) were de-trended with a high-pass Butterworth filter with a pass-band above 2 Hz, and 40 dB attenuation at the stop-band of 1 Hz. Time series were subsequently low pass filtered with a Butterworth filter with a 200 Hz pass-band limit, with 60 dB attenuation in the stop band at 240 Hz.

Normalized trial average event-locked spectral estimates were performed on 2-second trials centered on the key-press. Spectra were estimated as an average over K=5 independent tapers using the multi-taper method (Thomson 1982; Percival 1993; Mitra and Pesaran 1999; Jarvis and Mitra 2001) based on a single-tapered sliding 250 msec

window with 10 msec overlap. The baseline period for a trial was the average spectral change of a given frequency band over the entire 2-second epoch. Significant deviations from baseline power were computed with a bootstrap method based on spectral estimates of each trial at 200 randomly selected latencies from the time-locking event.

Spectral and coherence estimates for channels and component signals exhibiting pathological slow wave activity were estimated as an average over 5 independent estimates using the multi-taper method applied to consecutive 10 second segments of time series data that was pre-filtered with a Butterworth low-pass filter with an edge frequency of 40 Hz and 60 dB attenuation by 60 Hz. The confidence limit for the magnitude of the coherence across all frequencies was estimated from the following:

$$| C | = \sqrt{P^{1/(NK-1)}}$$

in which p=0.05 represents the 95% confidence limit, N is the number of trials or epochs, and NK is the number of degrees of freedom (Jarvis and Mitra 2001; Berg, Whitmer et al. 2006).

4.5 Results

The results of ICA applied to an input matrix of time series data are both a component weights matrix and a matrix of component time series. The weights matrix indicates how much of each independent component contributes to each channel signal. We first ask whether the time series from intracranial ICA are more statistically independent than the time series of the original channel data. We computed mutual information between all pairs of channels and between all pairs of component time series.

The histograms in Figure 4.3 demonstrate that pairs of channels have higher mutual information than pairs of independent components, with a greater reduction achieved by ICA for scalp EEG channels than for intracranial channels. Table 4.2 indicates the mean and range of values.

The quantitative relationship between channels and components was then assessed with a "percent variance accounted for" metric. The percent variance of each iEEG channel accounted for by its maximum component is depicted for Patient 1 (Figure 4.4A). If intracranial channels were independent, the maximal component would be close to 100% and the plot close to white for all channels. Instead, we find that the maximum contribution to each intracranial channel by its single largest-contributing component ranges from 21.5% to 92.6% (Figure 4.4B). For patients 2,3,4, these quantities ranged from 15.9% to 77.6%, from 21.1% to 90.1%, and from 5.42% to 94.9%, respectively, the distribution from all four patients combined in Figure 4.4C and exhibited a broad range.

We next examined the maps contained in the inverse weights matrix and asked whether they were ordered and consistent with directly connected brain areas, by i.e. resembling plausible projections of distal sources contributing to the affected channels through volume conduction. We find that the iEEG component maps fall into a few different categories: focal components that project largely to a single iEEG channel, diffuse components that project to a range of contiguous channels, typically with a single dominant channels, complex components that project to discontiguous grid areas, and noisy (mostly small) components that appear to combine channels in a disordered manner. Figure 4.5 illustrates example component maps that fall into each category for

Patient 1. The bar chart in Figure 4.6 depicts the fraction of component maps that fall into each category for each patient.

The strongest assessment of the utility of ICA for the analysis of intracranial data is to examine whether independent components separate out functionally meaningful brain signals. Because these data are acquired from epilepsy patients who performed a visually-cued movement task, we looked for both interictal pathological, as well as task-related brain dynamics. Patient 1 had a 6x8 iEEG grid implanted over right frontal cortex, and strips over a variety of locations including lateral temporal lobe, medial temporal lobe, and medial frontal areas (Table 4.1). The etiology of Patient 1 partial epilepsy was a structural abnormality in the medial frontal lobe, with pathology demonstrating cortical dysplasia (Kuzniecky, Morawetz et al. 1995). The iEEG demonstrated episodes of rhythmic moderate amplitude delta frequency activity on the following set of frontally located channels: Grid1, Grid2, Grid9, Grid10, SFO4, and SFO3. Five of the 87 components, totaling 21.8% of the variance of the intracranial data, had component maps weighting some combination of these six channels. Figure 4.7 depicts an example of one of these components, IC3, which is strongly weighted both on a single lateral frontal channel (Grid1), as well as on the most anterior two channels of the orbito-frontal strip (SFO3, SFO4). An example 2-second segment from IC3 and the two channels to which it most strongly projects depicted in Figure 4.7B illustrates the iEEG channel domain abnormal delta activity. The log power spectrum of IC3, based on the average of spectral estimates of contiguous 10-second segments of the data, reveals a peak at 3 Hz (Figure 4.8). The coherence of these two channels was statistically significant in the 2 Hz to 6 Hz range. For comparison, the coherence between Grid1and Grid8 was computed. Grid8 was

an arbitrary grid channel chosen because it did not exhibit pathological delta activity and was not weighted in any of the maps with weights on Grid1. The coherence between Grid1 and Grid8 is insignificant at all frequencies (Figure 4.8).

ICA also identified components exhibiting classic movement related dynamics. Grid24, an iEEG channel in or near primary motor cortex Brodmann area 4 of Patient 1, exhibited classic movement-related spectral changes including peri-movement alpha and beta range power decreases and simultaneous gamma band power increases. ICA decomposition of this patient's data revealed one component with a strong projection to Grid24. IC18 accounted for 89% of the activity on Grid24 (Figure 4.9), and demonstrates the same alpha, beta, and gamma band movement-related spectral changes seen on Grid24 (Figure 4.9). An additional two components demonstrated event-related spectral changes time-locked to the movement, but with slightly different temporal dynamics of gamma power and with maps projecting to different subsets of channels. IC68 shows a strong gamma power increase time-locked to the movement and projects most strongly to Grid15 which is in or near Brodmann area 6 corresponding to premotor and supplementary motor areas. IC63 shows a gamma power increase tens of milliseconds after the movement and a strong projection to Grid8, which is in or near the superior temporal gyrus. IC23 (Figure 4.10C) is a component that separates out the alpha and beta activity associated with mu blocking, but without the gamma component. IC23 projects predominantly to Grid23, which is in or near Brodmann area 6 corresponding to pre-motor and supplementary motor cortex.

4.6 Discussion

To the best of our knowledge, this is the first peer-reviewed study in which ICA has been applied to human intracranial data for interpretation of functional brain signals. Hu et al. (Hu, Stead et al. 2007) applied ICA to concurrently recorded iEEG and scalp EEG to attempt to remove the contributions of sources near the scalp reference channel to the iEEG channel data. We applied ICA to intracranial data recorded during a cognitive task because it has been instructive for other researchers in decomposing the linear mixtures recorded by scalp EEG data into maximally independent model sources whose dynamics are modulated on a task basis. To the extent that the assumptions underlying ICA are reasonable approximations for scalp EEG, they are equally reasonable for iEEG. ICA is a model built upon the assumption that the voltages recorded at the level of sensors, are produced by (nearly) independent current sources that sum linearly and are spatially stationary over the duration of the recording. Linearity is accepted as a reasonable approximation based on the biophysics of electromagnetism through brain tissue at the macroscopic level measured in scalp EEG and iEEG recordings (Nunez, Wingeier et al. 2001; Nunez 2006). The spatial stationarity of sources at the scale recorded by 1-cm spaced electrodes during ~20 minute recordings is an empirical question that may or may not be factual, but may plausible as a gross approximation. Traveling waves are observed in cortical recordings on much finer spatial scales (Rubino, Robbins et al. 2006) and spread to a small enough extent that they could appear synchronous in the cm^2 scale of standard iEEG recordings (Freeman, Holmes et al. 2006). It should be noted that ICA does not exclude moving sources; rather, it would need to

account for the dynamics of a moving source as successive, temporally overlapping activity across multiple components. Although ICA may not capture all the aspects of spatiotemporal dynamics of cortical signals, we propose the use of ICA to spatially filter iEEG signals, with the goal of improving on the standard approach in which each intracranial channel is implicitly regarded as an independent source whose activity is open to visual inspection.

We propose that ICA is useful for the interpretation of intracranial data by un-mixing and separating functionally meaningful signals having biologically plausible component maps, and by separating pathological activity from task-based activity. We first tested the independence of intracranial recordings by comparing their degree of independence to that of component signals found by infomax ICA, which are guaranteed to be the maximally independent signals linearly combining to produce the data. Both the mutual information histogram and the percent-variance-accounted-for measures demonstrated that ICA decomposed the data into a set of signals with much greater independence than the original signals. Although ICA decomposition can identify maximally independent signals in any dataset, and independent component signals are never *less* independent than the recorded signals), our results nonetheless demonstrate that intracranial signals are not independent *as recorded*, and ICA finds yet more temporally independent or distinct signals in iEEG, many of which, in addition, have grid maps that may plausibly be associated with a source not located under any single iEEG electrode.

We then asked whether and how many of the spatial patterns exhibited by the component maps from the ICA decomposition appear biologically meaningful. We found

that only a fraction of the component maps identify components projecting to single channels, components we categorized as "focal," while the vast majority project to multiple electrodes. Another set of component maps, those projecting to multiple nearby electrodes, were categorized as "diffuse." Diffuse component maps project to channels in brain tissue likely to be anatomically connected. A second type of component map projecting to multiple electrodes was categorized as "complex" because the affected electrodes were not located in contiguous brain regions. We hypothesized that these component maps identify functionally distinct brain processes. Finally, we demonstrated examples of components with coherent pathological activity projecting to multiple electrodes.

We cannot make any concrete claims about the location of sources based on ICA alone, without first building individualized forward head model to predict how current sources generate the electric fields that appear as voltage changes on the sensors. However, we postulate that the most parsimonious explanation for focal component maps is that they represent brain sources in close proximity to the affected electrode. Our interpretation of the diffuse component maps is that they represent either 1) wide (multi-cm) areas of local cortical field activity coupled synchronously through synaptic coupling, or 2) the projection through volume conduction of activity generated in a (smaller) distal source area to a wide array of sensors. For example, a radially-oriented focal source on the inferior cortical surface might project to a much wider area on the superior cortical surface. These two quite different possibilities cannot be disambiguated without a forward model of the current flow through the brain volume conductor. Although synchronous activity across a multi-cm cortical region has not been reported in

the normal awake brain, in fact few studies have looked in detail and the extent and dynamics of synchrony within either animal or human cortex.

The ‘complex’ component maps in some cases suggested origins near electrodes that were functionally coupled. Again, the dipolar nature of cortical fields signify that each source has two opposite projection directions (in which the projected signal has opposite sign). In some cases, ‘complex’ maps might thus be generated by a small number of bi-valent dipolar projects to the iEEG grid.

Finally, some fraction of the independent components was not categorizable as focal, diffuse, or complex and was therefore described as “noisy.” The ICA algorithm, by design, decomposes the data into the same number of components as there are sensors. Some number of the independent components may fall below the threshold of those that can be resolved from the available length of the data. Also, the number of potential proximal and distal source signals contributing by volume conduction to an iEEG data set is larger than the number of electrode signals. ICA typically mixes the contributions of small source signal contributions into the available number of components. Thus, the smallest components returned by ICA may not be dominated by a single source signal, as is also the case for scalp EEG data decomposition.

An additional test of the utility of intracranial ICA, beyond the qualitative assessment of the biological plausibility of component maps, was to determine whether the time series of independent components group signals from disparate areas of the brain that are functionally linked. The prevalence of stereotyped pathological signals in these data provided the opportunity to use signals that are well characterized in the channel domain. We identified one type of clinically important signal, frontal rhythmic

intermittent delta activity, to test whether ICA can successfully separate pathological signals from non-pathological signals. Frontal intermittent rhythmic delta activity (FIRDA) is a nonspecific, but common, pathological brain signal that can be seen in patients with tumors (Kubota and Ohnishi 1997), increased intracranial pressure, and toxic-metabolic disorders (Niedermeyer 2003). ICA decomposition of scalp EEG data has been shown to successfully separate FIRDA from other brain activity in patients with Creutzfeld-Jakob disease, and associates FIRDA with periodic lateralized epileptiform discharges (PLEDs) (Hung, Wang et al. 2007). In our intracranial data, ICA separated FIRDA from other ongoing brain activity. Further, ICA separated 12 components having maps including projections to some subset of the six channels clinically identified as exhibiting frontal intermittent delta activity. Four of these components showed maximal spectral peaks at 3 Hz, and the remainder exhibited a maximum at 6 Hz with a smaller peak near 3 Hz.

Why were the FIRDA signals accounted for by multiple independent components rather than being aggregated into a single component? ICA models the data as the weighted mixture of independent source signals that remain spatially stationary through the duration of the recording. Different FIRDA trains may have appeared on different subsets of channels through the course of the 20-minute recording. Else, the source generators of FIRDA may have been hierarchical rather than independent, as is suggested by analysis of ictal epilepsy data (Repucci, Schiff et al. 2001).

As a further test of whether ICA separates functionally meaningful signals in intracranial data, we also examined how the decomposition parsed event-related signals triggered from cued finger movements. The cortical dynamics associated with finger

movement are well characterized and therefore provide a good model for testing ICA. The mu rhythm is a periodic signal with a stereotyped morphology including a sharply contoured wave followed by a rounded phase, observed over rolandic cortex of humans during periods of stillness and is attenuated with motor activity. Mu, like posterior alpha activity, is therefore viewed as an "idling" brain rhythm (Jasper 1938; Gastaut, Terzian et al. 1952; Niedermeyer 1999). The suppression of this rhythm during movements is a well-known phenomenon first observed in the time domain of scalp EEG during movement (Jasper 1938), and later determined by spectral decomposition to be comprised of alpha and beta components (Pfurtscheller and Aranibar 1977; Pfurtscheller and Aranibar 1980). This classical movement-induced brain signature is robustly evident across imaging modalities including EEG (Stancak and Pfurtscheller 1996), MEG (Salmelin and Hari 1994), and intracranial recordings (Arroyo, Lesser et al. 1993; Crone, Miglioretti et al. 1998; Crone, Miglioretti et al. 1998; Aoki, Fetz et al. 1999; Ohara, Ikeda et al. 2000; Klopp, Marinkovic et al. 2001; Miller, Leuthardt et al. 2007), and in response to movements of different modalities including the tongue, foot, and hand (Pfurtscheller, Pregenzer et al. 1994). Hand movement paradigms that have elicited this stereotyped pattern have include manually squeezing of rubber ball (Pfurtscheller, Aranibar et al., 1980; Pfurtscheller, 1982), finger movements from visual cue (Pfurtscheller, Neuper et al., 1997; Klopp et al., 2001); fist clenching and relaxing (Miller, Leuthardt et al. 2007), sustained muscle contraction (Crone, Miglioretti et al. 1998; Crone, Miglioretti et al. 1998), and more complex tasks involving the hand (Aoki, Fetz et al. 2001; Rektor, Sochurkova et al. 2006). Recent studies with data acquired at higher sampling rates have demonstrated an increase in gamma band power concurrent with the alpha and beta

power decreases associated with mu (Crone, Miglioretti et al. 1998; Miller, Leuthardt et al. 2007).

It is therefore expected that our visually-cued finger movement task would also elicit mu blocking in the time domain associated with alpha and beta power decreases, concurrent with gamma power increases over motor cortex. Indeed, a couple of intracranial channels from Patient 1, who had electrodes implanted over peri-rolandic area, exhibited these well-established spectral changes time-aligned to the finger movement. We examined a single electrode over pre-central cortex as an example. ICA decomposition revealed one component (IC18) with strong projections to that channel, and weaker projections to the neighboring channels, which exhibited salient movement-locked alpha, beta, and gamma band changes. The wider spatial extent of the beta dynamics than the gamma dynamics is consistent with the findings of other researchers (Crone, 1998; Miller, 2007). The effectiveness of ICA to separate predicted event-related dynamics in our intracranial data, as a proof of principle, suggests that ICA could be applied to data acquired during more sophisticated cognitive and perceptual tasks for identifying novel brain dynamics and functionally connected regions.

The infomax ICA algorithm used here has a strong and possibly fallible assumption of spatial stationarity of the source areas over the entire length of the recording. Newer decomposition methods have been developed that explicitly account for moving sources, such as complex ICA (Anemuller, Sejnowski et al. 2003; Anemuller, Duann et al. 2006; Dyrholm, Makeig et al. 2006; Dyrholm, Makeig et al. 2007) and the "amica" algorithm for multiple mixtures (Palmer 2006), all of which have been applied

to EEG data. The application of these algorithms to intracranial data could refine and extend the results reported here, and will be investigated in future research.

In summary, ICA is an algorithm for identifying and characterizing brain sources underlying mixed signals, without any constraints on where those sources are distributed. The results from ICA decomposition of EEG data may be used in conjunction with source localization models, such as equivalent single dipole or multiple dipole modeling with boundary element (BEM) or finite element (FEM) head models, to answer both "what" and "where" questions about brain function – i.e., What source activities produce the observed brain electrical data, and where are they generated? The putative sources of intracranial data identified by ICA can only be used for source localization by incorporating a sophisticated forward model, as forward models for EEG assume an intact skull, and are thus insufficient for use with epilepsy patients with craniotomies. Skull anisotropy has an effect on the accuracy of dipole localization to begin with (Yvert, Bertrand et al. 1997), and the hole produced from a craniotomy has significant effects on volume conduction (Oostenveld and Oostendorp 2002). Therefore, a critical step in extending this work will be the development of forward head models of patient-specific craniotomized skulls (Akalin Acar 2008). When used in conjunction with patient-specific forward models, can likely give more information about the distribution of both pathological and normal brain activities recorded by iEEG and/or scalp EEG sensors.

In conclusion, we demonstrate that ICA is useful for the interpretation of intracranial data. While intracranial recordings from patients with focal refractory epilepsy provide the unique opportunity for analysis of human brain signals with sub-millisecond resolution and without the low pass filtering from the skull and scalp, there

may be limitations to the extrapolation of healthy, normal-functioning brain activity from these studies performed on pathological brain tissue. It is therefore critical to find a robust means for separating epileptic and otherwise pathological brain signals from the task-related brain signals under investigation. ICA is one approach for solving this problem. Furthermore, our analyses demonstrate that intracranial signals are not independent as recorded, suggesting that analysis of event-related brain dynamics in the "component domain" can offer additional insight not readily apparent from the traditional channel domain analysis. Our simple task paradigm, with previously characterized dynamics, validates the use of ICA-based analysis of intracranial data. The success of this approach suggests that new discoveries of brain dynamics associated with novel, more complicated novel cognitive and behavioral tasks, could be discovered with the use of ICA.

4.7 Acknowledgments

Chapter IV is a preprint of a manuscript to be submitted to *Human Brain Mapping*. The dissertation author is the primary author of this work. I would like to thank Scott Makeig and Greg Worrell for co-authoring this work. Co-author Matthew Stead was instrumental in setting up the data acquisition system for the recordings, and co-author Il Keun Lee was responsible for designing the behavioral paradigm. I'd also like to thank Karla Crockett for her assistance in acquiring behavioral data from patients, and Andrey Vankov for his development of software that helped import the data into Matlab.

Table 4.1 Numbers and Locations of Electrodes

Patient	Intracranial electrodes*	Scalp electrodes
1	**88 total, 87 used** 1 6x8 right frontal grid 3 1x4 frontal strips 1 1x4 orbito-frontal strip 2 1x8 lateral frontal strips 2 1x4 mesial temporal surface	31 recorded, 30 used
2	**52 total, 49 used** 1 3x8 left temporal grid 2 1x8 frontal strips 3 1x4 mesial temporal depth probes	21 recorded, 16 used
3	**60 total, 60 used** 1 4x6 right temporal grid 1 8-contact R depth probe 1 8-contact L depth probe 1 8-contact strip 3 1x4 frontal strips	30 recorded, 30 used
4	**44 total, 39 used** 1 6x6 right frontal grid 1 1x8 parietal strip	23 recorded, 16 used

*The number of scalp electrodes varied because of differences in the surgical craniotomy size and location.

Table 4.2 Statistics on histogram of the pairwise mutual information for Patient 1.

Type of Pairs	N	Mean MI (nats)	Median MI (nats)	Range MI (nats)
Intracranial Channels	3741	0.0138	0.0068	Min: 0.0017 Max: 0.4159
Intracranial Components	3741	0.0052	0.0045	Min: 0.0013 Max: 0.0684
Scalp EEG Channels	465	0.0859	0.0510	Min: 0.0056 Max: 0.6857
Scalp EEG Components	465	0.0166	0.0139	Min: 0.0015 Max: 0.1326

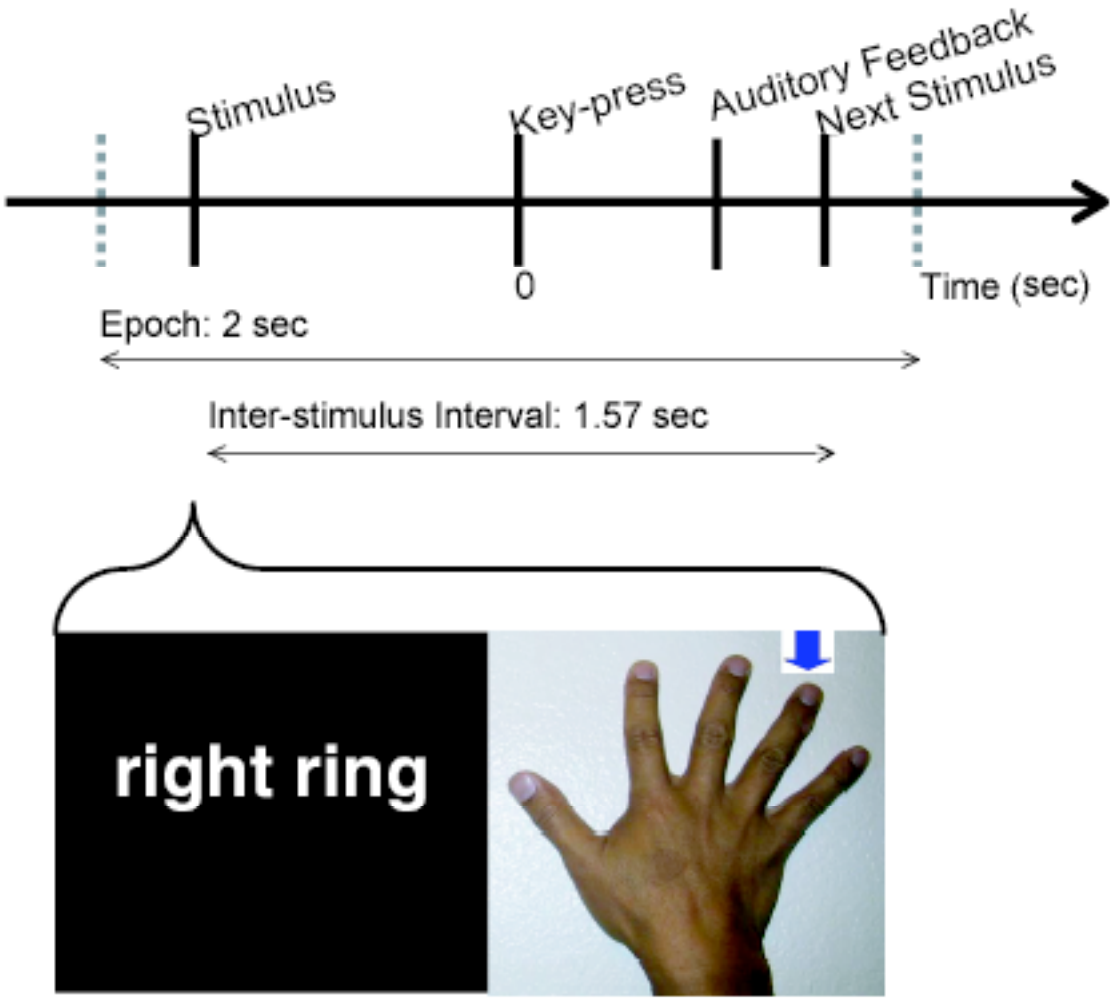

Figure 4.1 Schematic of Visually-cued Finger Movement Task

One of 20 stimuli indicating which finger to move is presented to the patient. Half of the stimuli are words naming a finger, and the other half are pictures of a hand with an arrow pointing to a finger. Stimuli are spaced 1.57 seconds apart. For trial-average spectral changes computed in this study, the data were parsed into 2-s epochs centered on the key-press. (ICA was performed on the continuous data before epoching.) Patients are presented with a tone indicating whether their performance on a given trial was correct or incorrect.

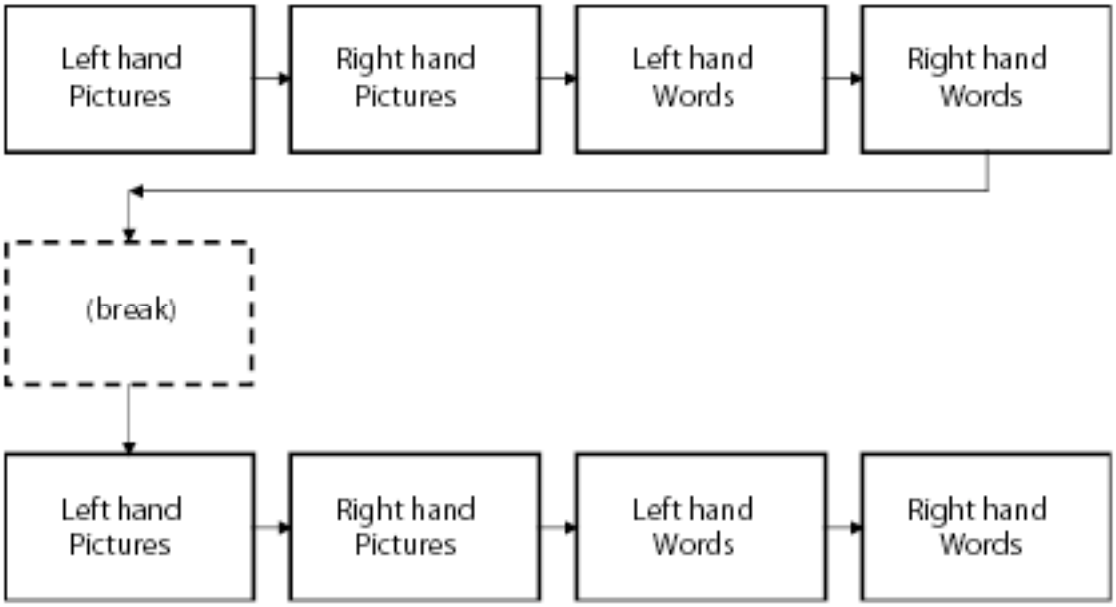

Figure 4.2 Presentation of Stimulus Types in Experimental Task

The study was a block design, with a block for each hand and stimulus type. The presentation of finger stimuli was randomized within a block. The entire experimental task was run through twice for Patients 1,2,3 and once through for Patient 4.

Figure 4.3 Reduction in Pairwise Mutual Information of Independent Components as Compared to Channels

Histograms of normalized pairwise mutual information between channels (top row) and between independent components (bottom row) returned from ICA performed on intracranial data (left) and on scalp EEG (right). As expected, the pair-wise mutual information of independent components is greatly reduced as compared to the pair-wise mutual information of channel recordings. The plot combines results from the recordings of four patients.

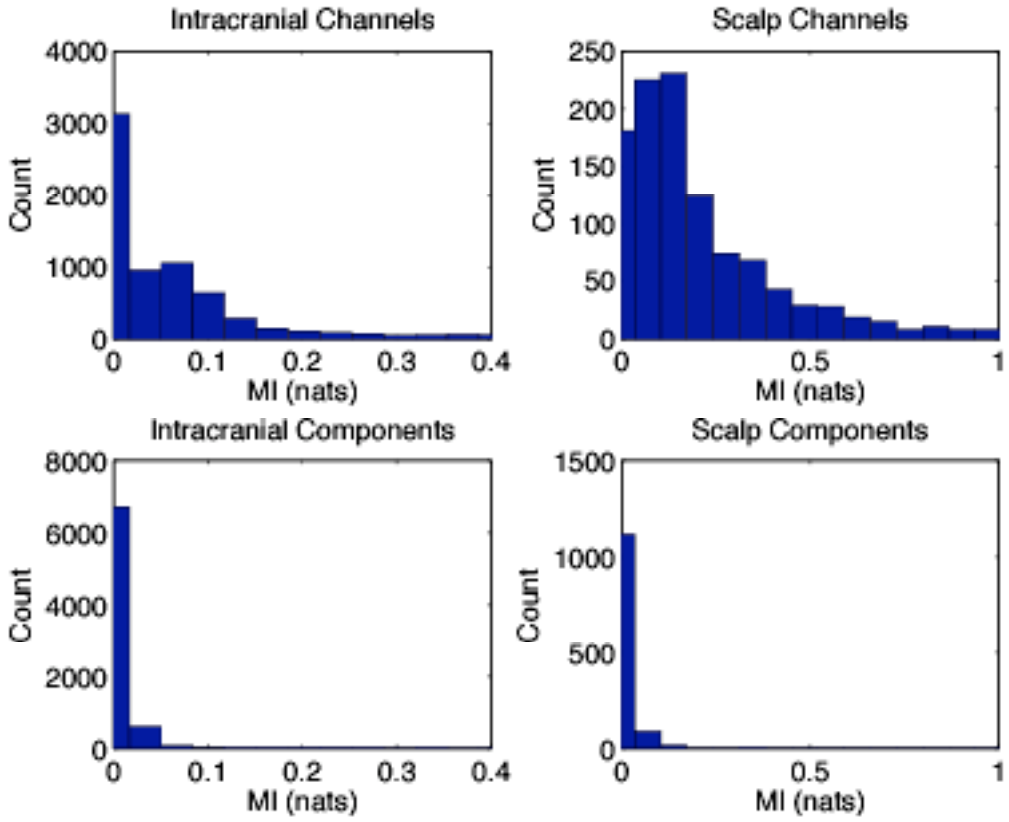
Intracranial Channels
Count
MI (nats)
Scalp Channels
Count
MI (nats)
Intracranial Components
Count
MI (nats)
Scalp Components
Count
MI (nats)

Figure 4.4 Range in Percent Variance of Each Intracranial Channel Accounted for by its Maximum Component

(A) Quasi-topographic display of intracranial (iEEG) channels for a single patient, from a medial view of the right hemisphere (left) and lateral view of the right hemisphere (right). The percent variance of an iEEG channel's activity accounted for by its maximum component indicated with the grey scale. Individual iEEG channels exhibit a wide range in how much of their variance is accounted for by a single component. Channels in white are dominated by a single independent component, whereas channels in dark grey are accounted for by a linear combination of multiple components.

(B) Histogram of maximum percent variance of iEEG channels shown in a). A range of values is demonstrated.

(C) Combined histogram of maximum percent variance of iEEG channels, for all four patients. The range in maximum percent variance accounted for is preserved across patients.

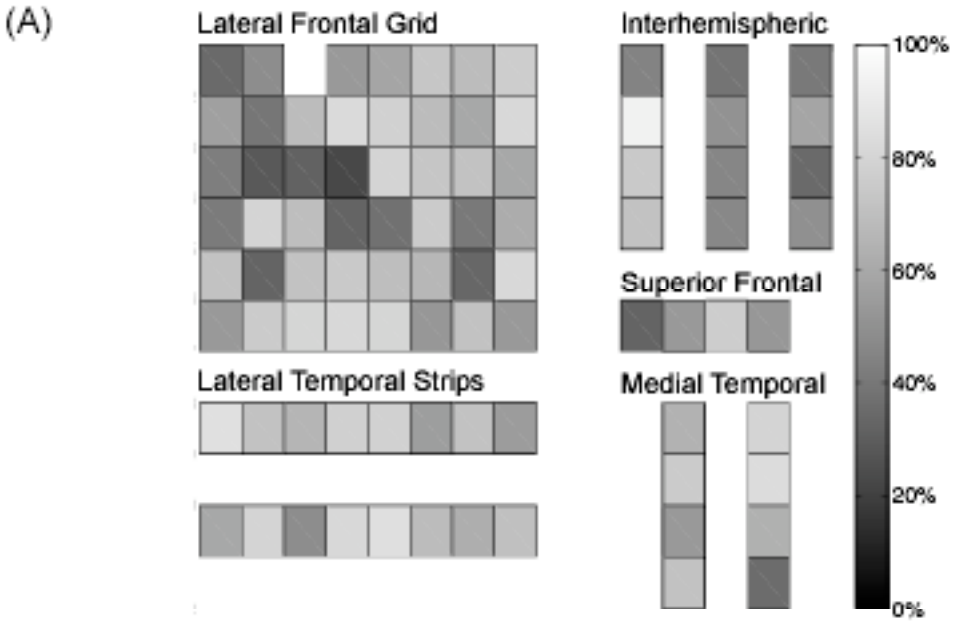
(A)
Lateral Frontal Grid
Interhemispheric
Superior Frontal
Lateral Temporal Strips
Medial Temporal
100%
80%
60%
40%
20%
0%

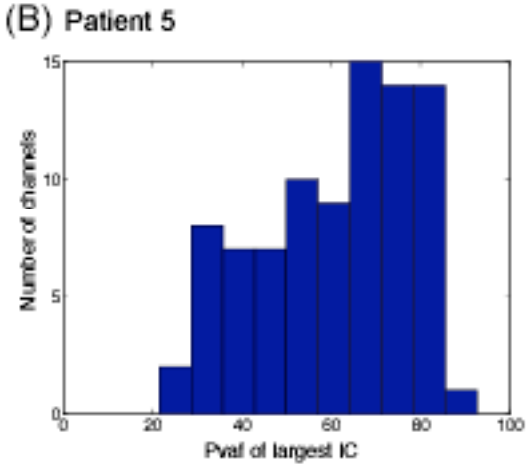
(B) Patient 5
Number of channels
Pval of largest IC

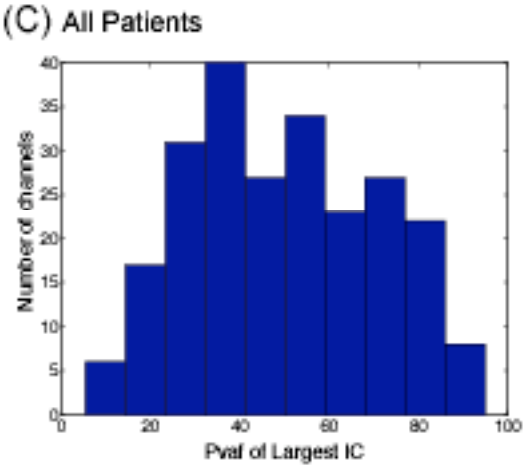
(C) All Patients
Number of channels
Pval of Largest IC

Figure 4.5 Examples of Independent Component Maps

(A) Four example components with focal grid maps.

(B) Examples of components with more diffuse grid maps. These component maps could represent synchronous activity of the cortex proximal to the implanted grid, or could represent the projections of more focal current sources distal from the grid.

(C) Set of components that back-project to both the frontal lateral corner of the intracranial grid, and the anterior end of the superior orbital frontal (SOF) strip. Each component captures a slightly different subset of intracranial channels, including the lateral anterior corner of the grid (Grid1, Grid 2, Grid 9, Grid 10), and the two most anterior channels of the superior orbital frontal strip (SOF3, SOF4). These channels are reported clinically to display coincident episodes of rhythmic moderate amplitude delta.

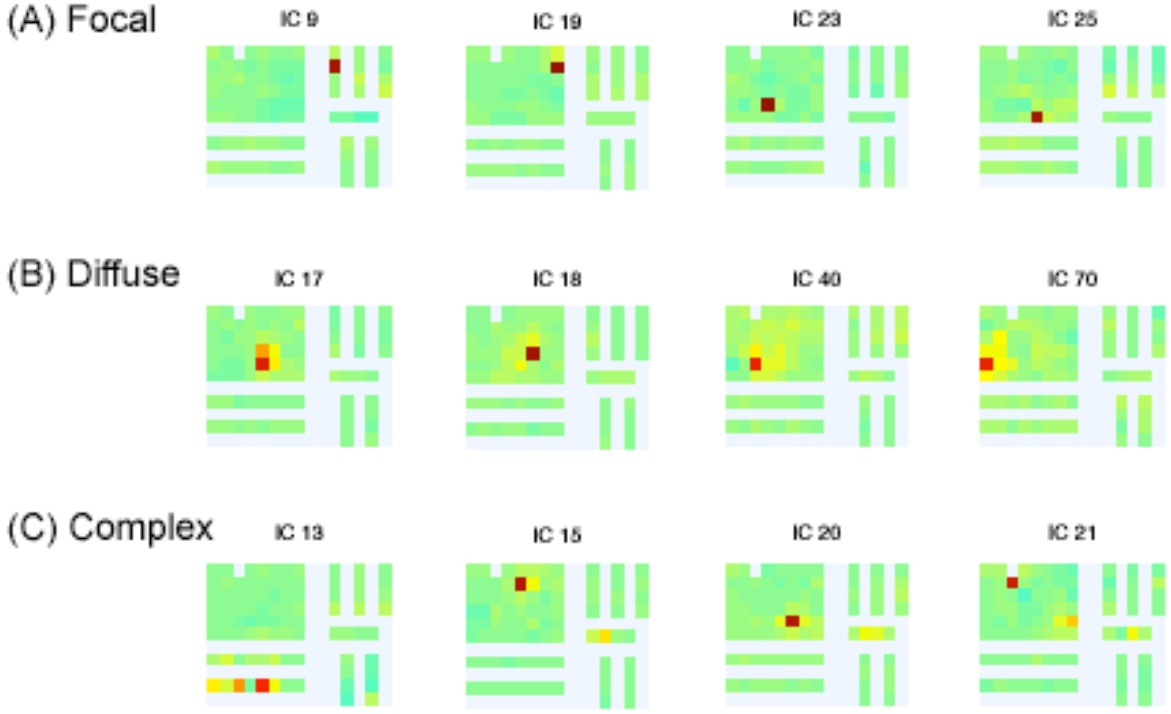
(A) Focal
IC 9
IC 19
IC 23
IC 25
(B) Diffuse
IC 17
IC 18
IC 40
IC 70
(C) Complex
IC 13
IC 15
IC 20
IC 21

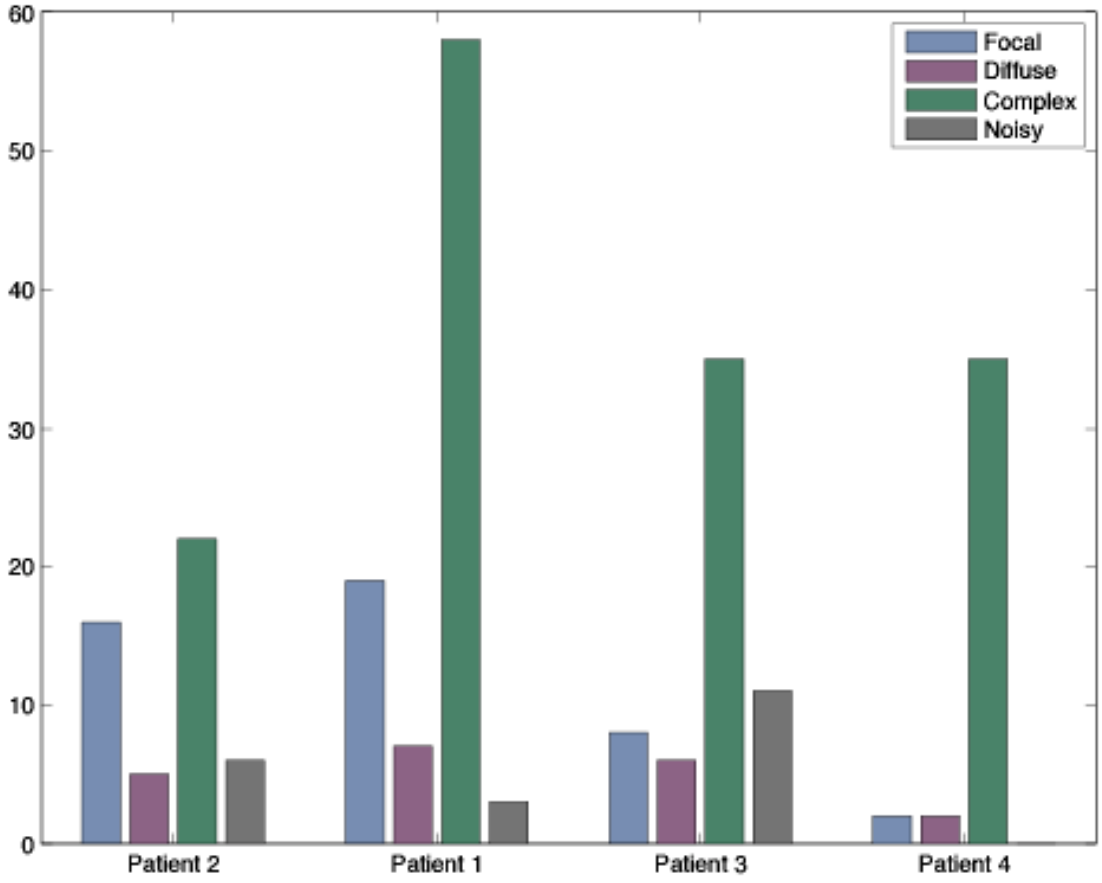

Figure 4.6 Classes of Component Maps

Percentage of components for each patient that fall in to each of the four categories based on visual inspection.

Figure 4.7 Multiple Independent Components Associate Lateral and Medial Frontal Channels with Interictal Delta Activity

(A) Schematic of electrode placement for Patient 1, with channels from independent component 3 (IC3) highlighted in color. Lateral view of right hemisphere on the left, and medial view of right hemisphere on the right.

(B) Map from IC3, which back-projects to Grid1, superior orbital frontal channel 4 (SOF4), and SOF3.

(C) Example 2-s time series from Grid1 (red), SOF4 (orange), and IC3 (black).
(D) Map of Independent Component 1, which projects most strongly to Grid9, but also to Grid1, SOF4, SOF2, and Grid10.

(E) Map of IC4, which back-projects most strongly to SOF3 (red), but also SOF4 (orange), Grid 1(yellow) and SOF2 (yellow).

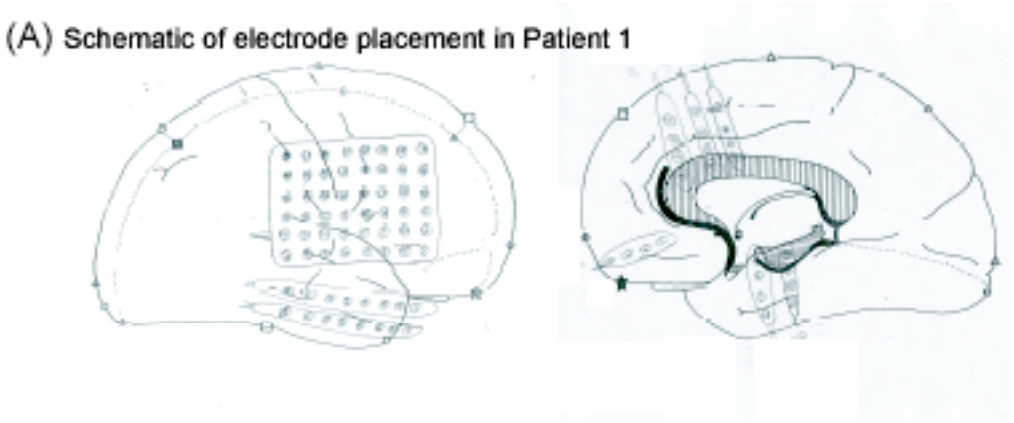
(A) Schematic of electrode placement in Patient 1

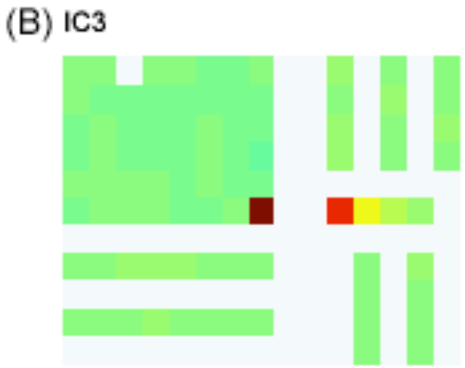
(B) IC3

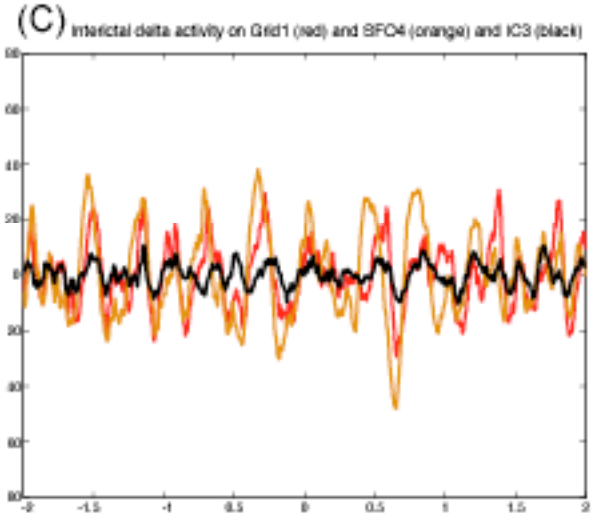
(C) Interictal delta activity on Grid1 (red) and SFC4 (orange) and IC3 (black)

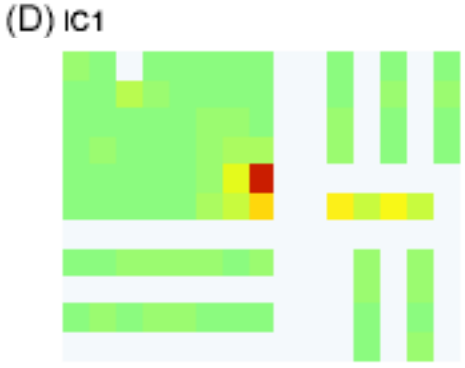
(D) IC1

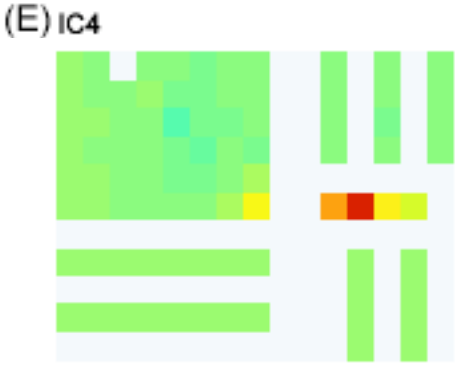
(E) IC4

Figure 4.8 Low Frequency Coherence between Channels Identified by Independent Component 1 (IC1)

(A) Multi-taper power spectral estimates, cross power spectra, and coherence of intracranial channels Grid1 and SOF4. The two channels, identified by IC3 in Figure 4.2, are significantly coherent in the delta band, consistent with the clinical report describing "episodes of coincident rhythmic moderate amplitude delta frequency" on these electrodes.

(B) By contrast, Grid 1 and Grid 8, two channels that do not appear weighted within the same component maps, are not significantly coherent, although they both have power in the delta band (not shown).

(A)

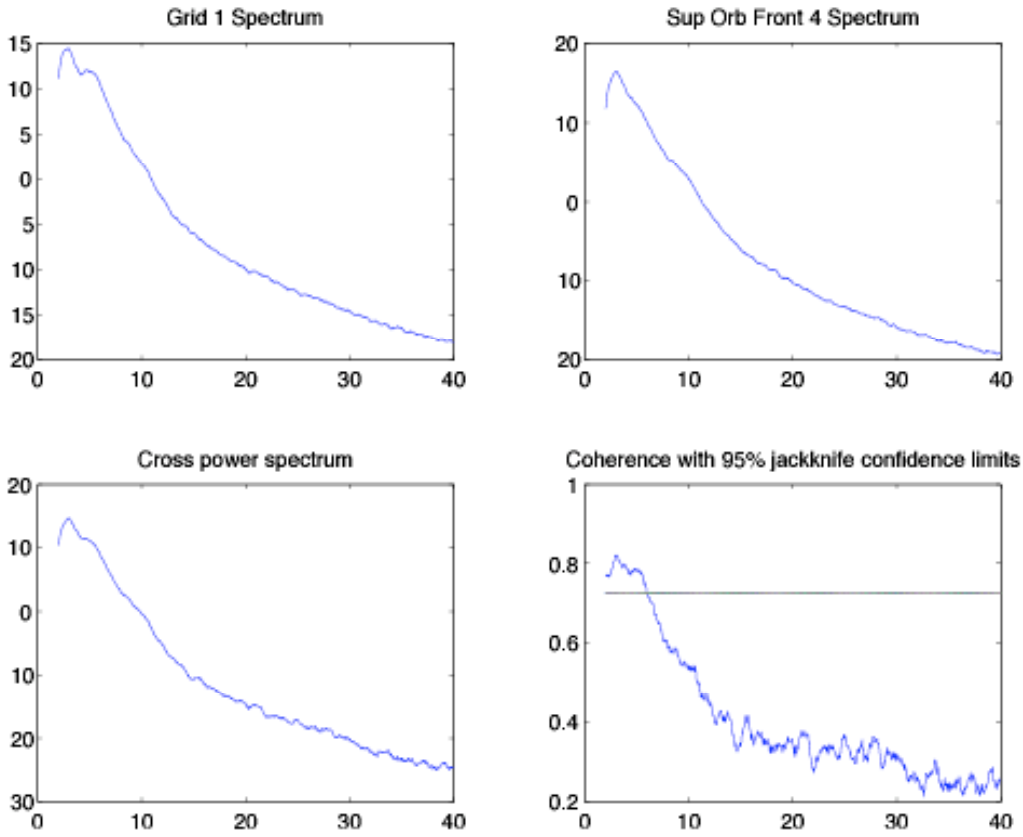
Grid 1 Spectrum
Sup Orb Front 4 Spectrum
Cross power spectrum
Coherence with 95% jackknife confidence limits

(B)

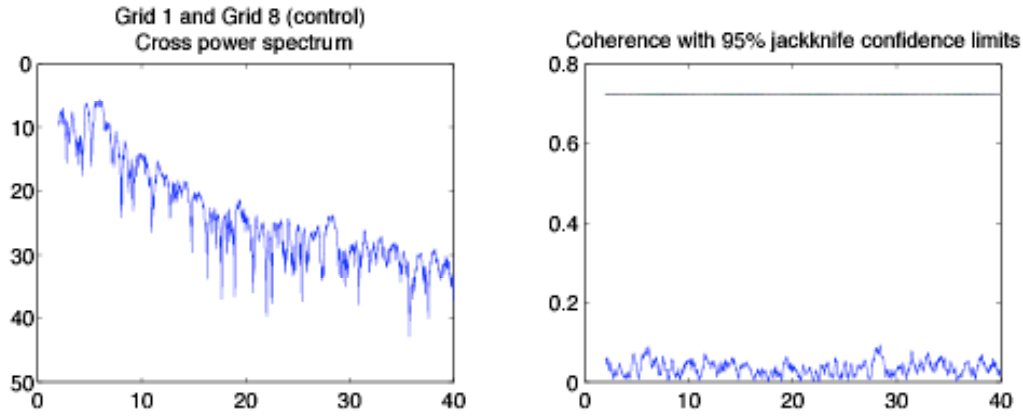
Grid 1 and Grid 8 (control)
Cross power spectrum
Coherence with 95% jackknife confidence limits

Figure 4.9 Mu Blocking and Movement-related Spectral Dynamics

(A) Trial-average event-locked log power spectrum for Grid24, an electrode in or near primary motor cortex.

(B) Time series of Grid24 (black) and IC18 (blue) from example 2-second segment zeroed on the finger movement. A suppression of mu starting approximately 1.7 seconds before the movement and lasting until 0.5 seconds afterwards is evident.

(C) Component map and trial-average event-locked log power spectrum for IC18. The grid map of IC18 maximally back-projects to Grid24 with a penumbra including neighboring channels. IC18 shows strong gamma increase during the movement and concurrent power decreases in both the beta and alpha power bands.

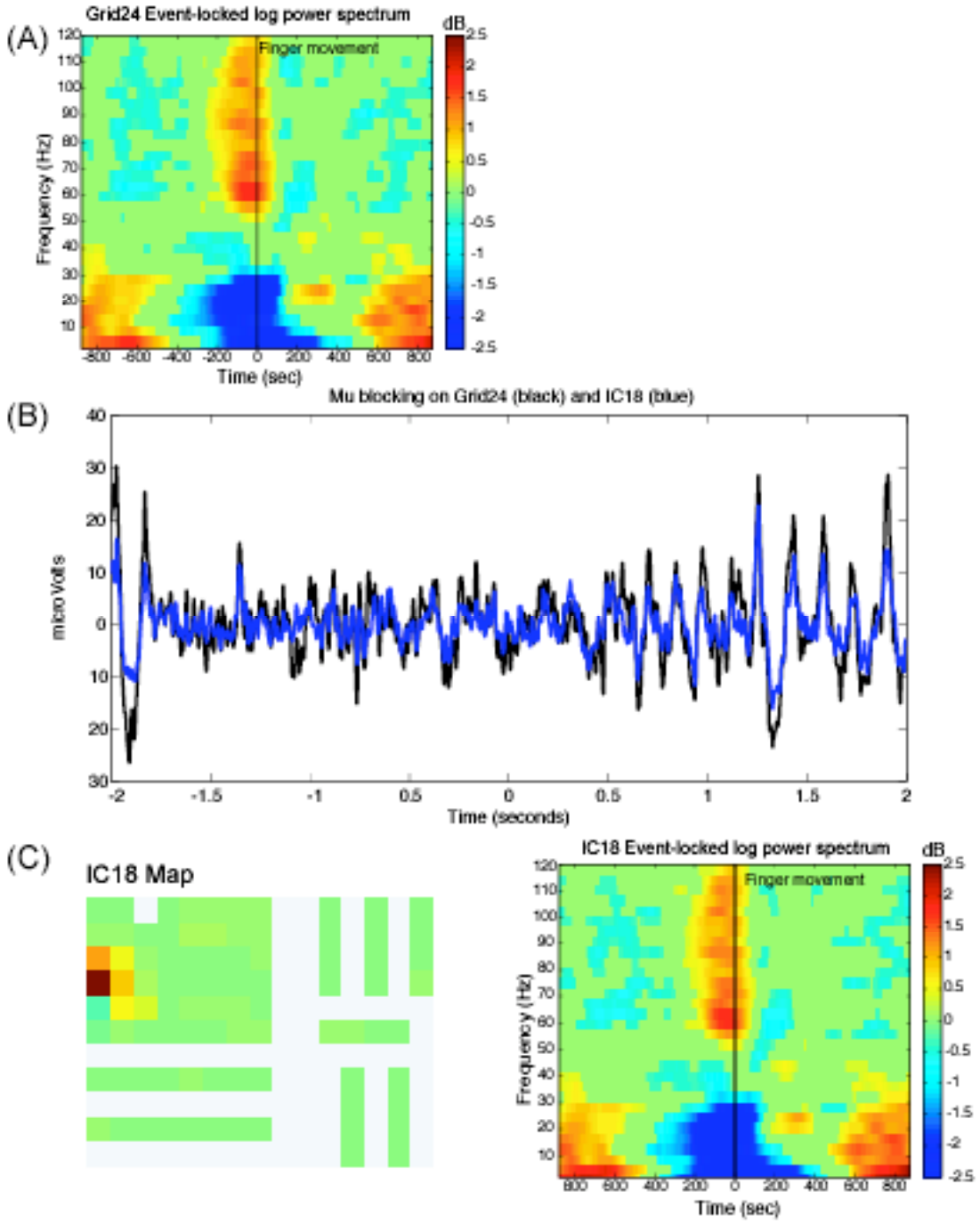
(A)
Grid24 Event-locked log power spectrum
Finger movement
dB
Frequency (Hz)
Time (sec)
(B)
Mu blocking on Grid24 (black) and IC18 (blue)
micro Volts
Time (seconds)
(C)
IC18 Map
IC18 Event-locked log power spectrum
Finger movement
dB
Frequency (Hz)
Time (sec)

Figure 4.10 Independent Components Capture Dynamics in Different Regions of Motor Cortex

Grid maps and event-locked log power spectra for three independent components.

(A) The grid map of IC23 projects most strongly to Grid23, which is located in or near Brodmann Area 6 of the precentral gyrus and also projects to neighboring electrodes. IC23 demonstrates an alpha and beta power decrease time-locked to the finger movement followed by a rebound power increase.

(B) The grid map of IC68 projects most strongly to Grid15, which is also in or near Brodmann Area 6. As compared to IC23, the movement-locked beta power decrease is smaller in amplitude. IC68 additionally demonstrates a broadband gamma power increase time-locked to the movement but with less precision in time than IC18 (Figure 4.9).

(C) The grid map for IC63 projects most strongly to Grid8, which is near the superior temporal gyrus and borders on Area 43 of the precentral gyrus. The event-locked spectral dynamics demonstrate a broadband gamma power increase within 100 msec after the finger movement

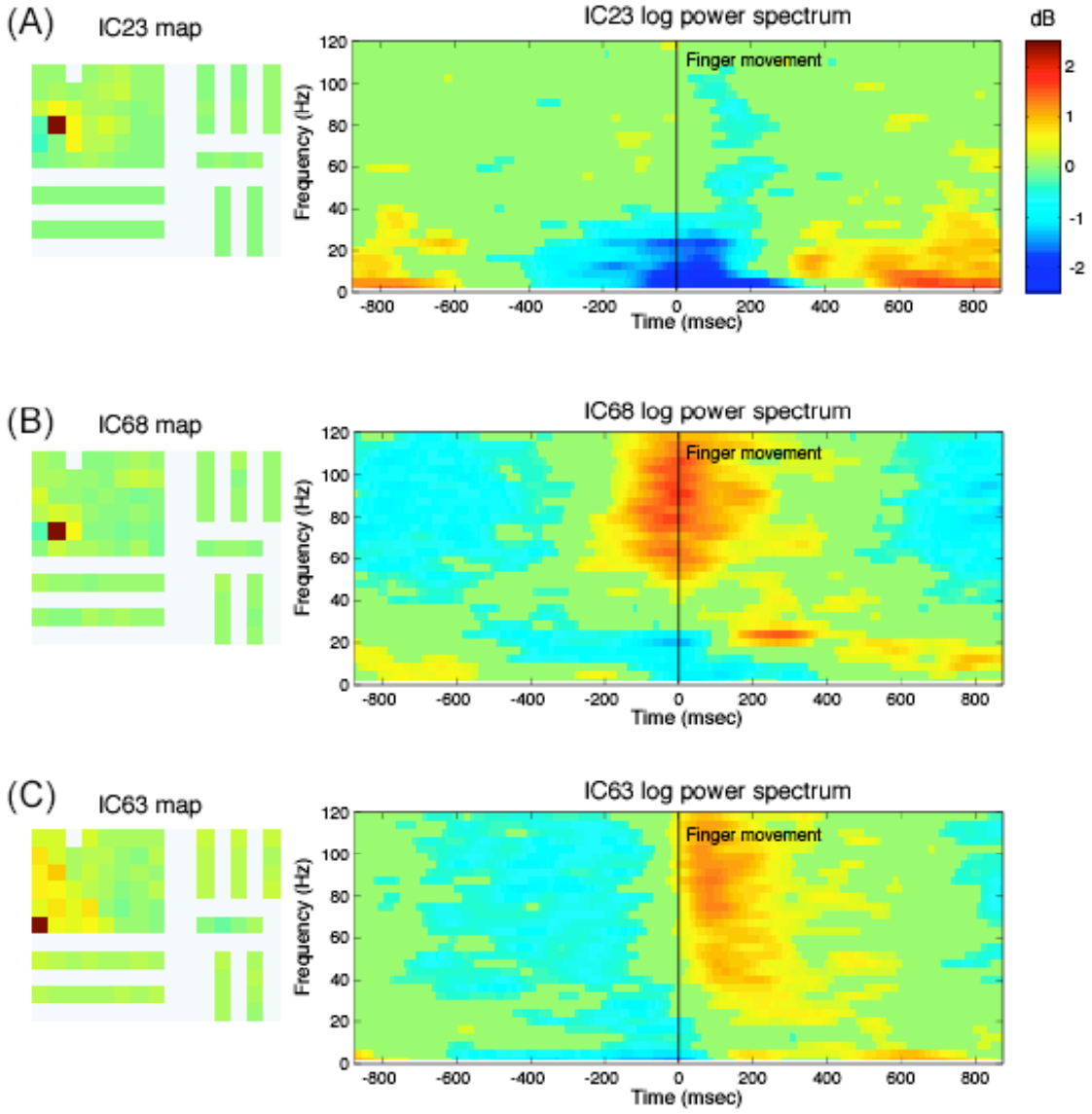
(A)
IC23 map
IC23 log power spectrum
dB
Finger movement
Frequency (Hz)
Time (msec)
(B)
IC68 map
IC68 log power spectrum
Finger movement
Frequency (Hz)
Time (msec)
(C)
IC63 map
IC63 log power spectrum
Finger movement
Frequency (Hz)
Time (msec)

REFERENCES

1. Akalin Acar, Z., Makeig, S. (2008). Head modeling and cortical localization in epilepsy. Proceedings of IEEE EMBC 2008, Vancouver, Canada.

2. Anemuller, J., J. R. Duann, et al. (2006). "Spatio-temporal dynamics in fMRI recordings revealed with complex independent component analysis." Neurocomputing **69**(13-15): 1502-1512.

3. Anemuller, J., T. J. Sejnowski, et al. (2003). "Complex independent component analysis of frequency-domain electroencephalographic data." Neural Netw **16**(9): 1311-23.

4. Aoki, F., E. E. Fetz, et al. (1999). "Increased gamma-range activity in human sensorimotor cortex during performance of visuomotor tasks." Clin Neurophysiol **110**(3): 524-37.

5. Aoki, F., E. E. Fetz, et al. (2001). "Changes in power and coherence of brain activity in human sensorimotor cortex during performance of visuomotor tasks." Biosystems **63**(1-3): 89-99.

6. Arroyo, S., R. P. Lesser, et al. (1993). "Functional significance of the mu rhythm of human cortex: an electrophysiologic study with subdural electrodes." Electroencephalogr Clin Neurophysiol **87**(3): 76-87.

7. Ball, T., E. Demandt, et al. (2008). "Movement related activity in the high gamma range of the human EEG." Neuroimage **41**(2): 302-10.

8. Bates, J. F. and P. S. Goldman-Rakic (1993). "Prefrontal connections of medial motor areas in the rhesus monkey." J Comp Neurol **336**(2): 211-28.

9. Bechara, A., H. Damasio, et al. (1998). "Dissociation Of working memory from decision making within the human prefrontal cortex." J Neurosci **18**(1): 428-37.

10. Bell, A. J. and T. J. Sejnowski (1995). "An information-maximization approach to blind separation and blind deconvolution." Neural Comput **7**(6): 1129-59.

11. Berg, R. W., D. Whitmer, et al. (2006). "Exploratory whisking by rat is not phase-locked to the hippocampal theta rhythm." J Neurosci **26**(24): 6518-22.

12. Berger, H. (1929). "Uber das Elektrenkephalogramm des Menschen." Arch. Psychiatr. Nervenkr **87**: 527-570.

13. Bullock, T. H., M. C. McClune, et al. (1995). "EEG coherence has structure in the millimeter domain: subdural and hippocampal recordings from epileptic patients." Electroencephalogr Clin Neurophysiol **95**(3): 161-77.

14. Burchiel, K. J., H. Clarke, et al. (1989). "Use of stimulation mapping and corticography in the excision of arteriovenous malformations in sensorimotor and language-related neocortex." Neurosurgery **24**(3): 322-7.

15. Cameron, K. A., S. Yashar, et al. (2001). "Human hippocampal neurons predict how well word pairs will be remembered." Neuron **30**(1): 289-98.

16. Cover, T. M., Thomas, J.A. (2006). Elements of Information Theory, John Wiley & Sons, Inc.

17. Crone, N. E., D. L. Miglioretti, et al. (1998). "Functional mapping of human sensorimotor cortex with electrocorticographic spectral analysis. II. Event-related synchronization in the gamma band." Brain **121 (Pt 12)**: 2301-15.

18. Crone, N. E., D. L. Miglioretti, et al. (1998). "Functional mapping of human sensorimotor cortex with electrocorticographic spectral analysis. I. Alpha and beta event-related desynchronization." Brain **121 (Pt 12)**: 2271-99.

19. Dewar, S., E. Passaro, et al. (1996). "Intracranial electrode monitoring for seizure localization: indications, methods and the prevention of complications." J Neurosci Nurs **28**(5): 280-4, 289-92.

20. Dyrholm, M., S. Makeig, et al. (2006). "Model structure selection in convolutive mixtures." Independent Component Analysis and Blind Signal Separation, Proceedings **3889**: 74-81.

21. Dyrholm, M., S. Makeig, et al. (2007). "Model selection for convolutive ICA with an application to spatiotemporal analysis of EEG." Neural Comput **19**(4): 934-55.

22. Engel, J., Jr. and P. H. Crandall (1987). "Intensive neurodiagnostic monitoring with intracranial electrodes." Adv Neurol **46**: 85-106.

23. Engel, J. J. (1996). Principles of epilepsy surgery. Oxford, Blackwell.

24. Fell, J., P. Klaver, et al. (2001). "Human memory formation is accompanied by rhinal-hippocampal coupling and decoupling." Nat Neurosci **4**(12): 1259-64.

25. Freeman, W. J., M. D. Holmes, et al. (2006). "Fine spatiotemporal structure of phase in human intracranial EEG." Clin Neurophysiol **117**(6): 1228-43.

26. Gastaut, H., H. Terzian, et al. (1952). "[Study of a little electroencephalographic activity: rolandic arched rhythm.]." Mars Med **89**(6): 296-310.

27. Halgren, E., P. Baudena, et al. (1994). "Spatio-temporal stages in face and word processing. 2. Depth-recorded potentials in the human frontal and Rolandic cortices." J Physiol Paris **88**(1): 51-80.

28. Halgren, E., P. Baudena, et al. (1994). "Spatio-temporal stages in face and word processing. I. Depth-recorded potentials in the human occipital, temporal and parietal lobes [corrected]." J Physiol Paris **88**(1): 1-50.

29. Hu, S., M. Stead, et al. (2007). "Automatic identification and removal of scalp reference signal for intracranial EEGs based on independent component analysis." IEEE Trans Biomed Eng **54**(9): 1560-72.

30. Hung, C. I., P. S. Wang, et al. (2007). "Blind source separation of concurrent disease-related patterns from EEG in Creutzfeldt-Jakob disease for assisting early diagnosis." Ann Biomed Eng **35**(12): 2168-79.

31. Jarvis, M. R. and P. P. Mitra (2001). "Sampling properties of the spectrum and coherency of sequences of action potentials." Neural Comput **13**(4): 717-49.

32. Jasper, H., Penfield, W (1949). "Electrocorticograms in man: effect of voluntary movement upon the electrical activity of the precentral gyrus." Arch Psychiatr Neurol **182**: 163-174.

33. Jasper, H. a. A., HL (1938). "Electro-encephalography. III. Normal differentiation of occipital and precentral regions in man." Arch Neurol Psychiat **39**: 96-115.

34. Kahana, M. J., J. B. Caplan, et al. (1999). "Using intracranial recordings to study thetaResponse to J. O'Keefe and N. Burgess (1999)." Trends Cogn Sci **3**(11): 406-407.

35. Klopp, J., K. Marinkovic, et al. (2000). "Early widespread cortical distribution of coherent fusiform face selective activity." Hum Brain Mapp **11**(4): 286-93.

36. Klopp, J., K. Marinkovic, et al. (2001). "Timing and localization of movement-related spectral changes in the human peri-Rolandic cortex: intracranial recordings." Neuroimage **14**(2): 391-405.

37. Kubota, F. and N. Ohnishi (1997). "Study on FIRDA and 3 Hz rhythmic slow wave bursts occurring in the frontal area of epileptic patients." Clin Electroencephalogr **28**(2): 112-6.

38. Kuzniecky, R., R. Morawetz, et al. (1995). "Frontal and central lobe focal dysplasia: clinical, EEG and imaging features." Dev Med Child Neurol **37**(2): 159-66.

39. Lancaster, J. L., M. G. Woldorff, et al. (2000). "Automated Talairach atlas labels for functional brain mapping." Hum Brain Mapp **10**(3): 120-31.

40. Lu, M. T., J. B. Preston, et al. (1994). "Interconnections between the prefrontal cortex and the premotor areas in the frontal lobe." J Comp Neurol **341**(3): 375-92.

41. Luders, H., I. Awad, et al. (1992). "Subdural electrodes in the presurgical evaluation for surgery of epilepsy." Epilepsy Res Suppl **5**: 147-56.

42. Luders, H. O., D. S. Dinner, et al. (1995). "Cortical electrical stimulation in humans. The negative motor areas." Adv Neurol **67**: 115-29.

43. Miller, E. K. and J. D. Cohen (2001). "An integrative theory of prefrontal cortex function." Annu Rev Neurosci **24**: 167-202.

44. Miller, K. J., E. C. Leuthardt, et al. (2007). "Spectral changes in cortical surface potentials during motor movement." J Neurosci **27**(9): 2424-32.

45. Miller, K. J., S. Makeig, et al. (2007). "Cortical electrode localization from X-rays and simple mapping for electrocorticographic research: The "Location on Cortex" (LOC) package for MATLAB." Journal of Neuroscience Methods **162**(1-2): 303-308.

46. Mitra, P. P. and B. Pesaran (1999). "Analysis of dynamic brain imaging data." Biophys J **76**(2): 691-708.

47. Niedermeyer, E. (2003). "Electrophysiology of the frontal lobe." Clin Electroencephalogr **34**(1): 5-12.

48. Niedermeyer, E. a. L. D. S., F. (1999). Electroencephalography: Basic principles, clinical applications, and related fields. Baltimore, Williams & Wilkins.

49. Nunez, P. L., Srinivasan, R. (2006). Electric Fields of the Brain: The Neurophysics of EEG. New York, Oxford University Press.

50. Nunez, P. L., B. M. Wingeier, et al. (2001). "Spatial-temporal structures of human alpha rhythms: theory, microcurrent sources, multiscale measurements, and global binding of local networks." Hum Brain Mapp **13**(3): 125-64.

51. Ohara, S., A. Ikeda, et al. (2000). "Movement-related change of electrocorticographic activity in human supplementary motor area proper." Brain **123 (Pt 6)**: 1203-15.

52. Ojemann, G. A. (1982). "Models of the brain organization for higher integrative functions derived with electrical stimulation techniques." Hum Neurobiol **1**(4): 243-9.

53. Oostenveld, R. and T. F. Oostendorp (2002). "Validating the boundary element method for forward and inverse EEG computations in the presence of a hole in the skull." Hum Brain Mapp **17**(3): 179-92.

54. Palmer, J. A., Kreutz-Delgado, K., Makeig, S. (2006). Super-gassian mixture source model for ICA. Proceedings of the 6th International Symposium on Independent Component Analysis, Springer.

55. Penfield, W. (1954). "Mechanisms of voluntary movement." Brain **77**(1): 1-17.

56. Penfield, W. a. K., K (1951). Epileptic Seizure Patterns. Springfield, IL, Charles C. Thomas.

57. Percival, D. B. a. W., A.T. (1993). Spectral Analysis for Physical Applications. London, Cambridge University Press.

58. Pfurtscheller, G. and A. Aranibar (1977). "Event-related cortical desynchronization detected by power measurements of scalp EEG." Electroencephalogr Clin Neurophysiol **42**(6): 817-26.

59. Pfurtscheller, G. and A. Aranibar (1980). "Changes in central EEG activity in relation to voluntary movement. I. Normal subjects." Prog Brain Res **54**: 225-31.

60. Pfurtscheller, G., M. Pregenzer, et al. (1994). "Visualization of sensorimotor areas involved in preparation for hand movement based on classification of mu and central beta rhythms in single EEG trials in man." Neurosci Lett **181**(1-2): 43-6.

61. Quiroga, R. Q., L. Reddy, et al. (2005). "Invariant visual representation by single neurons in the human brain." Nature **435**(7045): 1102-7.

62. Ray, S., E. Niebur, et al. (2008). "High-frequency gamma activity (80-150Hz) is increased in human cortex during selective attention." Clin Neurophysiol **119**(1): 116-33.

63. Rektor, I., D. Sochurkova, et al. (2006). "Intracerebral ERD/ERS in voluntary movement and in cognitive visuomotor task." Prog Brain Res **159**: 311-30.

64. Repucci, M. A., N. D. Schiff, et al. (2001). "General strategy for hierarchical decomposition of multivariate time series: implications for temporal lobe seizures." Ann Biomed Eng **29**(12): 1135-49.

65. Rizzuto, D. S., J. R. Madsen, et al. (2006). "Human neocortical oscillations exhibit theta phase differences between encoding and retrieval." Neuroimage **31**(3): 1352-8.

66. Rubino, D., K. A. Robbins, et al. (2006). "Propagating waves mediate information transfer in the motor cortex." Nat Neurosci **9**(12): 1549-57.

67. Salmelin, R. and R. Hari (1994). "Spatiotemporal characteristics of sensorimotor neuromagnetic rhythms related to thumb movement." Neuroscience **60**(2): 537-50.

68. Stancak, A., Jr. and G. Pfurtscheller (1996). "Mu-rhythm changes in brisk and slow self-paced finger movements." Neuroreport **7**(6): 1161-4.

69. Tharin, S. and A. Golby (2007). "Functional brain mapping and its applications to neurosurgery." Neurosurgery **60**(4 Suppl 2): 185-201; discussion 201-2.

70. Thomson, D. J. (1982). "Spectrum estimates and harmonic analysis." Proc. IEEE **70**: 1055-1096.

71. Wyler, A. R., G. A. Ojemann, et al. (1984). "Subdural strip electrodes for localizing epileptogenic foci." J Neurosurg **60**(6): 1195-200.

72. Yvert, B., O. Bertrand, et al. (1997). "A systematic evaluation of the spherical model accuracy in EEG dipole localization." Electroencephalogr Clin Neurophysiol **102**(5): 452-9.

Chapter V. Conclusions and Future Work

In Chapter II, we used a behavioral paradigm to test the rat's ability to localize objects in space with its whiskers. The translation from touch to the position of an object requires that the animal keep track of its own body position. Our study demonstrated that rats could use a single actively moving whisker to search for, locate, and differentiate objects in space. Rats were able to keep track of their vibrissa motion with a resolution less than 100 msec. The ability of the rat to accomplish this task with only a single whisker suggests that the phase of a whisking cycle could be used as a reference signal to compare with a contact signal and compute an object's position.

Similar findings by Knutsen and colleagues (Knutsen, Pietr et al. 2006) were published contemporaneously with these results. In their experimental paradigm, rats compared the rostro-caudal position of two different objects on opposite sides of its head. The rat's performance was at chance in the absence of whisking movements and was improved when the animal had a stable head and body (Knutsen, Pietr et al. 2006). Both the findings of Knutsen et al. and the work presented in Chapter II filled a fundamental gap in our understanding of how object location in 3-d space can be represented by the nervous system the rat and its a two-dimensional sensor array. The neural code must disambiguate confounds of object position in the medial and rostro-caudal directions and ambiguities introduced by the movement of the whiskers themselves. Ahissar and Knutsen (Ahissar and Knutsen 2008) used our results as a building block for their comprehensive model for the neural code of spatial position. They propose that vertical position is encoded with a labeled-line code, radial position is encoded with firing rate,

and rostro-caudal position is encoded with timing. They argue that this triple-coding scheme allows for efficiency within the nervous system.

In Chapter III, we computed the coherence between a salient hippocampal brain signal and whisker movements, both which occur in the theta frequency band, to determine whether these signals are related and phase-locked. Given that theta in the rat co-occurs with voluntary movements, it was a plausible hypothesis that whisking and theta would be synchronous, suggested by visual inspection of some of the data. Our work demonstrated that extracting phase information from the complex-valued coherence measure to quantify phase locking, and with the use of statistics, hippocampal theta and whisking oscillations are not coherent. Our careful analyses and quantification disambiguated competing theories (Vanderwolf 1969; Komisaruk 1970) and resolved a thirty-year-old debate in neuroscience literature.

In Chapter IV, human data acquired during a visually-cued finger movement task was analyzed both with independent component analysis and spectral estimations. We showed that ICA could be used to decompose intracranial data into a set of independent model sources, where a "source" is the activity from a nearly synchronous patch of cortex. Moreover, ICA was shown to separate the pathological brain signals that contaminate these types of recordings, from the cognitive/perceptual signals under investigation.

A theme that emerges from this work is the notion of phase for information processing of the nervous system. The earliest work in neuroscience from single unit recordings in the olfactory and visual system focused on rate codes. Neuroscience research has evolved to consider timing as an essential aspect of the neural code.

Rhythmicity is inherent in the nervous system: both in specialized motor outputs such as the natural and ethologically important whisking movements of rats, and in oscillations at many different frequency bands throughout the brain. The phase of the motor output of the whisking system is a necessary parameter for the accurate encoding of spatial position of objects. Oscillations at the level of spikes, local field potentials, intracranial EEG, and scalp EEG are the signatures of fine non-rhythmic motor movements such as human finger movements and of a variety of behaviors and cognitive events. Future work will take the exploration of oscillations one step future and examine phase relationships among different frequency bands and between disparate brain areas. Independent component analysis can help identify spatially discontiguous brain areas that exhibit synchronous activity in response to behavioral and cognitive events. Additionally, scientists will use results from basic science experiments on cognition and motor output to develop neural prosthetics. We may still be decades away from determining the cortical signature(s) of consciousness (and even of agreeing upon on a clear definition of this term), but in the interim, phase-locking is proving to play an essential role, at least for the creation of single conscious percepts of visual stimuli.

5.1 Future work with Intracranial ICA

Independent component analysis is a model that presumes spatial stationarity of independent sources over the duration of the recording. In recent years, more sophisticated ICA algorithms have been developed that relax this assumption and could be applied to intracranial data for more accurate descriptions of underlying brain processes.

Complex ICA is one technique that improves upon the infomax ICA model. With complex ICA, a source regarded as dynamic spatio-temporal pattern, i.e. one that can move across cortex. This is modeled as convolutive mixing in the temporal domain, where an impulse-like EEG activation can be smeared out into a sequence of maps with different spatial topographies. Convolutive mixing in time translates to multiplicative mixing in the frequency domain. Complex ICA is therefore performed on complex-valued spectra in the frequency domain, after having spectrally decomposed the time series. In the work of Anemuller, Sejnowski and colleagues (Anemuller, Sejnowski et al. 2003), EEG data is first spectrally decomposed into the classical EEG bands (theta, alpha, beta, etc.) and subsequently decomposed by the complex ICA algorithm. The results from this approach suggest an improvement in the separation of sources from infomax ICA. Further, it successfully identified sources with spatial dynamics in EEG data acquired during a visual spatial attention task.

A further extension of the ICA algorithm is to relax the assumption of zero time delays in addition to the spatial stationarity constraint. Dyrholm, Makeig and colleagues (Dyrholm, Makeig et al. 2007) implemented an algorithm that used autoregressive filter to find maximally independent components in the frequency domain. Their technique also separated out independent components suggestive of biologically plausible brain sources based on their spatial maps and temporal dynamics.

Another new approach for using ICA is the Mixture ICA algorithm developed by Palmer and colleagues (Palmer 2008). This approach relaxes the spatial stationarity constraint and the constraint of a fixed number of sources equal to the number of sensors. The algorithm decomposes the data into multiple mixtures of independent sources that

change as a function of time over the length of the recording. Preliminary results suggest that this technique can parse out the evolving dynamics of epileptic seizure activity (Palmer 2008; Palmer, Akalin-Acar et al. 2008).

5.2 Forward Models for Intracranial ICA

Independent component analysis is a methodology that answers the "what" question about brain sources without answering the question of where the sources are located. It is therefore necessary to combine ICA results with source localization methods such as current equivalent dipole models to a more complete interpretation of the results. To date, most source localization methods have been developed based on the fully intact skulls of normal subjects. In intracranial studies, however, the participating patients have typically undergone craniotomies for the implantation of electrodes and have large portions of skull removed. The propagation of electrical signals through the brain volume conductor is dramatically changed by the craniotomy. Even small holes from local skull defects have been shown to produce an abnormal EEG signal known as the "breach rhythm" (Niedermeyer 1999).

The forward problem of how to calculate the electromagnetic fields observed on intracranial and scalp EEG sensors given a distribution of brain sources, is a fundamental step in accurately solving the inverse problem of localizing sources. Akalin-Acar and colleagues (Akalin Acar 2008a; Akalin Acar 2008b) have recently developed a toolbox for producing patient-specific realistic head models for the modeling of forward current flow in intracranial patients. They extracted and modeled segmented tissue volumes for scalp, skull, and cerebral spinal fluid, using magnetic resonance (MR) images. The

boundary element model (BEM) was implemented for the numerical solution of the forward flow of electromagnetic signals. This approach has been applied to epilepsy seizure data and, in conjunction with ICA, has been used to localize independent seizure sources (Akalin Acar 2008b). The application of this method to intracranial data from patients participating in cognitive experiments, will further our understanding of cognition, perception, and behavior.

5.3 Microwires Recordings in Humans

Another direction for the advancement of human research is the use of microwire recordings in epilepsy patients. Recent technological advances for epilepsy research have resulted in the implementation of microwire recordings in human epilepsy patients concurrently with traditional macro-electrode intracranial recordings (Howard et al., Garrett, 1996; Ulbert et al., 2001). This clinical development has provided the opportunity for neuroscientists to 1) obtain better spatial sampling of the electrical signals of human brain dynamics, 2) fill in the gaps between animal research and human research, and 3) begin to address the multi-scale problem by measuring relationships between spikes, LFP recordings, and iEEG recordings. For example, Kraskov and colleagues (2007) have recorded simultaneous spikes and LFPs from the medial temporal lobe of human patients. Microwire recordings from the human medial temporal lobe have revealed single neurons that are selective (Fried et al., 1997; Kreiman et al., 2000) and invariant (Quiroga et al., 2005) in their responses to categories of objects and of human faces. The responses of medial temporal single units and LFPs can be used to decode the semantic category of stimuli (Kraskov et al, 2007), providing a basic step toward the

development of cognitive neural prosthetics (Pesaran et al., 2006). Studies of motion perception (Ulbert et al., 2001) and emotional processing (Kawasaki et al., 2001) have also been achieved with microwire recordings, along with studies of language. The development of microelectrodes allows for finer spatial sampling than can otherwise be obtained given that language studies with animal models are not possible. Randomly sampled single neuron recordings from the temporal cortex are selectively responsive to language tasks such as naming, reading, or listening to words (Ojemann et al., 1988; Haglund et al., 1994; Schwartz et al., 1996; Ojemann & Shoenfield-McNeill, 1999). The use of concurrent microwires and clinical iEEG macroelectrodes during movement paradigms has not yet been undertaken and is likely to enable significant advances in the development of neural prosthetics.

5.4 Applications to Brain-Computer Interfaces

One the ultimate goals of neuroscience research is to elucidate basic mechanisms of brain function for the development of clinical treatments and applications. Approximately 2.4 million patients in the U.S. are paralyzed from a variety of medical conditions including traumatic head or spinal cord injury, stroke, and amyotrophic lateral sclerosis (ALS). The development of neural prosthetics and other brain-computer interfaces (BCI) is essential for the treatment of these patients. Basic neuroscience research on sensorimotor systems and the application of tools like ICA can facilitate the progress of developing brain-computer interfaces.

For example, both the alpha band of the mu rhythm (Wolpaw, McFarland et al. 1991) and sensorimotor beta activity (Kubler, Nijboer et al. 2005; Bai 2008) have been

effective signals for non-invasive brain-based control of cursor movements. In separate work, ICA was shown to be instrumental for removing artifacts and improving classification performance of a reaching task based on EEG signals (Hammon, Makeig et al. 2008). The cortical signals used for BCI implementations of cursor movements and/or robot arms have spanned the range of single unit recordings (Taylor et al., 2002; Hochburg et al., 2006), LFPs (Donoghue, 2007; Rickert, 2005), human intracranial recordings (Leuthardt et al, 2004; Mehring, 2004; Pistohl, 2008), and whole brain EEG (McFarland, Wolpaw et al., 2006). Local field potential recordings from monkey (Rickert, Oliveira et al. 2005) have shown great promise for read-out of movement direction and better classify movement direction than iEEG signals (Mehring, Nawrot et al. 2005), suggesting that the implementation of microwires in humans is an important research direction.

Better understanding of the classic issues explored in basic neuroscience of sensorimotor processing is critical for the development of brain-controlled prosthetic limbs. For example, how different are the cortical dynamics associated with active movements versus passive movements? Is sensory input required for accurate movement of a prosthetic effector, and how can the absence of sensory input be compensated in the design? Alternatively, should sensors be included in the design of prosthetic limbs and what is the best approach for integrating that sensory information with the efferent motor commands?

The advancements in our understanding of sensorimotor systems and of the utility of ICA for clarifying the nature of large scale brain signals based on the work presented

here, will hopefully lay a few more stones on the path toward the development brain-computer interfaces.

REFERENCES

1. Ahissar, E. and P. M. Knutsen (2008). "Object localization with whiskers." Biol Cybern **98**(6): 449-58.

2. Akalin Acar, Z., Makeig, S., and Worrell, G. (2008a). Neuroelectromagnetic forward modeling toolbox. Proc. of IEEE EMBC, Vancouver, British Columbia.

3. Akalin Acar, Z., Makeig, S., and Worrell, G. (2008b). Head modeling and cortical localization in epilepsy. Proc. of IEEE EMBC, Vancouver, British Columbia.

4. Anemuller, J., T. J. Sejnowski, et al. (2003). "Complex independent component analysis of frequency-domain electroencephalographic data." Neural Netw **16**(9): 1311-23.

5. Bai, O., Lin, P., Vorbach, S., Floeter, M.K., Hattori, N., Hallett, M. (2008). "A high performance sensorimotor beta rhythm-based brain-computer interface associated with human natural motor behavior." J. Neural Eng. **5**: 24-35.

6. Dyrholm, M., S. Makeig, et al. (2007). "Model selection for convolutive ICA with an application to spatiotemporal analysis of EEG." Neural Comput **19**(4): 934-55.

7. Hammon, P. S., S. Makeig, et al. (2008). "Predicting reaching targets from human EEG." IEEE Signal Processing Magazine **25**(1): 69-77.

8. Knutsen, P. M., M. Pietr, et al. (2006). "Haptic object localization in the vibrissal system: behavior and performance." J Neurosci **26**(33): 8451-64.

9. Komisaruk, B. R. (1970). "Synchrony between limbic system theta activity and rhythmic behavior in rats." J Comp Physiol Psychol **70**(3): 482-492.

10. Kubler, A., F. Nijboer, et al. (2005). "Patients with ALS can use sensorimotor rhythms to operate a brain-computer interface." Neurology **64**: 1775-1777.

11. Mehring, C., M. P. Nawrot, et al. (2005). "Comparing information about arm movement direction in single channels of local and epicortical field potentials from monkey and human motor cortex." Journal of PHysiology-Paris **98**(4-6): 498-506.

12. Niedermeyer, E. a. L. D. S., F. (1999). Electroencephalography: Basic principles, clinical applications, and related fields. Baltimore, Williams & Wilkins.

13. Palmer, J. A., Z. Akalin-Acar, et al. (2008). AMICA: Adaptive Newton Method for Non-stationary ICA - ECoG Recording Epileptic Seizure. Collaborative Research in Computational Neuroscience, University of Southern California.

14. Palmer, J. A., Makeig, S., Kreutz-Delgado, Rao, B.D. (2008). Newton method for the ICA mixture model. Proceedings of the 33rd IEEE International Conference on Acoustics and Signal Processing (ICASSP), Las Vegas, NV.

15. Rickert, J., S. C. Oliveira, et al. (2005). "Encoding of movement direction in different frequency ranges of motor cortical local field potentials." J Neurosci **25**(39): 8815-24.

16. Vanderwolf, C. H. (1969). "Hippocampal electrical activity and voluntary movement in the rat." Electroencephalogr. Clin. Neurophysiol. **26**(4): 407-418.

17. Wolpaw, J. R., D. J. McFarland, et al. (1991). "An EEG-based brain-computer interface for cursor control." Electroencephalogr Clin Neurophysiol **78**(3): 252-9.